Fall 2016

Generalized Partial Directed Coherence and centrality measures in brain networks for epileptogenic focus localization

Joshua Aaron Adkinson

GENERALIZED PARTIAL DIRECTED COHERENCE AND

CENTRALITY MEASURES IN BRAIN NETWORKS FOR

EPILEPTOGENIC FOCUS LOCALIZATION

by

Joshua Aaron Adkinson, B.S., M.S.

A Dissertation Presented in Partial Fulfillment
of the Requirements of the Degree
Doctor of Philosophy

COLLEGE OF ENGINEERING AND SCIENCE
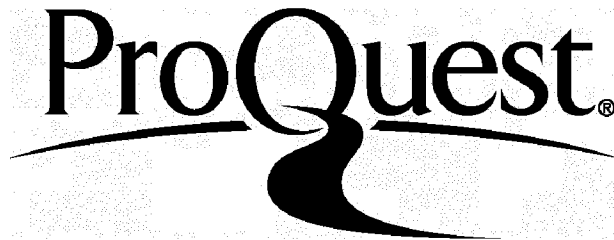LOUISIANA TECH UNIVERSITY

November 2016

ProQuest Number: 10307764

ProQuest 10307764

LOUISIANA TECH UNIVERSITY

THE GRADUATE SCHOOL
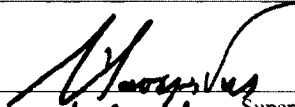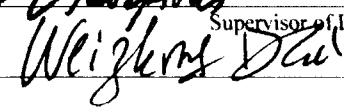
October 5th, 2016
_____
Date
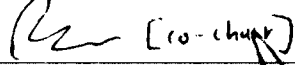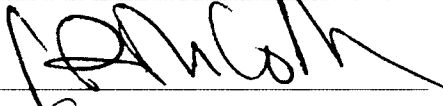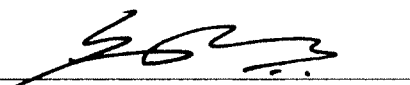
We hereby recommend that the dissertation prepared under our supervision

by Joshua Aaron Adkinson
_____

entitled _____

Generalized Partial Directed Coherence and

Centrality Measures in Brain Networks for

Epileptogenic Focus Localization

_____

be accepted in partial fulfillment of the requirements for the Degree of

Doctorate of Philosophy in Computational Analysis and Modeling

_____
Supervisor of Dissertation Research

_____
Head of Department

Computational Analysis and Modeling
_____
Department

Recommendation concurred in:

[co-chair]

_____

_____   Advisory Committee

_____

Approved:

_____
Director of Graduate Studies

_____
Dean of the College

Approved:

_____
Dean of the Graduate School

ABSTRACT

Accurate epileptogenic focus localization is required prior to surgical resection of brain tissue for treatment of patients with intractable temporal lobe epilepsy, a clinical need that is partially fulfilled to date through a subjective, and at times inconclusive, evaluation of the recorded electroencephalogram (EEG). Using brain connectivity analysis, patterns of causal interactions between brain regions were derived from multichannel EEG of 127 seizures in nine patients with focal, temporal lobe epilepsy (TLE). The statistically significant directed interactions in the reconstructed brain networks were estimated from three second intracranial multi-electrode EEG segments using the Generalized Partial Directed Coherence (GPDC) and validated by surrogate data analysis. A set of centralities per network node were then estimated. Compared to extra-focal brain regions, regions located anatomically within the epileptogenic focus (focal regions) were found to be associated with enhanced inward directed centrality values at high frequencies (γ band) during the initial segments of seizures (within nine seconds from seizures onset) and led to correct localization of the epileptogenic focus in all nine patients. Therefore, an immediate application of the employed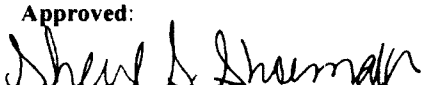 novel network framework of analysis to intracranial EEG recordings may lead to a computerized, accurate and objective localization of the epileptogenic focus from ictal periods. The proposed framework could also pave the way for studies into network dynamics of the

epileptogenic focus peri-ictally and interictally, which may have a significant impact on

current automated seizure prediction and control applications.

APPROVAL FOR SCHOLARLY DISSEMINATION

The author grants to the Prescott Memorial Library of Louisiana Tech University the right to reproduce, by appropriate methods, upon request, any or all portions of this Dissertation. It is understood that "proper request" consists of the agreement, on the part of the requesting party, that said reproduction is for his personal use and that subsequent reproduction will not occur without written approval of the author of this Dissertation. Further, any portions of the Dissertation used in books, papers, and other works must be appropriately referenced to this Dissertation.

Finally, the author of this Dissertation reserves the right to publish freely, in the literature, at any time, any or all portions of this Dissertation.

Author _Joshua Atkinson_

Date _11/1/2016_

DEDICATION

To my family:

Thank you all for always believing in me and showing me what it means to be like Christ. Without each one of you in my life, I would not be the person I am today. I love you all.

-Joshua

TABLE OF CONTENTS

LIST OF TABLES

ACKNOWLEDGEMENTS

coincidence that I have met so many people who have made such a huge impact on my life.

The last few years of my life have been quite an experience. Through this time, not only have I grown as an academic but also as a person. I believe I have been changed for the better, and I hope that someday I can return the favor and ultimately make a positive impact on the world.

CHAPTER 1

INTRODUCTION

Epilepsy is a neurological disorder characterized by a predisposition to recurring

seizures. This abnormal brain activity causes clinical symptoms to arise, and it is from

these symptoms and the accompanying electroencephalographic (EEG) activity that

epilepsy is diagnosed. It is estimated that about 1% of the global population suffers from

epilepsy, making epilepsy the fourth most common neurological disorder today after

stroke, Alzheimer's, and migraines.

While the causes and neuroanatomical substrates of epilepsy are pretty diverse,

the resulting seizures can be primarily generalized, where seizure activity appears in both

brain hemispheres simultaneously (according to EEG readings), or focal where the

seizure (a.k.a. ictal) activity begins in a localized region and subsequently propagates to

other brain regions. In focal epilepsy, the brain region that first exhibits ictal activity is

called the epileptogenic focus.

For 60-70% of people with epilepsy, the occurrence of seizures can be controlled

pharmacologically via antiepileptic drugs. For the remaining 30-40% patients with focal

epilepsy, surgical resection of the epileptogenic focus may be a viable option. Improving

the likelihood of surgical success requires accurate localization of the epileptogenic focus

thus minimizing the inherent risks of brain tissue resection. Surgical removal of the

epileptogenic focus yields positive but not always ideal results, with about one-third of

1

patients with mesial temporal lobe epilepsy continuing to have seizures within five years of surgical intervention. Furthermore, 75% of patients with remission of seizures after surgery still require the use of antiepileptic drugs to prevent a relapse of epileptic symptoms.

Multiple recording modalities (e.g. EEG, MRI, PET, MEG) and clinical psychological tests are typically utilized for localization of the epileptogenic focus at specialized epilepsy centers. Noninvasive EEG monitoring followed by invasive long-term EEG monitoring to electrographically capture typical seizures of patients remains the most important clinical tool. The epileptogenic focus is determined by visual inspection of the EEG by a specialist and/or software looking for brain regions that first exhibit the onset of seizure activity, which is the current gold standard for focus localization.

In order to improve upon the success of surgical intervention, better algorithms for focus localization from the EEG still need to be developed. Such analytical algorithms should ideally be objective and patient independent, and one approach to this problem involves Brain Connectivity Analysis (BCA). BCA is a rapidly growing field in the study of complex brain networks from an anatomical and functional perspective. In BCA, the connectivity between brain regions can be quantified by a multitude of measures depending on the type of network features one would like to investigate. Once connectivity between every two regions is measured, a network representation of the brain's activity can be constructed. Using the constructed networks as a model of brain activity during a defined event, metrics from graph theory and network science can be employed to further analyze the networks. Metrics that measure the connectivity

importance of a given node to all the other nodes in the network fall under the category of

centrality measures. Many different centrality metrics exist and provide different

interpretations of the function of a node in the network.

In this study, we employed centrality metrics to identify the characteristic

behavior of the epileptogenic focus in patients with temporal lobe epilepsy undergoing

phase II EEG monitoring. Statistically significant causal interactions between brain

regions were determined using the measure of Generalized Partial Directed Coherence

(GPDC). Surrogate data analysis was used to further identify only the statistically

significant causal interactions, and the thus derived brain networks were then analyzed to

determine the centrality of each brain region and subsequently investigate the possibility

of localizing the epileptogenic focus on the basis of its centrality characteristics. Under

this methodology we were successful in associating certain centrality metrics with the

epileptogenic focus in all patients.

Chapter 2 covers the primary background information needed to understand this

research topic. This chapter covers basic concepts of the brain and how brain activity is

measured using electroencephalography (EEG). In Sections 2.3, 2.4 and 2.5, epilepsy,

focal epilepsy and focus localization are described in further detail. Section 2.6 describes

the fundamental concept of Graph Theory, which is an important basis for explaining the

ideas of brain connectivity analysis discussed in Section 2.7.

Chapter 3 provides a detailed description of the methods used in this research.

After discussing the EEG data used in this research and any processing performed prior

to analysis (Sections 3.1 and 3.2), the basic statistical tools needed to analyze the data as

a time series are discussed in Section 3.3. Section 3.4 covers the theory behind

Generalized Partial Directed Coherence (GPDC), the measure used to describe the connectivity between EEG signals. Section 3.5 covers surrogate data analysis, which is the technique used in this research to determine which GPDC values are significant. Sections 3.6, 3.7, and 3.8 describe concepts from Graph Theory in more detail, focusing primarily on fundamental concepts needed to understand how the significant GPDC values can be modeled as a network of connections and how this network can be described using a mathematical structure known as an adjacency matrix. Section 3.9 describes a series of measures known as centralities, and each subsection explains in detail how each centrality is measured. Sections 3.10 and 3.11 cover how each measured centrality is processed and how it associates with the epileptogenic focus for each patient, and Section 3.12 describes the parameters utilized for this research and the rationale for the choice of those parameters.

Chapter 4 is an overview of the results from this research investigation. An example of a derived network and its resulting centrality values are described in Section 4.1. Section 4.2 then describes how centrality values change over the duration of seizure events, and Section 4.3 describes these changes over different frequency spectra. Section 4.4 shows the effects of averaging centralities over specified windows of time and frequency bands with respect to localization of the epileptogenic focus. In Section 4.5, the focus localization results from undirected networks reconstruction are compared to the results derived from directed networks reconstruction from the recorded EEGs. Section 4.6 compares the focus localization results when either all seizures or only a subset of clinical seizures from each patient are considered. Lastly, Section 4.7 shows the final results obtained in this research.

Chapter 5 provides a discussion of the results and the nuances of this research. Section 5.1 covers the primary conclusions made from the results obtained during this research. Section 5.2 then explains how these results relate to current clinical and neurophysiological evidence on this topic. Section 5.3 then compares the methodology and results of this research to other similar epilepsy research in the literature, specifically research surrounding the concept of brain connectivity analysis and focus localization. Sections 5.4 describes possible challenges that can occur using this methodology, and Section 5.5 completes this chapter with descriptions of other possible approaches/extensions to this research.

Finally, two appendices have been added. Appendix A includes additional research that was performed on the intracranial EEG data from four of the patients studied. Here, the entire EEG dataset (seizure and non-seizure segments) of each patient was used for analysis to understand where prominent GPDC values arise between pairs of electrodes. Appendix B provides more supporting results similar to the final results shown in Section 4.7.

CHAPTER 2

BACKGROUND

2.1 The Brain

The human brain is one of the most complex systems in existence. Generally considered the "control center" of the body, the brain is involved either directly or indirectly in almost every ongoing process. The complexity of this system comes from amalgamations of neurons, that is, cells that communicate by sending electrochemical signals (called action potentials) to other cells, especially other neurons. Estimates place the total number of neurons in the human brain between 86 billion [1] and 100 billion [2]. Each neuron communicates with other neurons via synapses, and a single neuron can have thousands of synapses that connect it to other neurons. Even by a low estimate of 1,000 synapses per neuron, this would mean that the human brain has at least 100 trillion synaptic connections [2]. Furthermore, the number and strength of synapses present in the brain are not static but dynamic, maintaining high levels of plasticity, which allows for the brain to adapt to external stimuli, learn, process and memorize information. Overall, this vast complex communication system makes the brain central to consciousness, cognition, regulation, and behavior.

Figure 2-1 provides a simple representation of a neuron including labels for the basic neuron structures. The complex branches emanating from the cell body, called the soma, are known as dendrites and are the primary place for synaptic input from other neurons. The neuronal branch surrounded by Schawnn cells is known as the axon, which

is the portion of the cell specializing in relaying chemical signals to other neurons. The

chemical signal propagates as a wave (action potential) initiating at the axon hillock, the

region where the axon connects to the cell body, moves down the axonal fiber, and

terminates at the axon terminal. This area, known as the presynaptic terminal, releases

neurotransmitters through a region called the synaptic cleft to a region on dendrites or

soma of another neuron, known as the postsynaptic terminal, where the action potential

may instigate the generation of an action or field post-synaptic potential in the next

neuron in line. Note that Schawnn cells are only present on neurons in the peripheral

nervous system.
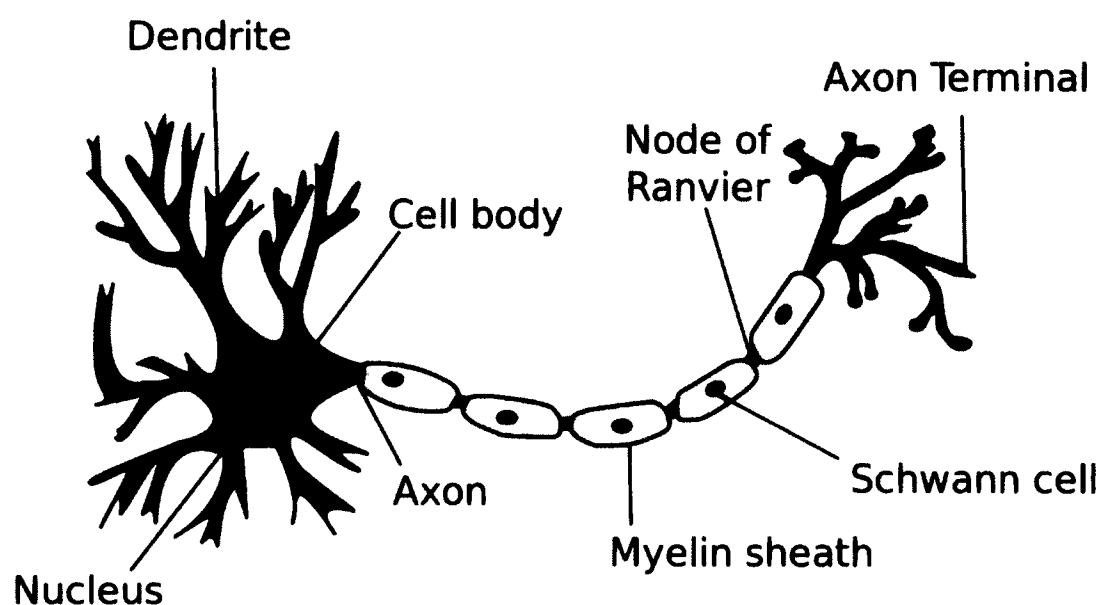
Figure 2-1: Basic neuron with labeled structures. (Image source:
http://commons.wikimedia.org/)

Although the brain is a highly complex system, all brains share common

structures, which can be roughly divided into the medulla, pons, midbrain, diencephalon,

cerebellum, and cerebrum, all of which have differing purposes and developed at

different stages in evolutionary history. Figure 2-2 provides a sagittal cross section of the

brain with labeled brain structures. The cerebrum with its superficial cortex is the most recently developed portion of the brain and is the primary driver of conscious thought and cognition. The cerebrum is made of two hemispheres which are symmetrical in structure and are primarily connected to one another via a structure called the corpus callosum. Furthermore, each cerebral hemisphere is subdivided into four regions named after the cranial bones that overlay each one: the frontal lobe, the parietal lobe, the occipital lobe, and the temporal lobe [3]. Each of these structures and substructures per region performs certain tasks (functional segregation) and communicates with the other regions to amalgamate these processes into more complex mental faculties (functional integration).
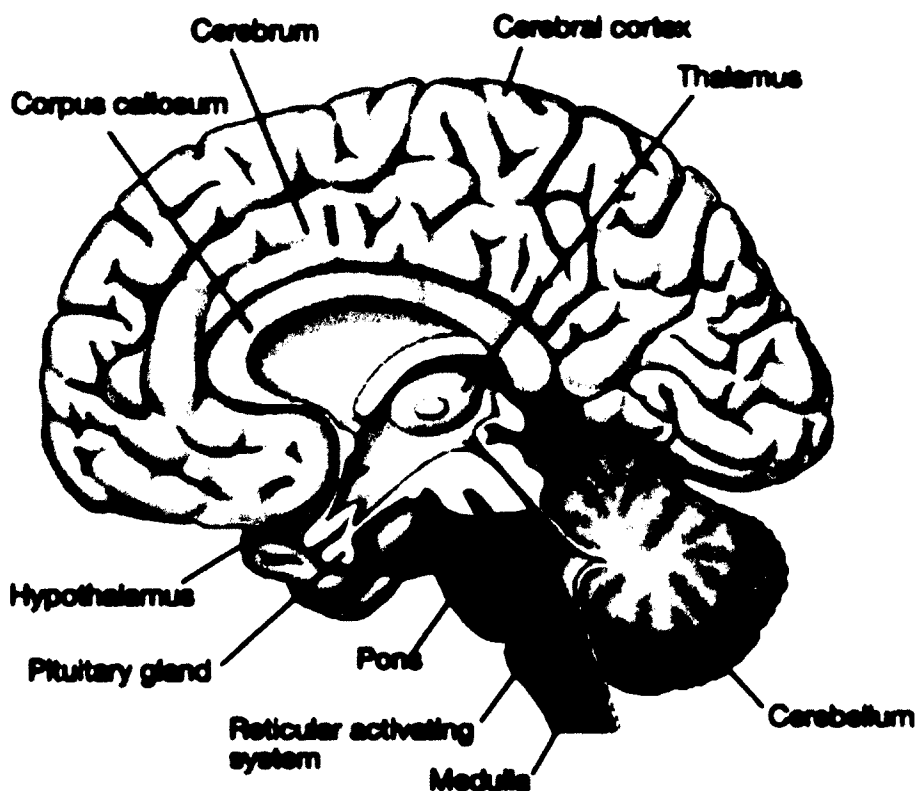
Figure 2-2: Sagittal cross section of the human brain with labeling of general brain structures. (Image source: http://www.prabusha.com/)

2.2 Electroencephalography

Electroencephalography (EEG) is an electrophysiological technique used to record the electrical activity of the brain with the use of sensors called electrodes. EEG measures the internal field potential changes due to ionic currents generated from inter-neuronal communication. Prior to the generation of an action potential, different concentrations of ions inside and outside of the cell membrane produce a membrane potential, and if this potential is depolarized sufficiently, rapid flux of ions into and out of the neuron generates the action potential. EEG takes advantage of this phenomena on a large scale, recording the electrophysiological behavior of thousands to millions of neurons simultaneously. The EEG signals are recorded by measuring the voltage potential difference between pairs of electrodes (channels). If electrodes placed at brain sites are compared to an electrode outside of the area of interest, called the reference electrode, each channel measures the activity of the brain at the site of interest. EEG can be recorded using scalp or intracranial electrodes. Scalp EEG records brain activity using electrodes placed on the scalp, whereas intracranial EEG require electrodes to be surgically implanted inside or on the surface of the brain.

Figure 2-3 provides an example of multichannel scalp EEG data. The data covers a period of 10 seconds of recorded scalp EEG data taken using a standard electrode placement setup known as the 10-20 system. The signal braced in red represents an EEG signal that contains oscillatory behavior in the α frequency band, which ranges between 8 Hertz (Hz) and 12Hz. Other studied frequency bands include the δ (0Hz to 4Hz), θ (4Hz to 8Hz), β (12Hz to 30Hz), and γ (30Hz to 50Hz) frequency bands. The area braced in green is an example of an eye-opening artifact (muscle movements near the eye, not

related to brain activity) picked up during the recording process. Artifacts are a major

challenge when reading and analyzing scalp EEG data.
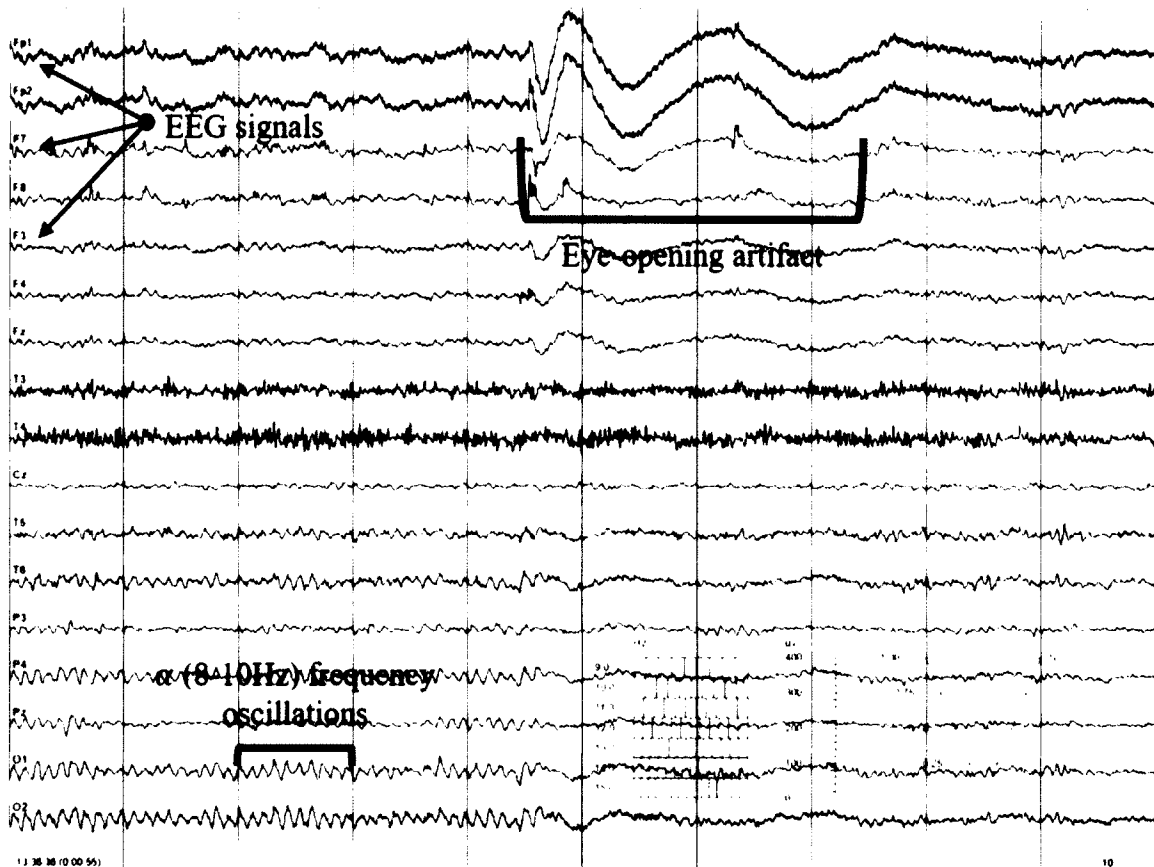
Figure 2-3: Example of multichannel scalp EEG data. The record is over 10 seconds, and a ruler (light orange, middle) provides the scale of the signals (in microvolts).

Although scalp EEG is noninvasive and cost effective, the signal quality is not

ideal. Voltage potentials measured by scalp electrodes are attenuated in amplitude and

frequency due to the low conductivity and low-pass characteristics of the skull.

Furthermore, the voltage potential of a given brain region is often also picked up by a

multitude of neighboring electrodes, so finding the exact source of given brain activity is

difficult by scalp EEG. Scalp EEG is also riddled with artifacts, signal data from sources

other than brain activity, such as voltage potentials generated from the muscles involved

in eye blinks (see Figure 2-3). Such factors make scalp EEG signals difficult to analyze.

To minimize these issues, intracranial EEG (iEEG) can be employed.

In iEEG, strips or grids of electrodes are surgically implanted directly onto the

brain surface to record highly local brain activity (see Figure 2-4), and electrodes

embedded along the length of a needle probe can be inserted into the brain tissue to

record deep brain activity. This recording method provides the best quality signal, but

because of the risks involved in surgical implantation of electrodes, iEEG is only

performed when it is deemed absolutely necessary.
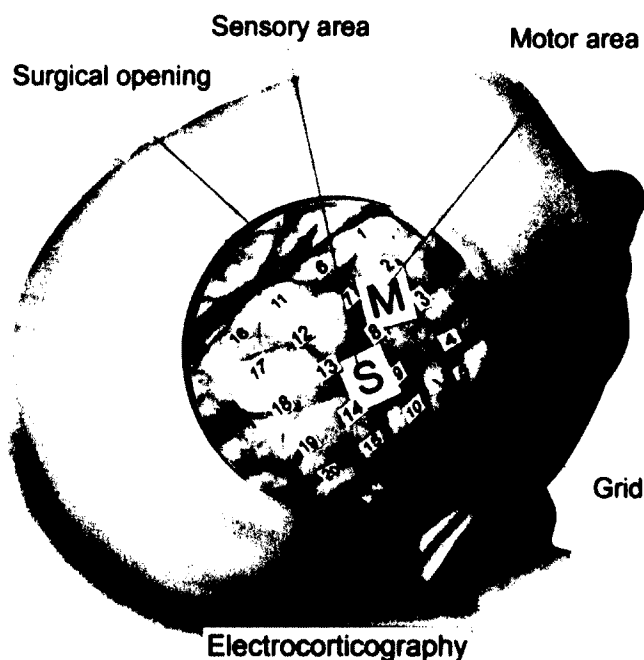
Figure 2-4: An artistic representation of a grid of electrodes covering the sensory and motor brain regions for intracranial EEG recording. (Image source: http://en.wikipedia.org/)

EEG has been the most widely adopted technique for monitoring brain activity for

research purposes and in clinical practice. First and foremost, EEG can record signals

derived from the electrophysiological phenomena unique to neurons. Along with EEG,

neuroimaging has become a common class of techniques designed to image the structural

and functional characteristics of the nervous system; many neuroimaging techniques rely on secondary processes caused by the neurophysiological activity. For example, functional Magnetic Resonance Imaging (fMRI) measures the amount of oxygen present in the blood throughout the brain; higher levels of blood oxygen in a given brain region are associated with increased metabolic activity, which is in turn related to increased electrophysiological activity in that brain region. Because of the relative simplicity of EEG machines, EEG recording devices are fairly affordable for most hospitals, and of greater portability compared to other machines (i.e. MRI). EEG recording systems also have the ability to record data with very high sampling rates (up to 20,000 Hz, currently), meaning that EEG data has a very high temporal resolution. EEG also has disadvantages which make its use not ideal for certain situations. Because a limited number of electrodes that can be placed on the scalp or implanted into the brain, EEG tends to have very low spatial resolution compared to other techniques. Furthermore, EEG electrodes are very sensitive; and therefore, electrodes tend to capture a significant amount of noise extraneous to the desired signals generated by the brain. This means that measures must be taken to mitigate the sources of noise. Also, surgical implantation of electrodes may cause problems (e.g. cerebral hemorrhage) to patients. Ultimately, the advantages of EEG still far outweigh their disadvantages, especially in the field of epilepsy research.

2.3 Epilepsy

Epilepsy is a broad class of neurological disorders characterized by a person's predisposition to recurrent seizures. The International League Against Epilepsy (ILAE) defines an epileptic seizure as "a transient occurrence of signs and/or symptoms due to abnormal excessive or synchronous neuronal activity in the brain"[4]. This excessive

neuronal activity lies outside the voluntary control of the person, and it is through this activity that clinical symptoms arise in the patient. Clinical symptoms can vary widely as well, ranging from brief loss of awareness (absence seizures) to complete loss of consciousness with loss of bodily control (tonic-clonic seizures). Furthermore, different clinical manifestations may arise depending on where this activity occurs in the brain. The type of epilepsy for a given person is based on the general behavior of his/her seizures. If seizure events initiate in a particular region of the brain, epilepsy is deemed as partial or focal, and if seizures initiate across the whole brain simultaneously, the patient is diagnosed with generalized epilepsy.

In the United States, roughly 2.2 million Americans have been diagnosed with epilepsy, and approximately 150,000 new cases are diagnosed annually [5]. From a financial standpoint, the direct medical cost of epilepsy in the U.S. is about $9.6 billion annually [6], and based on estimates from 1995, the annual total cost (direct and indirect) of epilepsy in the U.S. is $12.5 billion [7], [8]. Adjusted for inflation, that value comes up to $19.7 billion as of 2016. Global estimates reveal that about 1% of the global population suffers from some form of epilepsy, making epilepsy the fourth most common neurological disorder today [5]. Causes for the manifestation of epilepsy can vary widely, but most epilepsy cases can be categorized into either genetic predispositions, congenital conditions, or acquired through events such as Traumatic Brain Injury (TBI). The recurrence of seizure events has a profoundly negative impact on the cognitive, psychological, and social well-being of those suffering from the condition, and therefore methods for controlling seizure generation are the primary treatment plan for people with epilepsy.

To diagnose a person with epilepsy physicians must observe the brain's electrophysiological behavior during a seizure event (also known as the ictal period). This electrical activity of the brain across different regions is observed using EEG. In about 70% of people diagnosed with epilepsy, the occurrence of seizures can be controlled via antiepileptic drugs (AEDs). The remaining 30-40% of patients have medically refractory (intractable) epilepsy, where AEDs have no or little beneficial effect [9]. For the subset of these people who suffer from focal epilepsy a viable option may be surgical intervention.

2.4 Focal Epilepsy

Focal epilepsy is the recurrence of seizures that have been electrographically observed to initiate in a specific brain region before (possibly) propagating to other brain regions. Focal epilepsies are often categorized by the location in the brain where seizures are initiated. For example, seizures in people with temporal lobe epilepsy are initiated in either the left or right temporal lobe. Electrographically, the type of focal seizure generated can be further described based on the degree of propagation that occurred relative to the seizure focus. If the seizure activity remains in the brain region in which it was initiated, the ictal event is called a simple partial seizure. Complex partial seizures initiate in a given region and spread throughout the same hemisphere and are often accompanied by a loss of consciousness. Secondarily generalized seizures initiate at the focal region, but then spread to both ipsilateral and contralateral hemispheres. Sampling statistics have shown that approximately 60% of people with epilepsy have some form of focal epilepsy [10]. For people with medically refractory partial epilepsy, surgical resection of the brain tissue involved in seizure generation has been found to be a more

effective means of controlling seizures than continued treatment with AEDs [11].

Regardless, resection of brain tissue is an incredibly high-risk endeavor, so an accurate

determination of the epileptogenic focus is of utmost importance.

2.5 Focus Localization

Multiple modalities and tests are utilized in order to localize the epileptogenic

focus. Brain imaging techniques such as magnetic resonance imaging (MRI) can be

utilized to reveal the existence of a malformation and determine its location. Single-

photon emission computed tomography (SPECT) is another common technique for

finding the epileptogenic focus. Like fMRI, SPECT takes advantage of the fact that blood

flow in the brain is closely related to local brain metabolism. In this method, a gamma

emitting radioisotope is injected into the patient at the moment of seizure initiation, and

the SPECT scanner records the path of the radioisotope throughout the brain. This is an

effective method for focus localization since the epileptogenic focus has increased

metabolic activity around the period of seizure initiation. However, this method requires

physicians and assistants to remain vigilant at the side of the patient in order to inject the

radioisotope into the blood stream of the patient very close in time to seizure initiation.

Although the two aforementioned methods are some of the most commonly used today,

the gold standard for focus localization remains a two-stage (phase I and II) EEG

monitoring performed at an Epilepsy Monitoring Unit (EMU).

Phase I EEG involves long-term monitoring of the brain activity by scalp EEG.

The patient is monitored over a sufficient period of time so that several ictal events

(seizures) occur. Even though visual inspection of phase I EEG gives a rough indication

of the location of the epileptogenic focus, heavy signal attenuation occurs through the

skull because of the low conductive properties of bone and thus localization of the focus can be done usually at a much more extended region than desired. Patients who exhibit epileptogenic foci validated in Phase I EEG recordings, and the focus location renders them good candidates for surgery, typically undergo Phase II monitoring to more accurately localize the focus. Phase II EEG monitoring requires placement of electrodes onto or inside the cerebrum. Placement of the intracranial electrodes is typically guided by the results of Phase I monitoring. Because of the vast enhancement in signal quality, intracranial EEG allows for improved understanding of the focal epilepsy of each patient. Optional video monitoring of the patient may be performed to help correlate clinical symptoms with the recorded EEG signals. Based on the results of Phase II monitoring and various other neurophysiological tests, physicians decide which tissue should be resected. In both phases of EEG monitoring, the epileptogenic focus is primarily determined by visual inspection of the EEG by an expert neurologist and often accompanied by computational analysis of the EEG via commercially available signal processing software; typically, the first location in which highly synchronous activity arises during the ictal period is deemed the focal region for that given seizure. Figure 2-5 is an example of a clinical seizure recorded during a Phase II multichannel iEEG monitoring in a patient with temporal lobe epilepsy. For this seizure, lasting roughly 30 seconds (framed by the green vertical bars), electrodes inserted near the left hippocampus (red brace) presented high amplitude and high frequency oscillatory behavior at the beginning of the seizure. Since this high frequency behavior was initiated at these electrodes, the epileptogenic focus likely was within or near this region.
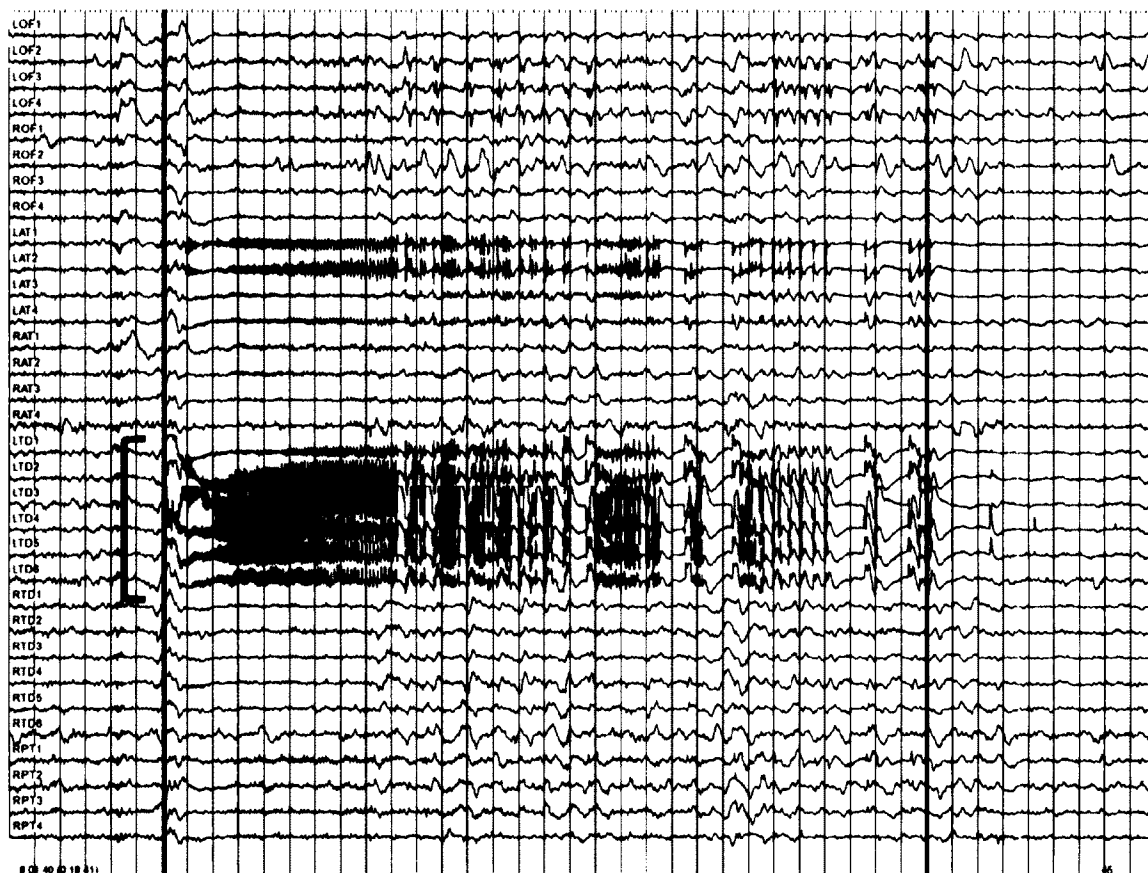
Figure 2-5: Intracranial EEG data of a clinical seizure.

Surgical removal of the epileptogenic zone has yielded an overall positive

outcome in patients. However, about one-third of patients with mesial temporal lobe

epilepsy continue to have seizures within five years of surgical intervention [12]–[14].

Furthermore, 75% of patients showed remission of seizures after surgery but still required

the use of antiepileptic drugs to prevent a relapse of seizure events [12]. Surgeries for

extratemporal lobe epilepsies tend to have even less success, with only 50% of patients

being seizure-free two years after surgery [15], [16].

As stated above, visual inspection of the iEEG to determine the epileptogenic

focus is the current gold standard used prior to brain resection, and the need for better

localization of the epileptogenic focus is still considered an important goal in epilepsy

research. Visual inspection is an inherently subjective diagnostic tool requiring extensive

training of the EEG reviewer. Additionally, EEG activity can be difficult to interpret due

to the variability of ictal events as well as the quality of EEG recordings, especially in

Phase I/scalp EEG. For example, inspection of ictal scalp EEG data recorded prior to

surgery from patients who were seizure free two years after surgery found that up to 20%

of temporal seizures and 40% of extratemporal seizures could not be lateralized [17].

Also, in patients who underwent brain surgery guided by intracranial EEG monitoring,

only ~45% were seizure free up to three years after surgery [18], [19].

To improve upon the success of the surgical intervention, more defined

algorithms for focus localization need to be developed. Underlying brain activity

indicative of the interactions between brain regions is not readily detectable visually and

requires the use of advanced computational tools. In addition, any analytical algorithms

should ideally be completely objective. A promising approach that could satisfy the needs

of such a brain connectivity analysis is methodology derived from concepts from Graph

Theory.

2.6 Graph Theory

Graph Theory, in general terms, is the study of the relationships that exist within a

set of discrete objects. A wide array of phenomena can be modeled using graphs

including physical structures such as roadways, electrical circuits, and the internet

infrastructure and less tangible interactions like social relationships, predator-prey

interactions, and citation networks. All of these data types can be modeled using a

combinatorial structure known as a graph, where the objects are represented as nodes

(also called vertices) and the relationships between objects are represented by edges

joining these nodes. Figure 2-6 provides as example of a simple graph containing 10

nodes and 38 edges connecting them. Additional characteristics can be included in the

graph such as numerical weights for the nodes and/or edges, the existence of multiple

edges between two nodes, edges joining a node to itself, or directionality present in the

edge. The choice to include any of these characteristics is dependent on the set of objects

being studied along with the relationship that the researcher wishes to observe.
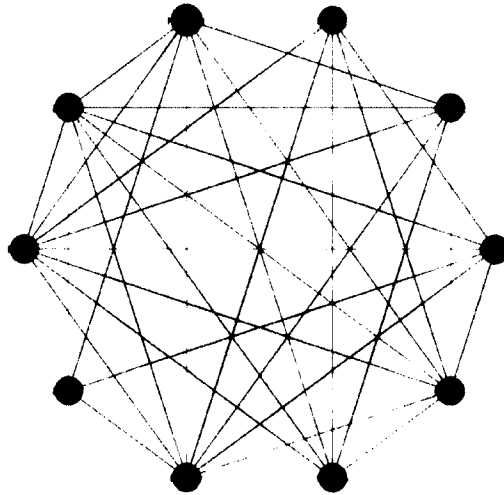
Figure 2-6: Graph example. The nodes are colored green with black lines line segments representing edges.

While pure graph theory looks to understand mathematically the general nature of

graphs, a subset of graph theory called Network Science uses the concept of graphs as the

basis for modeling real-world phenomena, and the constructed networks can be studied in

order to better understand the system under investigation. Brain connectivity analysis is a

field that uses network science to study the brain as networks.

2.7 Brain Connectivity Analysis

Brain Connectivity Analysis (BCA) has been a rapidly growing field in recent

years, looking to study the complex network structure of the brain from anatomical,

functional, and/or effective perspectives using various neuroimaging techniques.

Anatomical studies in BCA aim to study the structural pathways linking neural elements,

which can range from the local circuitry of a few neurons up to the axonal fiber tracts in

the brain acting as a "wiring diagram" connecting different brain regions. This "wiring

diagram" between brain regions, coined the connectome, can be obtained using

neuroimaging techniques such as diffuse tensor imaging (DTI) [15], which measures the

direction of diffusive motion of water molecules, and 3D polarized light imaging (3D-

PLI) [16]. Recent advances have improved the spatial resolution of the imaging

techniques down to 100μm. Furthermore, the connection between neural elements can be

considered either a static or dynamic system, depending on the time scale utilized by the

researcher. Functional connectivity relies on the statistical dependencies that arise

between brain regions and is often utilized to determine which brain regions are

interacting during a given task. The primary datatype used in functional connectivity

studies comes from time series data derived from neural recordings. Effective

connectivity investigates the cause-effect relationship between neural elements. Like

functional connectivity, effective connectivity uses time dependent data, but infers a

causal relationship between neural elements either by finding temporal precedence

between neural elements in the time series data or via a structural model such as

anatomical pathways used in conjunction with statistical analysis of functional

interactions. Figure 2-7 provides a flowchart of the brain connectivity analysis process

divided into three fundamental steps. First, data are collected that capture the behavior

that is of interest. The acquired data are then processed in such a manner that

relationships between different brain regions can be extracted and the behavior is

modeled at the network level. Lastly, the derived network is studied in order to determine

if any qualities of the network are associated with the observed behavior.
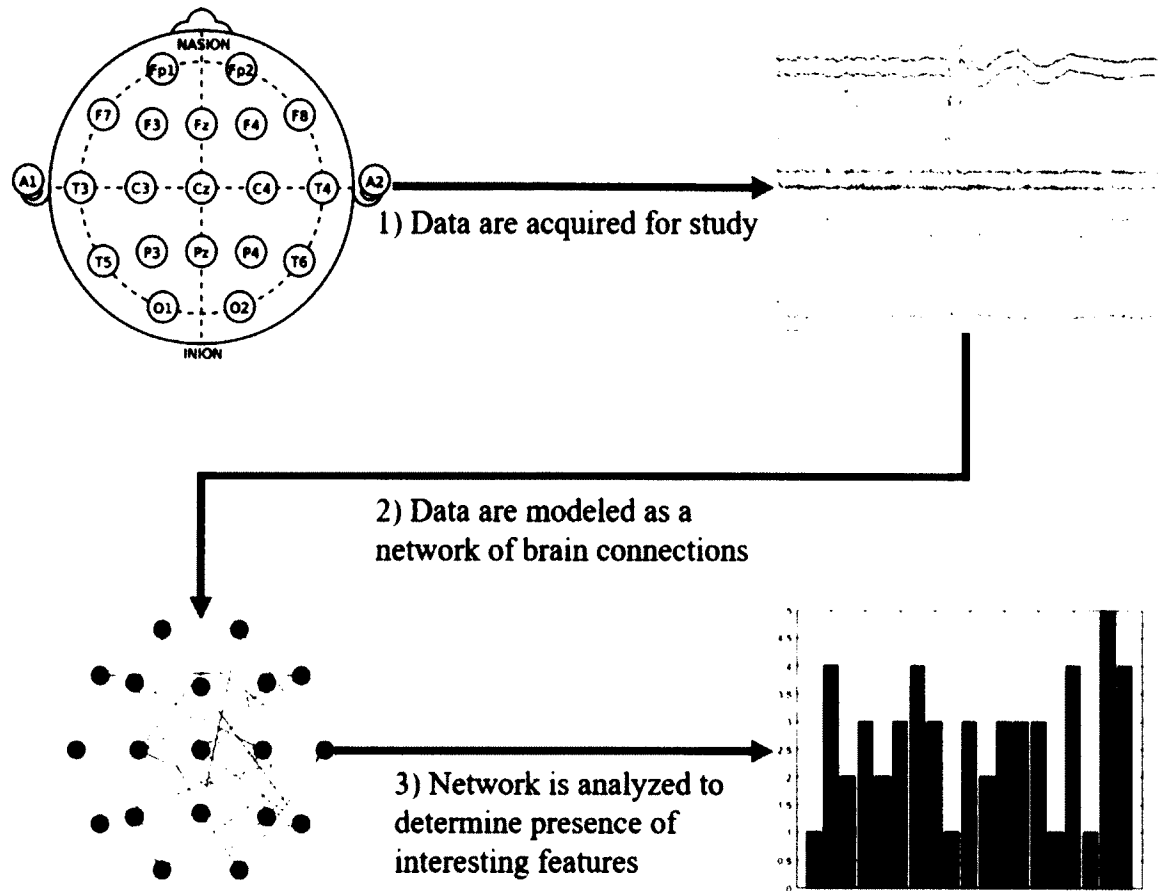
Figure 2-7: Flowchart representing the general process for studying the connectivity of different brain regions.

For both functional and effective connectivity, researchers have employed a

multitude of electrophysiological and neuroimaging techniques, each having tradeoffs in

terms of the characteristics of the data acquired. On one end of the spectrum, fMRI uses

blood oxygen level dependent (BOLD) signals as a method to elucidate functional

connectivity between voxels of brain tissue. Although fMRI has the advantage of high

spatial resolution, fMRI imaging has a low sampling frequency, requiring studies to use

analytical techniques that utilize static connectivity patterns. Neuroimaging techniques

that can collect data with a high sampling frequency, such as EEG and

magnetoencephalography (MEG), allow for the creation of multiple networks spanning a

short period of time, providing an opportunity to study the dynamic behavior of the brain.

The tradeoff with current EEG recording techniques is the lack of high spatial resolution

which is inherent in fMRI. Regardless of the neuroimaging technique being employed,

the next common aspect for many BCA studies is the creation of a network derived from

the neuroimaging data.

Along with the various datatypes/modalities employed in BCA, researchers have

utilized a multitude of measures to quantify the connectivity between brain regions.

Typically, these measures estimate the pair-wise relationship between neural elements

using the signals generated by the given technique. Correlation, for example, estimates

interaction between brain regions in the time domain, whereas coherence estimates

similar interactions in the frequency domain. However, more advanced measures such as

Directed Transfer Function (DTF) [20] or Partial Directed Coherence (PDC) [21] have

been developed to allow for the observation of the interaction between brain regions

while accounting for the possible effects of contributing interactions from all other

regions. Measures can provide directional information, that can be used to infer causal

relationships between brain regions, and may consider all interactions, whether direct or

indirect, as in the case for DTF, or only direct interactions, as in the case of PDC.

Furthermore, modifications to the above methods, such as the Generalized Partial

Directed Coherence (GPDC), have been developed to better model specific aspects in the

data [22].

The type of connectivity measure used can, however, restrict the type of network that can be reconstructed. Connectivity estimates from coherence, for example, can only be used to create undirected networks unless parameters relating to the anatomical structure can also be implemented to account for directionality (a possible approach of effective connectivity). Another consideration is whether to provide edge weights in the network. If weighted networks are desired, then the weights can be taken directly from the estimated measure. To create unweighted networks, a thresholding method can be used such that only connections above a threshold are considered for the reconstructed network. Conversely, connectivity values below the threshold are considered insignificant and are not present in the network. Therefore, directed networks can be used to create undirected networks by removing the directionality present in directed networks, which can be useful when measuring certain characteristics of a network.

Once a network model is reconstructed from the measures of connectivity between brain sites, metrics from graph theory and network science can be utilized to further analyze it. These metrics can then be reinterpreted as characteristics of the connectivity behavior of the brain. Metrics that summarize the adjacency of a given node to all other nodes in the network fall under the category of centrality measures. Many different centrality measures exist, each providing a different perspective of the importance (or centrality) of a node in the network. A node may be important if it is adjacent to many other nodes, or may be important on a global scale, that is, important to the overall structure of the network. On the other side of the network analysis, measures such as small-worldness and clustering describe characteristics of the network as a whole. These measures quantify topological characteristics of the network, and may reflect the

overall functional behavior of the network and therefore the brain. In BCA, extensive

research has gone into the small-world nature of the brain network [23]-[25] as well as

its possible scale-free architecture [26].

In epilepsy research, brain connectivity analysis using EEG has recently become a

popular approach for epilepsy diagnosis, seizure prediction, and epileptic focus

localization, and has advanced the understanding of the functional behavior of the

epileptic brain. Using interictal scalp EEG recordings, knowledge of characteristics

derived from weighted functional networks has been shown to improve diagnostic

accuracy in children with partial epilepsy [27]. Furthermore, the overall connectivity

structure of the functional brain networks derived during resting state recorded scalp EEG

from patients with temporal lobe epilepsy seem to have noticeable differences compared

to healthy controls [28], a result that is also seen in resting state functional MRI (rsfMRI)

[23]. For focus localization, a significant portion of research has focused on the

functional behavior of the seizure onset zone. One research group found high correlation

between the seizure onset zone and increased information outflow in higher brain

frequency bands (β: $13 - 30Hz$; γ: $30 - 50Hz$) when measuring the connectivity of the

brain using DTF from EEG signals taken from the ictal periods of patients with neo-

cortical onset epilepsy, and more importantly, showed that graph measures can provide

information related to the seizure onset zone [29], which was supported some years later

when another group found similar results using a modified DTF function estimated from

a time-variant vector autoregressive model to develop the network, with increased out-

degree values associated with the ictal onset zone [30], [31]. Dynamic behavior of the

functional network during ictal events has also been studied in partial epilepsy, revealing

that connectivity patterns can be associated with finite, sequentially progressive brain states where the seizure onset zone is more isolated from the rest of the network at seizure initiation [32]. For a more in-depth review of the functional brain connectivity analysis and graph theory in epilepsy research, we refer to [33] for an overview of the topic, to [34] using EEG and to [35] using rsfMRI.

CHAPTER 3

METHODOLOGY

3.1 <u>Materials</u>

For this research, all EEG data analyzed comes from the EEG database of the

Brain Dynamics Laboratory at Louisiana Tech University. The EEG data were obtained

from patients diagnosed with temporal lobe epilepsy (TLE) who were admitted to an

epilepsy monitoring unit (EMU) for Phase II monitoring in order to determine the

location of their seizure onset zone. Every patient used in this research had a minimum of

four clinical seizures recorded during their stay at the EMU. Strip electrodes on the

cortex and needle electrodes near the hippocampus were surgically implanted in a

stereotactic fashion. The data originated from two different EMUs: Shands Hospital in

Gainesville, Florida (electrode montage A) and Barrow Neurological Institute in Phoenix,

Arizona (electrode montage B). EEG data from Shands Hospital were recorded with a

200Hz sampling frequency, and the data from Barrow Neurological Institute were

recorded with a sampling frequency of 400Hz. All data are currently stored using the

European Data Format, a common format used to exchange and store multichannel

biological signals. Figure 3-1 shows the placement of electrodes for the two montages as

well as 10 seconds of multichannel EEG signal taken from 1 second prior to 9 seconds

after seizure initiation. Table 3-1 provides patient data relevant for this research.
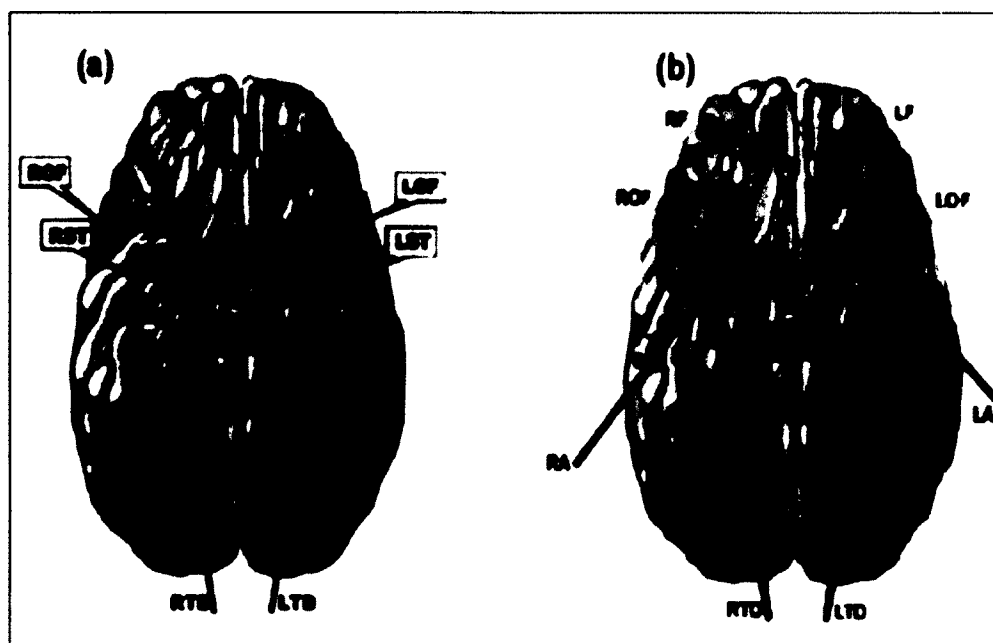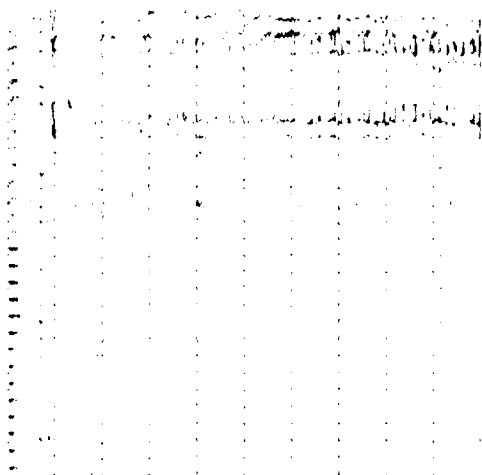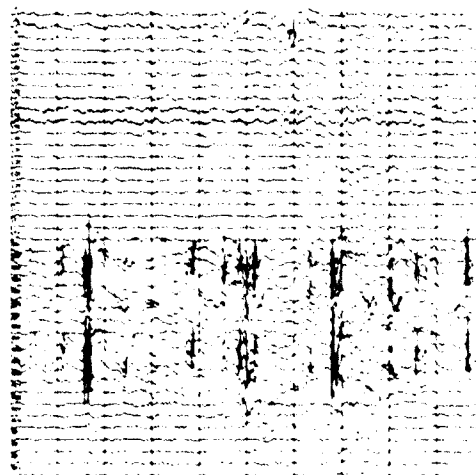
Figure 3-1: Top panel: Intracranial electrode montages that were used for the iEEG monitoring. EEG montage A on the left with 28 electrodes from four electrode strips (four electrodes per strip) on the left/right orbitofrontal (LOF/ROF) and left/right subtemporal (LST/RST) brain regions and two left/right temporal depth (LTD/RTD) 1-dimensional electrode arrays (six electrodes per array) inside the hippocampus. Montage B on the right with 64 electrodes from four electrode strips (eight electrodes per strip) in the left/right frontal (LF/RF) and left/right orbitofrontal (LOF/ROF) regions, and four depth 1-dimensional electrode arrays (eight electrodes per array) in the amygdala and temporal lobe (LA/RA) and hippocampus (LTD/RTD). For all depth electrode arrays, contact #1 is the most anterior one and for the strip electrodes the most mesial one. Bottom panel: Two examples of EEG recordings around seizure onset by montage A (left) from patient P7 (28 electrodes used), and montage B (right) from patient P2 (40 out of 64 electrodes were actually used in this recording).

TABLE 3-1: PATIENT INFORMATION

Patient	Electrode Setup	iEEG Recording Duration (days)	Subclinical Seizures Analyzed	Clinical Seizures Analyzed	Number of Seizures Analyzed	Number of Electrodes Utilized	Clinically Determined Focus/Foci
P1	B	~2	0	26	26	36	Left Amygdala (LA)
P2	B	~1.4	2	5	7	40	Right Amygdala (RA) Right Hippocampus (RTD)
P3	A	~11.7	0	6	6	28	Right Hippocampus (RTD)
P4	A	~3.6	0	23	23	28	Right Hippocampus (RTD)
P5	A	~13.9	6	8	14	28	Right Hippocampus (RTD)
P6	A	~3.5	0	4	4	28	Right Hippocampus (RTD)
P7	A	~6.5	17	5	22	28	Left Subtemporal (LST) Left Hippocampus (LTD)
P8	A	~6	10	9	19	28	Right Hippocampus (RTD)
P9	A	~0.75	0	6	6	28	Left Hippocampus (LTD)

3.2 Preprocessing

Due to the quality of the signals obtained using intracranial EEG monitoring,

minimal prepossessing was required. No filtering was performed on the data, but if an

EEG channel was found to have a low quality recorded EEG signal in a given patient,

that channel as well as the contralateral one were removed prior to analysis. In this case, a

total of four channels were removed from patient P1. Also, the recordings from the

Barrow Neurological Institute were downsampled to 200Hz to keep them consistent with

the data from Shands Hospital. Lastly, seizure times were obtained from the de-identified

clinical reports written by the attending physicians that were provided with the EEG data.

3.3 Time Series

EEG data represents the potential difference between two electrodes over time,

and therefore can be considered a realization of a time series process which can be

modeled using statistical techniques from time series analysis. In order to model EEG

data as a stochastic process using classical time series techniques the data must be

stationary. In general, if $\{X_t\}$ is a stochastic process where $F_X(x_{t_1+\tau}, \ldots, x_{t_n+\tau})$ represents

the cumulative distribution function of the joint distribution function of $\{X_t\}$ for times

$t_1, \ldots, t_n$, then $\{X_t\}$ is a strictly stationary stochastic process if $F_X(x_{t_1+\tau}, \ldots, x_{t_n+\tau}) =$

$F_X(x_{t_1}, \ldots, x_{t_n})$ for all $t_1, \ldots, t_n$ and integer τ. Simply put, the stochastic process $\{X_t\}$ is a

strictly stationary process if the joint probability distribution of $X_1, \ldots, X_t$ does not change

when the process is shifted by any integer τ. A weaker definition of stationarity exists,

which only requires the time series process to remain constant over time for the first and

second statistical moments. In this case, a process is called second-order stationary (or

weakly stationary) if the process maintains constant mean and autocovariance for any lag

τ such that

$$E[X_t] = \mu \tag{3.1}$$

and

$$Cov(X_t, X_{t+\tau}) = Cov(X_0, X_\tau) \tag{3.2}$$

where $E[X_t]$ represents the expected value of X_t such that $E[X_t] = \int_{-\infty}^{\infty} x(t) f_X(t) dt$.

The previous definitions of stationarity are defined for univariate time series. For

the case of multivariate time series, stationarity is satisfied if each of the univariate

signals of the multivariate process is stationary. One notable time series process, called

the white noise process, is defined as a sequence of independent, identically distributed

random variable $\{e_t\}$. White noise is characteristically strictly stationary, and has the

quality that the autocovariance of the process is equivalent to the variance of $\{e_t\}$, and the

covariance at any nonzero lag is zero. White noise are not themselves very interesting, but are very important for constructing many useful models.

Assuming that a given time series satisfies at least second-order stationarity, the series may be modeled using one of many models derived from a general linear process. A general linear process (GLP), $\{Y_t\}$, is a stationary time series process which can be represented as a weighted linear combination of present and past white noise terms such that

$$Y_t = e_t + \sum_{i=1}^{\infty} \psi_i e_{t-i}. \tag{3.3}$$

For the above equation to have meaning and allow for a reasonably manageable model, the coefficients of the process should satisfy the condition that

$$\sum_{i=1}^{\infty} \psi_i^2 < \infty \tag{3.4}$$

which ultimately implies that the process is stationary. For this condition to be satisfied either a finite number of ψ coefficients can be nonzero, some sequence of ψ coefficients must exponentially decay towards zero, or some combination of these cases must occur.

One of the most common processes modeled in time series analysis is the autoregressive processes. An autoregressive process $\{Y_t\}$ of order p satisfies the equation

$$Y_t = e_t + \sum_{k=1}^{p} \phi_k Y_{t-k} \tag{3.5}$$

where the current value of Y_t is a linear combination of the p previous values plus a white noise term e_t, independent from the past values of Y_t, that accounts for the variance in the data that is not be explained by the previous values. For the case of multivariate time series such as multichannel EEG data, the autoregressive process for each individual time

series might not only take into account the past values of the individual time series, but also the past values of other time series in the multivariate process. Such a multivariate autoregressive process can be modeled using a Vector Autoregressive Model. Let $X(t) = [x_1(t), x_2(t), x_3(t), \dots, x_N(t)]'$ be an N-dimensional time series vector representing the recorded iEEG signals at N brain sites, where each vector component $x_i(t)$ denotes the iEEG signal recorded at the ith brain site. Then, a vector autoregressive model (VAR) of order p can be constructed for X as

$$X(t) = \sum_{k=1}^{p} B(k)X(t-k) + \epsilon(t) \tag{3.6}$$

where $B(k)$ is the model's $N \times N$ coefficient matrix at lag k, and $\epsilon(t)$ is the residual vector of the model following a multivariate Gaussian white-noise process if the EEG signal from each brain site is at least weakly stationary.

In order to develop a VAR model for the given set of time series, it is necessary to first determine the optimum model order p for the best fitting model. Several model selection criteria exist that may accomplish this task, but typically Bayesian Information Criterion is often considered the most accurate for this [36]. Formally, Schwarz Bayesian Information Criterion (BIC) is defined as

$$BIC = -2 \cdot \ln(\hat{L}) + k \cdot \ln(n) \tag{3.7}$$

where $\hat{L}$ is the maximum value for the likelihood function, k is the number of free parameters to be estimated, and n is the number of observations used to develop the model. The likelihood function is itself a function of the model parameters θ given the known data x and is equivalent to the probability of the obtaining x given the parameters θ, i.e. $L(\theta|x) = P(x|\theta)$. Furthermore, the number of free parameters depends on the

number of multivariate signals being modeled N and the model order size being tested p

such that $k = N^2 \cdot p$. The number of observations n is dependent on the number of

signals being modeled N and the number of time samples s being observed such that $n =$

$N \cdot s$. The primary idea behind BIC is that maximum likelihood values become larger as

the order of the model is increased, making for increasingly negative BIC values but is

counteracted by the punitive effects of $k \cdot \ln(n)$ since increasing the tested model order

increases k. This leads to a sequence of BIC values that behave as a function of tested

model orders p. Therefore, the best fitted model is derived by taking the model order p

which provides the smallest BIC value. For this research, it was desired to use a single

model order for all estimated time windows, so BIC was performed for several time

windows to determine which model order gave the smallest BIC value among the tested

samples.

Once the order of the model is selected, we proceed to estimate the model

coefficients of the VAR model. Many methods exist for estimating the model coefficients

such as ordinary least squares (OLS) and Yule-Walker estimation, however, many of the

classical techniques cannot handle adequately the statistical phenomenon of

multicollinearity. Multicollinearity is the phenomenon that occurs when model

coefficients in a multivariate dataset are highly correlated such that one variable can be

modeled as a linear combination of other variables in the model, which can relate to large

fluctuations in the estimation of model coefficients when small changes occur in the data.

To resolve this potential issue when estimating the VAR model coefficients, one solution

is to use a stepwise regression technique such as the Viera-Morf Method [37] with

unbiased covariance estimation, which has been found to provide the most accurate

model estimates compared to other model estimation techniques [38]. The method works

by first initializing forward and backward predictor matrices A and B so that

$$A_{0,0}^{-1} = \left[\sum_{i=1}^{T} y_i y_i^T\right]^{\frac{1}{2}} \tag{3.8}$$

$$B_{0,0}^{-1} = \left[\sum_{i=0}^{T-1} y_i y_i^T\right]^{\frac{1}{2}} \tag{3.9}$$

where y_i is the m-vector construction of the m signals at time i. Then, a for-loop from

$n = 0$ to sample size N initializes, which in one cycle

-computes the normalized errors generated from the forward and backward predictor

matrices

$$\epsilon_{n,t} = \sum_{k=0}^{n} A_{n,k} y_{t-k} \tag{3.10}$$

$$r_{n,t} = \sum_{k=0}^{n} B_{n,n-k} y_{t-k} \tag{3.11}$$

-estimates the normalized reflection coefficients used to generate the VAR coefficients

$$R_n^\epsilon = \sum_{t=n+1}^{T} \epsilon_{n,t} \epsilon_{n,t}^T \tag{3.12}$$

$$R_n^r = \sum_{t=n+1}^{T} r_{n,t-1} r_{n,t-1}^T \tag{3.13}$$

$$R_n^{\epsilon r} = \sum_{t=n+1}^{T} \epsilon_{n,t} r_{n,t-1}^T \tag{3.14}$$

$$\hat{\rho}_{n+1} = [R_n^\epsilon]^{1\backslash 2}[R_n^{\epsilon r}][R_n^r]^{-\frac{T}{2}} \tag{3.15}$$

-updates the normalized predictors P and Q such that

$$P_{n+1} = I - \rho_{n+1}\rho_{n+1}^T \tag{3.16}$$

$$Q_{n+1} = I - \rho_{n+1}^T\rho_{n+1} \tag{3.17}$$

-runs a nested for-loop from $k = 0$ up to $n + 1$ in order to update the forward and

backward predictor matrices

$$A_{n+1,k} = P_{n+1}^{-\frac{1}{2}}\left[A_{n,k} - \rho_{n+1}B_{n,n-k+1}\right] \tag{3.18}$$

$$B_{n+1,k} = Q_{n+1}^{-\frac{1}{2}}\left[B_{n,k} - \rho_{n+1}^T A_{n,n-k+1}\right] \tag{3.19}$$

and, lastly, n is incremented up by one step to complete a single loop in the algorithm.

Upon completion, the forward and backward predictors A and B give the same and

unique estimate of the power spectral matrix, thus producing a stable VAR model.

With the help of the modeling methodology described above we determine, based

on provided data, the existence or not of causal relations between the various signal

processes of the multivariate time series. As defined by Clive W.J. Granger, two signals

have a causal relation if the prediction of one signal is improved when knowledge of the

other signal is taken into account. Formally, let $\{A_t\}$ be a stationary stochastic process, U_t

be all the information in the universe up to time $t - 1$, let $U_t - B_t$ denote all information

in the universe, except that from process B_t, and let $\overline{A}_t$ represents any set $\{A_{t-j}|j =$

$1,2,\ldots,\infty\}$. Also, let $\sigma^2(A|B)$ be the variance of the error derived by predicting series A_t

using information from B_t. If $\sigma^2(A_t|U_t) < \sigma^2(A_t|\overline{U_t - B_t})$, then signal B_t is said to

cause signal A_t. Furthermore, if $\sigma^2(A_t|U_t) < \sigma^2(A_t|\overline{U_t - B_t})$ and $\sigma^2(B_t|U_t) <$

$\sigma^2(B_t|\overline{U_t - A_t})$, then each signal influences the other, and, in this case, there exists

feedback between the two signals. For example, assume a matrix Z composed of two

weakly stationary stochastic processes $Z = [X_t, Y_t]'$ are modeled using a vector

autoregressive equation of order $p = 1$ such that

$$Z(t) = \begin{bmatrix} a & b \\ c & d \end{bmatrix} Z(t-1) + \epsilon(t). \tag{3.20}$$

If the coefficient $b \neq 0$, then it may be said that there existed information in past values

Y_t that can be used to better predict the future values of X_t, and therefore Y_t causes X_t.

Using the same logic, if the coefficient $c \neq 0$, then X_t causes Y_t. Therefore, non-diagonal

entries of the coefficient matrix for the VAR model which are nonzero provide some idea

of the causal relationships that arise between stochastic processes. However, approaching

the problem from the time domain prevents the researcher from finding underlying

aspects of the causal relationship present in the data. First, the values of the non-diagonal

entries are not directly related to the strength of the causal relationship between two

signals. Second, weakly stationary processes, like EEG, often have oscillatory behavior,

and analyzing these processes in the frequency domain allows for linearly causal

relationships to be measured not only by their relative strengths but also at which

frequencies these causal relations arise. A spectral representation of these stationary

processes ultimately leads us to the causal connectivity measure used in this research, the

Generalized Partial Directed Coherence.

3.4 Generalized Partial Directed Coherence

For stationary process $\{Y_t\}$, the autocovariance of the signal at lag k, denoted γ_k,

measures the similarity in behavior of the signal Y_t with the signal Y_{t-k} and is defined as

$\gamma_k = Cov(Y_t, Y_{t-k}) = E[(Y_t - \mu_Y)(Y_{t-k} - \mu_Y)]$. The autocorrelation function, defined as

$\rho_k = \gamma_k/\gamma_0$, is a normalization of the covariance to values between -1 and 1. For ρ_k, 1

represents identical behavior occurring between the signal at the lag k, and -1 represents

exactly opposing behavior. For a multivariate time series $X(t) =$

$[X_1(t), X_2(t), X_3(t), ..., X_N(t)]^T$ where $E[X_i(t)] = 0$ for $i = 1, ..., N$, the autocovariance

and cross-covariances are given as functions of lag k using the covariance matrix $R(k) =$

$E[X(t)X^T(t - k)]$, and each element $r_{ij}(k)$ of the covariance matrix can be normalized

to a (auto or cross) correlation coefficient as

$$\rho_{ij}(k) = \frac{r_{ij}(k)}{\sqrt{r_{ii}(k)r_{jj}(k)}}. \tag{3.21}$$

Furthermore, the partial correlation, defined as the correlation between signals when

associations arising from the influence of other signals is excluded, comes from the

inverse of the covariance matrix $R(k)^{-1}$ which is normalized in the same manner as the

correlation coefficient. Both matrices have frequency-domain counterparts which allow

for spectral analysis of the multivariate process. Taking the Fourier Transform (FT) of the

covariance matrix $R(k)$ gives the spectral density matrix, denoted $S(f)$. The inverse

spectral density matrix $P(f)$ can be obtained directly from the inverse of $S(f)$ (i.e.

$P(f) = S(f)^{-1}$) or by taking the FT of the inverse covariance matrix. Normalizing the

elements of the spectral matrices $S(f)$ and $P(f)$ in the same manner used to create the

correlation coefficient give the measures known as coherence and partial coherence,

respectively.

For any VAR process, spectral analysis of the signal can also be performed by

taking the FT of the coefficient matrix of the VAR model such that

$$B(f) = \sum_{k=1}^{p} B(k)e^{-i2\pi fk}. \tag{3.22}$$

The spectral factorization theorem [39] allows the partial coherence matrix $P(f)$ to be written in terms of the Fourier Transformed coefficient matrix $B(f)$ as

$$P(f) = \bar{B}^H(f)\Sigma^{-1}\bar{B}(f) \tag{3.23}$$

where $\bar{B}(f) = I - B(f)$, H represents the Hermitian transpose (taken as the complex conjugated elements of the transposed matrix), and Σ^{-1} is the inverse of the covariance matrix of the white noise $\epsilon(t)$ taken from the VAR model. Note that Σ is treated as a diagonal matrix since the created model should not have remaining structural behavior residing in $\epsilon(t)$, and therefore the ith diagonal element of Σ^{-1} is $1/\sigma_i^2$. From here, the element-wise definition of the inverse spectral density between signals X_i and X_j is

$$P_{ij}(f) = \sum_{n=1}^{N} \frac{1}{\sigma_n^2} \bar{B}_{ni}^*(f)\bar{B}_{nj}(f) \tag{3.24}$$

which leads to the partial coherence between the signals X_i and X_j defined as

$$\Pi_{ij}(f) = -\frac{P_{ij}(f)}{\sqrt{P_{ii}(f)P_{jj}(f)}} \tag{3.25}$$

$$= -\sum_{n=1}^{N} \frac{\left(\frac{1}{\sigma_n}\right)\bar{B}_{ni}^*(f)}{\sqrt{P_{ii}(f)}} \frac{\left(\frac{1}{\sigma_n}\right)\bar{B}_{nj}(f)}{\sqrt{P_{jj}(f)}} \tag{3.26}$$

$$= -\sum_{n=1}^{N} \pi_{ni}^*(f)\pi_{nj}(f). \tag{3.27}$$

The element in the above equality $\pi_{nj}(f)$ contains the Generalized Partial Directed Coherence ($GPDC$) from signal X_j to signal X_i at frequency f and is defined as

$$GPDC_{j \to i}(f) = \pi_{ij}(f) = \frac{\left(\frac{1}{\sigma_i}\right)|\bar{B}_{ij}(f)|}{\sqrt{\sum_{n=1}^{N}\left(\frac{1}{\sigma_n^2}\right)|\bar{B}_{nj}(f)|^2}}. \tag{3.28}$$

Thus, through the decomposition of the (symmetric) partial coherence matrix $\Pi(f)$, an asymmetric matrix in the form of $GPDC$, π, is derived. This provides a measure of the directional influence of one signal onto another while excluding the influences generated by other signals. Furthermore, $GPDC$ has the properties that $0 \le |\pi_{ij}(f)|^2 \le 1$ and $\sum_{n=1}^{N} |\pi_{nj}(f)|^2 = 1$. Thus, the value π_{ij} is a normalized measure of the coupling from X_j onto X_i relative to the coupling from X_j to all other signals $X_{1,\dots,N}$ (including coupling to X_j itself) [21], [22], [40].

In Figure 3-3 an example of GPDC values is shown. Six channels of EEG data over a period of three seconds (Figure 3-2) are used, and GPDC value between each directional pair of signals is estimated for frequencies from 0Hz to 50Hz. Figure 3-3 shows the GPDC estimates with an exploded view of $GPDC_{5\to6}(f)$ for all estimated frequencies.
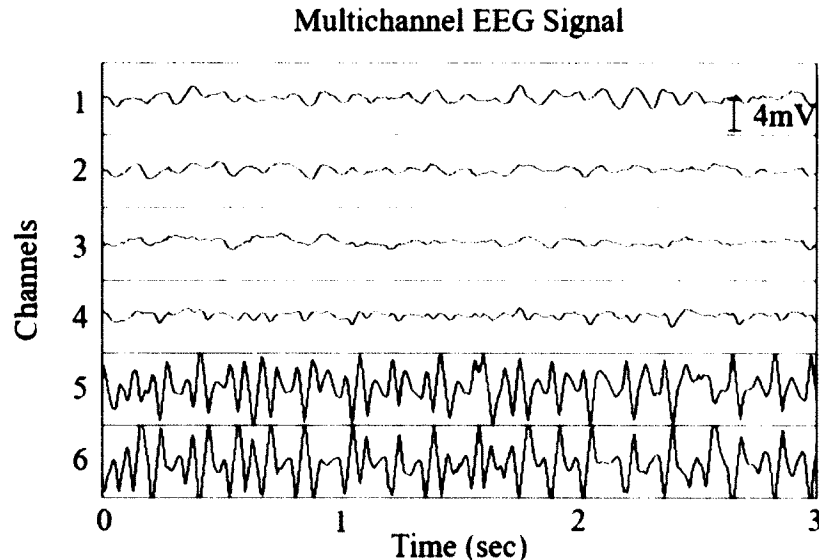
Figure 3-2: Six signals taken from multichannel intracranial EEG data.
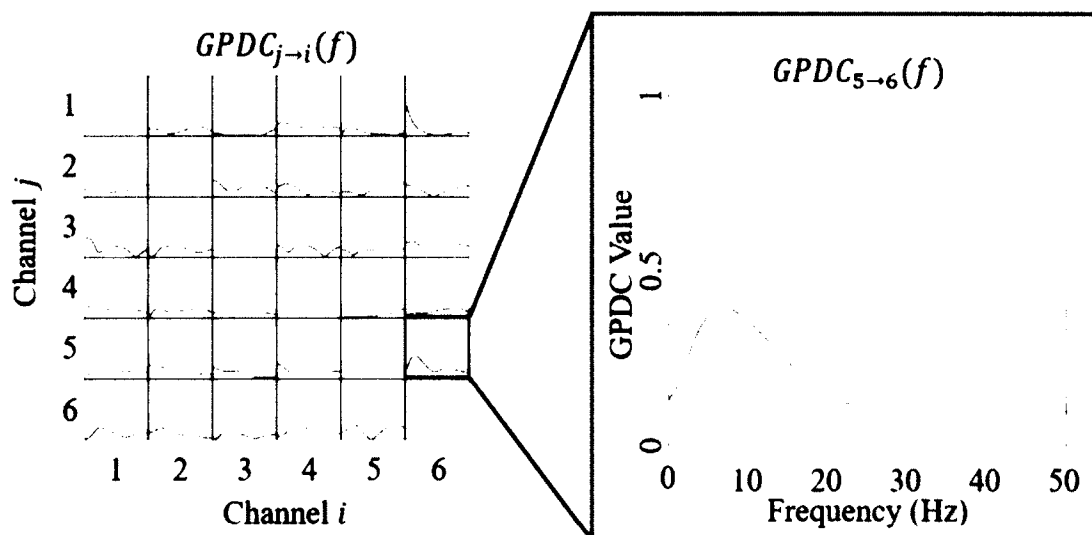
Figure 3-3: (Left Panel) GPDC estimated from signals shown in Figure 3-2. (Right Panel) Exploded view of the GPDC estimated from signal 5 to signal 6.

Ultimately, because generalized partial directed coherence measures the relative signal strength arising from one structure to another, the measure is treated as a spectral interpretation of Granger causality, and thus, in this research, is related to directional connectivity between brain structures. Compared to other popular connectivity measures, GPDC also has the advantage of measuring partialized coupling strengths between brain structures. In other words, GPDC measures the direct connectivity between pairs of brain structures while ignoring the common effects from other sources, thus abating values of coupling strength between brain structures that are connected indirectly. However, the inverse spectral density matrix $P(f)$ from which GPDC is derived does not have a clear relationship to the physiological behavior in the brain. Therefore, a technique is required that would allow for the utilization of the direct coupling values of GPDC and for only the significant connections to be considered important and used for further analysis.

3.5 Surrogate Data Analysis

Surrogate data analysis is a statistical technique used in this research to determine which directional connectivity interactions are considered statistically significant based on the GPDC values of the given data. Surrogate data analysis is a proof by contradiction method used commonly to determine if a time series has non-linearity, but has been repurposed to test if the measured GPDC values are statistically different from the distribution of simulated GPDC values. Since the distribution of simulated GPDC values is not directly known, Monte Carlo simulation methods can be utilized on the time series to generate M surrogate time series which are used to generate a probability distribution for each GPDC values [41]. The Monte Carlo simulations used to generate surrogate data can be used to determine if a feature of the time series is significant. For our study, we assume that we have the null hypothesis

$$H_0: GPDC_{j \to i}(f) = 0. \tag{3.29}$$

To generate the M surrogate data sets, we used the improved amplitude-adjusted Fourier Transform (iAAFT) algorithm [42], which provides randomized time series data that share the same amplitude distribution and power spectrum with the original time series. The algorithm uses an iterative process performed individually to each time series in the multivariate process. First, the power spectrum of $X_i(t)$ is estimated using the squared amplitudes of its Fourier transformation of $X_i(t)$ as

$$X_i(f)^2 = \left| \sum_{t=1}^{N} X_i(t) e^{\frac{i2\pi ft}{N}} \right|^2. \tag{3.30}$$

Then, the order of the values in $X_i(t)$ are randomly selected in time without replacement to generate $X_i^{(0)}(t)$, a random shuffling of the original time series. By shuffling $X_i(t)$, the

phase angles associated with each frequency $X_i^{(0)}(f)$, denoted $\theta_i^0(f)$, are randomized.

However, the power spectrum of $X_i^{(0)}(t)$ needs to be adjusted so that it matches the

power spectrum of $X_i(t)$. This is accomplished via an iterative process where a new

signal $X_i^{q,0}(t)$ is generated by taking the inverse Fourier transformation of the power

spectrum $X_i(f)$ with phase angles $\theta_i^q(f)$. Then, a new sequence $X_i^{q,1}(t)$ is generated by

replacing the values $X_i^{q,0}(t)$ with the rank-ordered equivalent values from $X_i(t)$ (i.e. the

lowest value of $X_i^{q,0}(t)$ is replaced by the lowest value in $X_i(t)$, the highest value of

$X_i^{q,0}(t)$ is replaced by the highest value in $X_i(t)$, etc). Finally, new phase angles $\theta_i^{q+1}(f)$

are estimated from $X_i^{q,1}(t)$. This iterative process terminates when either $q = 1000$

iterations are completed or the rank-order of $X_i^{q,1}(t)$ is equivalent to the rank order of

$X_i^{q,0}(t)$. Through the iAAFT algorithm, a random time series process is generated that

maintains similar power spectra and probability distribution to $X_i(t)$ but different phase

angles for each frequency component. Furthermore, because the iAAFT algorithm is

performed for each time series in the multivariate process independently, no causal

relationship between the time series should remain since any phase relationships should

be destroyed. Therefore, GPDC values estimated from the generated surrogate dataset

will produce estimates corresponding to unrelated (no underlying causal relationship)

pairs of signals. Figure 3-4 provides an example of a set of time series data that is run

through the iAAFT algorithm to provide surrogate time series. As shown in the two right

panels, the power spectrum of the surrogate data remains mostly the same as the power

spectrum of the original time series.
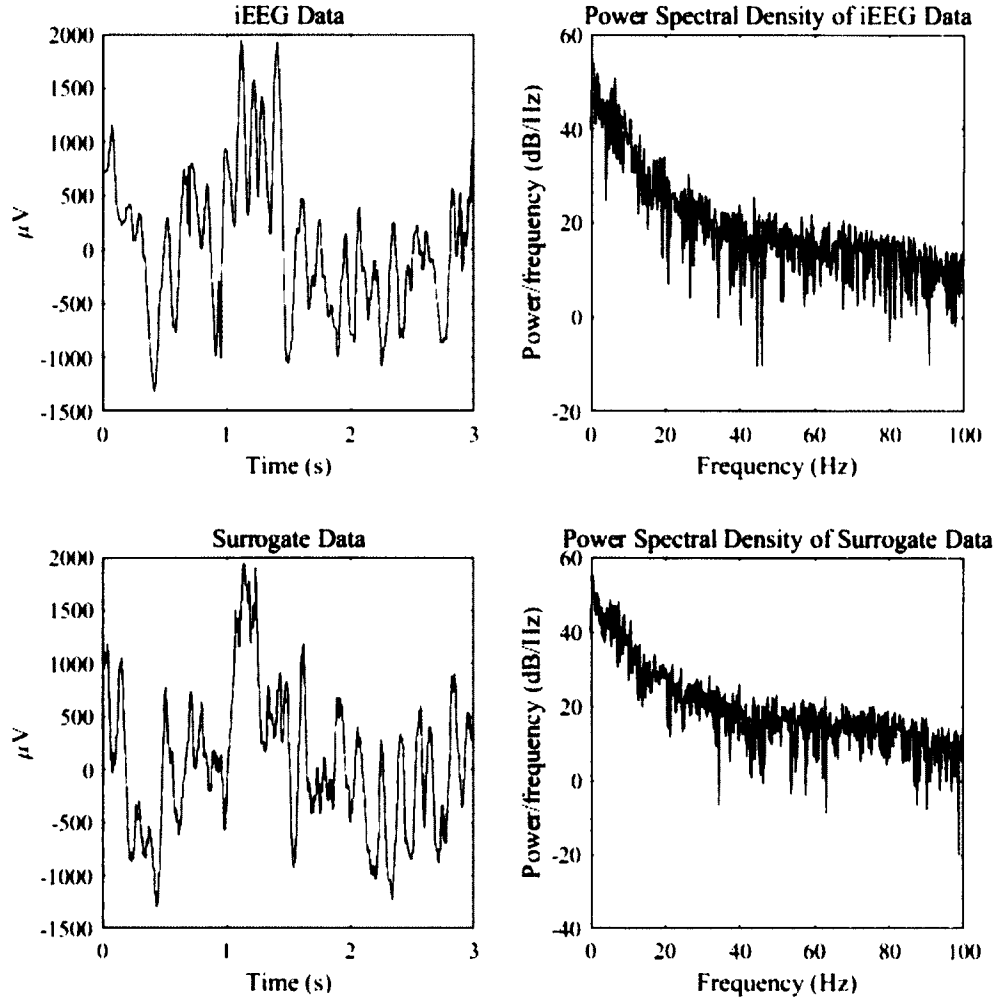
Figure 3-4: Example of surrogate data output from iAAFT.

For $M = 30$ surrogate datasets, GPDC values are estimated and stored for each

$GPDC_{j \to i}(f)$ from signals X_i and X_j as $\pi_{ij}^m(f), m = 1,2, ..., M$. The mean $\mu_{ij}(f)$ and

standard deviation $\sigma_{ij}(f)$ are estimated such that $\mu_{ij}(f) = \frac{1}{M}\sum_{m=1}^{M} \pi_{ij}^m(f)$ and $\sigma_{ij}^m(f) = $

$\frac{1}{M-1}\sum_{m=1}^{M} \left(\pi_{ij}^m(f) - \mu_{ij}(f)\right)^2$, respectively. Assuming that the GPDC values follow a

normal distribution, statistical hypothesis testing is performed with the null and

alternative hypotheses set as:

$$H_0: \pi_{ij}(f) = \mu_{ij}(f) \tag{3.31}$$

$$H_1: \pi_{ij}(f) > \mu_{ij}(f), \tag{3.32}$$

and is tested using a critical value $c_{ij}(f) = \mu_{ij}(f) + 1.96\sigma_{ij}(f)$ which provides an $\alpha = 0.05$ significance level (5% chance of Type I error, i.e. rejecting a true H_0). If $\pi_{ij}(f) > c_{ij}(f)$, then there is sufficient deviation from the mean to reject H_0, and, therefore, a causal relationship from signal $X_j(f)$ to $X_i(f)$ is deemed to exist.

Because GPDC values are limiting in their ability to clearly describe physiological behavior of the brain, further analysis of the relationships arising between brain regions is considered using the above hypothesis testing in order to identify the presence of a significant causal connection between brain regions. In this manner, a new matrix $A(f) = [a_{ij}]_{i,j=1,\ldots,N}$ can be derived based on the above hypothesis test such that

$$a_{ij} = \begin{cases} 1 & Reject\ H_0 \\ 0 & Do\ Not\ Reject\ H_0 \end{cases}. \tag{3.33}$$

This derived matrix $A(f)$ is a binary adjacency matrix describing the significant causal connections that occur between brain regions when observing a given epoch of time series data (further discussion about adjacency matrices is given in the Section 3.8).

Figure 3-5 represents the entire surrogate data analysis process as a flowchart using two EEG signals over a three second epoch. The directional connection from signal 2 to signal 1 is estimated throughout the figure for integer frequencies from 0Hz to 50Hz.
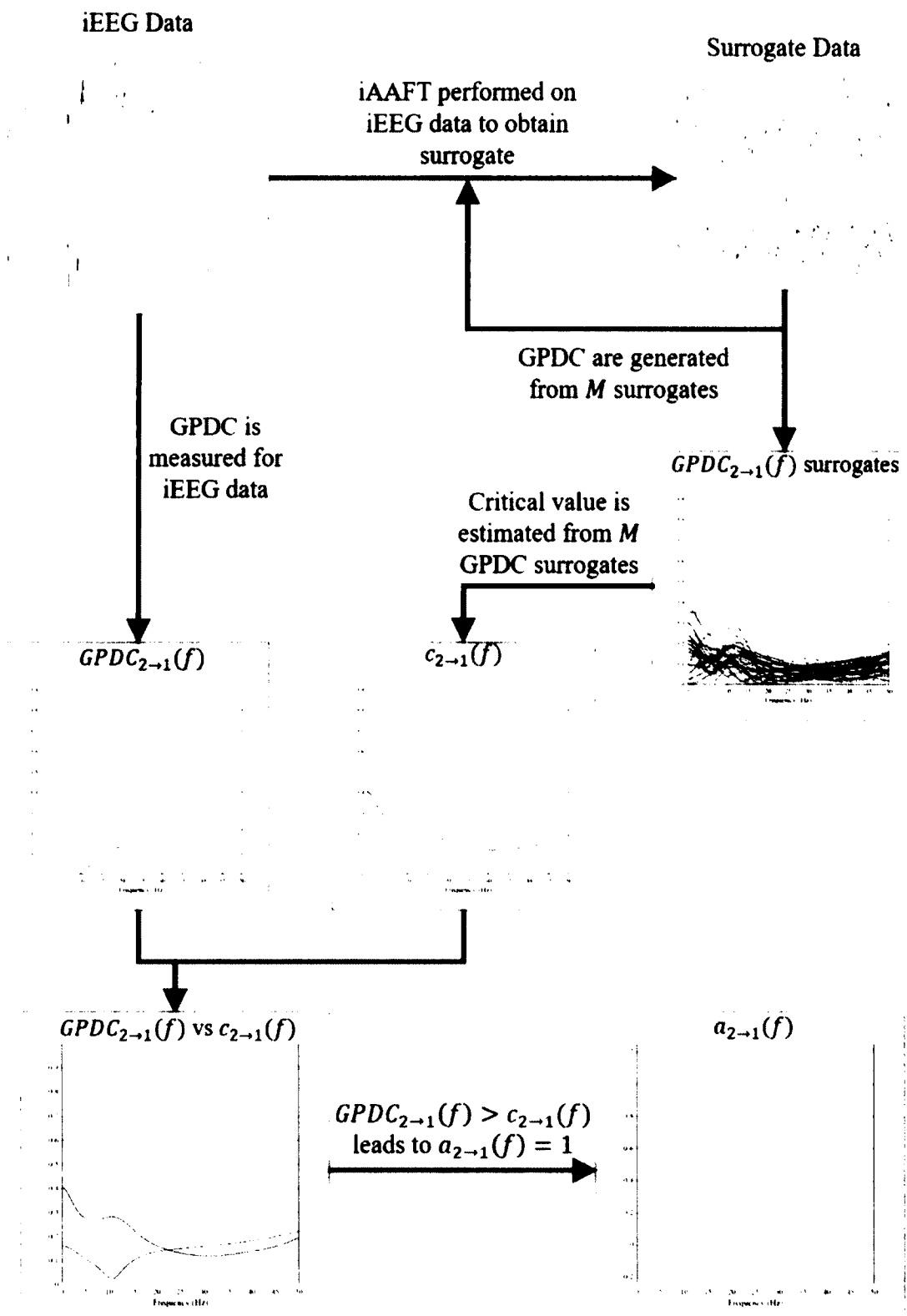
Figure 3-5: Flowchart of surrogate data analysis to find significant causal connections from channel 2 to channel 1 across frequencies (0Hz to 50Hz).

3.6 Graph Theory

Graph Theory is the study of a set of discrete objects and the relationships that exist between these objects. In order to discuss graphs in the context of brain networks, it is important to define basic terminology required to understand how the brain networks will be analyzed. To start, a graph $G = (V, E)$ is a mathematical structure consisting of two sets V and E. The set V contains the elements called nodes (or vertices) and represent the discrete objects to be studied, which in our case are the brain regions surrounding electrode recording sites, and the elements in the set E are called edges and are comprised of pairs of node elements which represent the endpoints of the edges. Considering the relationship between nodes and edges, two nodes are called adjacent if they are joined by a common edge, and a node v is incident to an edge e if it is an endpoint of e, and also e is therefore incident on v.

Although the set of nodes V in graph G are consistent across different types of graphs, by redefining the rules for what may exist in the edge set E, different types of graphs may be studied. For example, if the edge set is allowed to have repeated but unordered node pairs, meaning multiple edges can join two nodes, or node pairs where each element is the same node, known as self-loops, then the type of graphs studied are called multigraphs. When these types of node pairs are not allowed in the edge set, then the type of graphs studied are called simple graphs, which may also be called undirected graphs. Furthermore, if the edge set is defined such that the node pairs are ordered with the first node representing the beginning, or tail, of the edge and the second node designating the end, or head, of the edge, then the edges are called directed edges, and the resulting graph is called a directed graph (or digraph). Lastly, the edges of the graph can

have numerical values associated with each edge and are said to be weighted. Likewise, one can also place weights on the nodes or on both nodes and edges. Typically, the use of weighted networks is dependent on the phenomena that is being studied. For example, a graph representing a road map may find it useful to use weighted edges where the weight reflects the distance between nodes, which could represent cities. Graphs where the weight of the edge is not necessary, or the researcher wishes to only see where edges are present in the graph, may simply use binary graphs where the presence on an edge between nodes is given a value 1 and no edge presence is given a value 0.

Figure 3-6 is a flowchart showing the generation of the brain connectivity network starting with a projection of the iEEG electrodes onto the underside of a brain producing six iEEG signals over a three second epoch. The signal is analyzed using GPDC, and surrogate data analysis is utilized to determine which directional connections are significant at integer valued frequencies from 0Hz to 50Hz. In this visualization, three connectivity networks from 5Hz, 15Hz, and 50Hz are projected back onto the electrodes on the brain with blue edges representing bidirectional connections and red edges being unidirectional edges. An edge joining two nodes represents a connection between the corresponding brain regions.
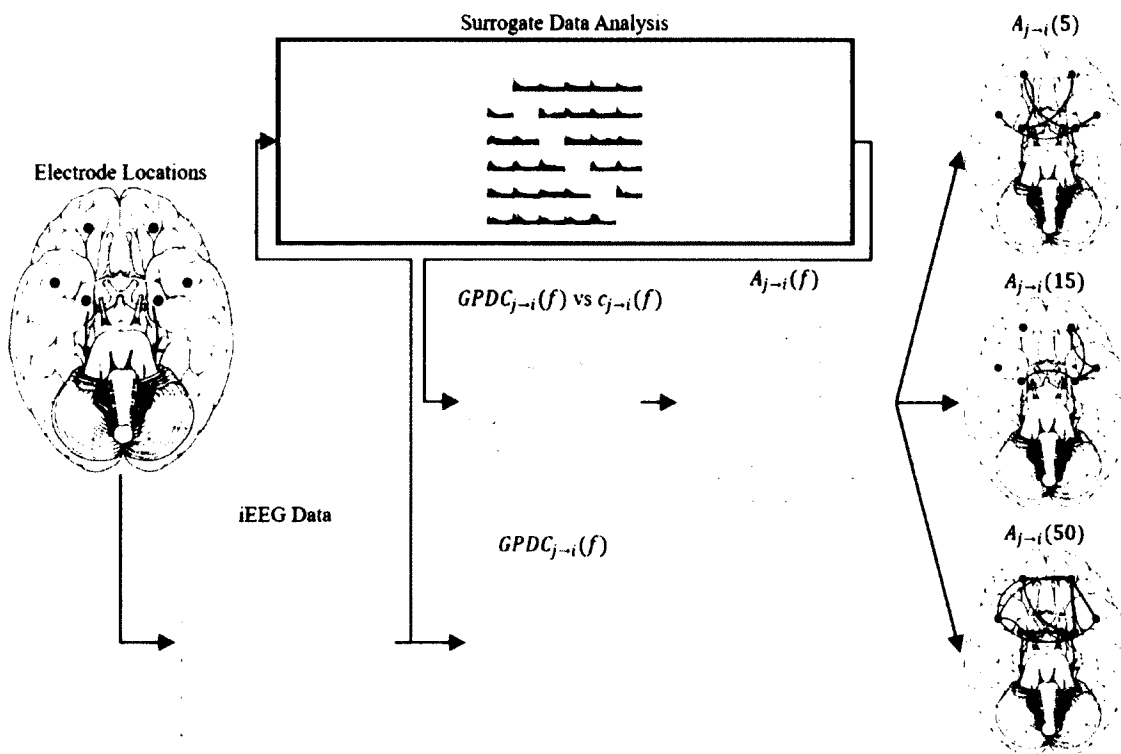
Figure 3-6: Flowchart of the network creation process.

3.7 Fundamental Graph Characteristics

A multitude of measures exists that measure characteristic qualities of the graph.

The three fundamental graph characteristics for comparison of a single node to other

nodes are degrees, walks, and paths. It is important to note that if a graph $G_1 = (V, E_D)$

consists of two nodes $V = \{v_1, v_2\}$ and directed edge set $E_D = \{(v_1, v_2), (v_2, v_1)\}$ and

graph $G_2 = (V, E_U)$ has the same vertex set V but an undirected edge set $E_U = v_1 v_2$ with

both edge sets having equivalent weighted edge relations, all three of the above

mentioned measures (degrees, walks, and path) will be similar. However, the definitions

for these characteristics are slightly altered with respect to the type of edge set being used

(directed or undirected). For example, the degree of a node v is the number of edges

incident to v, but for directed graphs, this definition of degree for each node v is

separated into in-degree, the number of edges directed towards v, and out-degree, the number of edges directed away from v. Relative to a graph G, in order to travel from one node to another, one must travel a sequence of nodes and edges. Formally, this traversal from node v_j to node v_i is referred to as a walk and is written as an alternating sequence $W_{ij} = \langle v_j, e_{m_1 j}, v_{m_1}, ..., e_{m_s m_{s-1}}, v_{m_s}, ..., e_{i m_s}, v_i \rangle$ where v_{m_s} is the mth node of the graph traversed at the $s \in \{1, ..., S\}$ step of the sequence. From this definition, walks allow for any node to be traversed more than once as long as there exists an edge that permits the traversal to occur, and multiple sequences W_{ij} may exist that satisfy the conditions for a walk. Furthermore, the length of a walk W_{ij} is equal to the number of edge-steps S in the sequence. Paths are another traversal upon the graph G, but include more stringent restrictions as to how G can be traversed. A path P_{ij}, by definition, is a walk from node v_j to node v_i where no node in the sequence can repeat. Note also that a cycle is a graph where the removal of any edge is a path. Like walks, multiple paths may exist that connect v_j to v_i, and the length of a path is the number of edge steps in the sequence. For paths, one additional measure of importance is the geodesic distance, or shortest path length, defined as the length of the path P_{ij} between nodes v_i and v_j with the fewest number of edge-steps S. Note that more than one path P_{ij} may exist having the shortest path length between v_i and v_j [43].

3.8 Adjacency Matrix

Because of the abstract nature of graphs, structural characteristics of the graph can be difficult to calculate using the set or graphical representations. Fortunately, simple directed and undirected graphs have an efficient representation known as the adjacency

matrix. For a given graph $G = (V, E)$ with node set $V = \{v_1, ..., v_N\}$, an adjacency matrix

A is an $N \times N$ (square) matrix whose elements a_{ij} represent a value of the edge from v_j

to v_i. The elements a_{ij} can have any numerical value if it represents a weighted graph, or

can be 0 or 1 if the network is binary, showing the absence or presence of an edge from

v_j to v_i, respectively. Furthermore, matrix symmetry provides insight into the directional

characteristics of the network. If the adjacency matrix is asymmetric, then it represents a

directed graph, while symmetric matrices are used for undirected graphs. As mentioned

above, the adjacency matrix used in this research represents the network of significant

causal connections that arises between brain networks at given points in time for

observed frequencies, as determined via GPDC and surrogate data analysis, with

$a_{ij}(f) = 1$ if a significant connection is observed from site j to site i, and $a_{ij}(f) = 0$

otherwise. Of course, it is possible to convert directed networks into undirected networks

by making the adjacency matrix symmetric, which is accomplished by setting $a_{ji} = 1$ if

and only if $a_{ij} = 1$. In this case, the edges of the network represent the presence of a

significant connection, or coupling, between sites i and j. Figure 3-7 shows the

relationship between a directed graph (top) generated from GPDC at 50Hz (see

Figure 3-6) and its associated adjacency matrix. By making the directed adjacency matrix

symmetric, an undirected graph (bottom) is produced.

Directed

$$A_{j\to i}(50) = \begin{pmatrix} 0 & 1 & 0 & 1 & 1 & 1 \\ 1 & 0 & 0 & 0 & 0 & 0 \\ 0 & 1 & 0 & 0 & 1 & 0 \\ 0 & 1 & 0 & 0 & 1 & 1 \\ 1 & 0 & 1 & 0 & 0 & 1 \\ 0 & 0 & 0 & 0 & 1 & 0 \end{pmatrix} j$$

Undirected

$$A_{j\to i}^{U}(50) = \begin{pmatrix} 0 & 1 & 0 & 1 & 1 & 1 \\ 1 & 0 & 1 & 1 & 0 & 0 \\ 0 & 1 & 0 & 0 & 1 & 0 \\ 1 & 1 & 0 & 0 & 1 & 1 \\ 1 & 0 & 1 & 1 & 0 & 1 \\ 1 & 0 & 0 & 1 & 1 & 0 \end{pmatrix} j$$
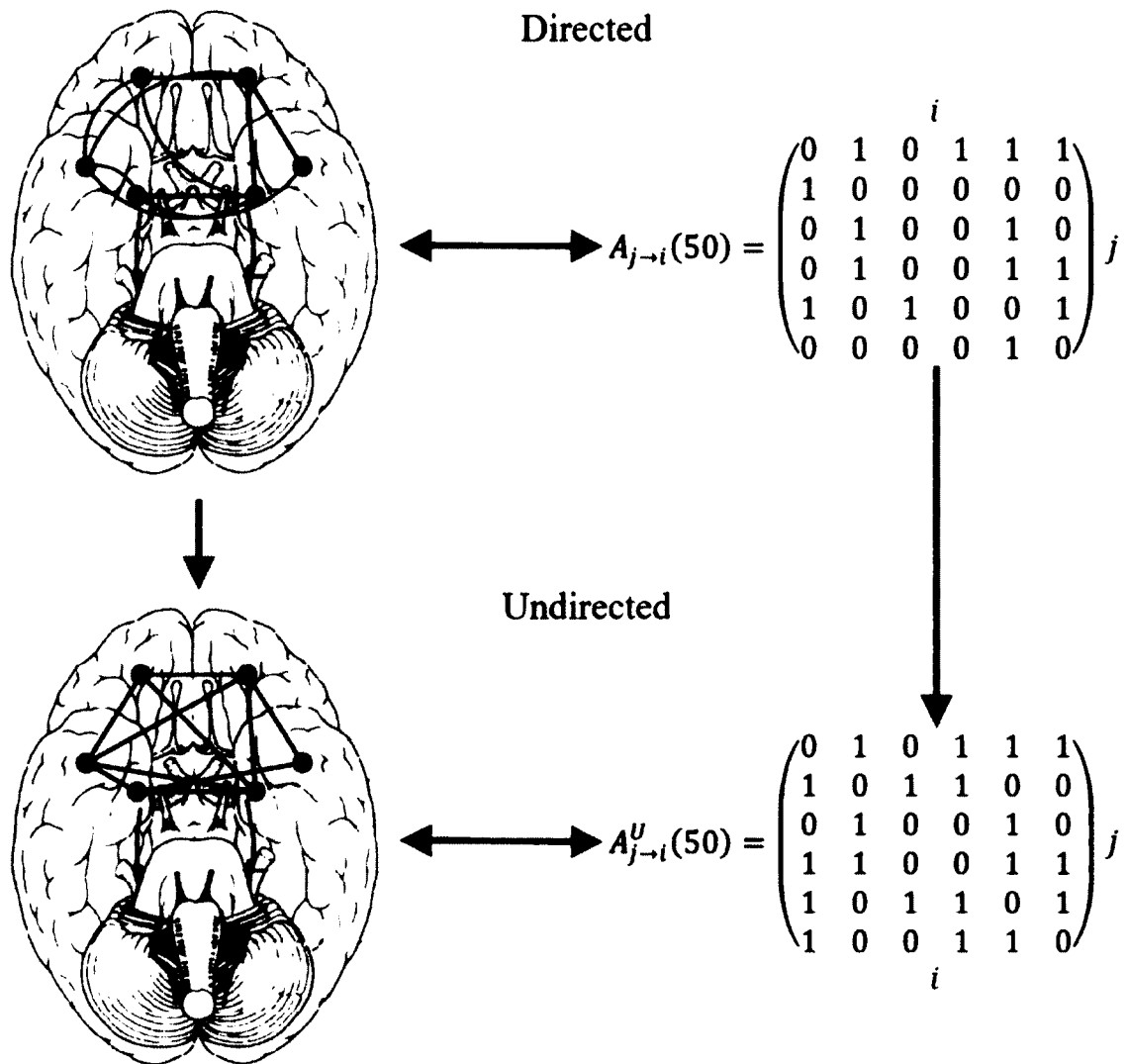
Figure 3-7: Directed and undirected graphs and their respective adjacency matrices. The undirected graph is created by generating a symmetric matrix from the directed graph's adjacency matrix.

Lastly, two operations performed upon adjacency matrices should be noted. First, the transpose of an $m \times n$ matrix A is the $n \times m$ matrix A^T created by interchanging the rows and columns of A such that element a_{ij} replaces element a_{ji} for all $i \in 1, \ldots, m$ and $j \in 1, \ldots, n$. For directed adjacency matrices, this becomes equivalent to changing the direction for each edge present in the graph. Since undirected adjacency matrices are square and symmetric, $A^T = A$ and no change occurs. Second, the number of unique

walks of length k between vertices i and j can be found by taking the adjacency matrix to

the kth power (A^k). For directed graphs, the walks must follow the direction of the edges,

and in that case the (i, j) element of the matrix A^k is the number of unique directed walks

of length k starting at node j and ending at node i [44].

3.9 Centrality

The significant part of network science is the study of the topological

characteristics of a graph in order to better understand the underlying system which it

represents. Although network science stems from the field of Graph Theory, slightly

different terminology has been adopted in the literature for the exact same concepts.

From here on out, the term "network" will be used in place of "graph", and the terms

"edge" and "connection" will be used interchangeably to weave together the concepts of

edges joining adjacent nodes in graphs and causal connections between EEG signals

constructing brain networks.

One topological characteristic of networks, centrality, measures relative

importance of each node in the network based on how it is joined to other nodes in the

network. In our research, the type of centrality most often associated with the

epileptogenic focus is unknown, so multiple centrality measures were estimated for each

node in the estimated networks. A total of seven different centrality measures were

estimated for both directed and undirected networks: Degree centrality [45], Eigenvector

centrality [46], PageRank centrality [47], Hyperlink Induced Topic Search (HITS) [48],

Katz Centrality [49], Harmonic centrality [50], and Betweenness centrality [51]. For

directed networks, centralities can be described with respect to the edge coming into the

node (inward centralities) or the edges coming from a node (outward centralities). For the

sake of consistency, when both element-wise and matrix equations clearly define the given centrality measure, the matrix equation form will be used. When using matrix equations, the vector $x = [x_1, x_2, \dots, x_N]^T$ where each x_i will represent the given centrality values for each node $i \in \{1, \dots N\}$ in the network, which is represented via the $N \times N$ adjacency matrix A. Lastly, both undirected centrality measures and inward centrality measures can be defined simultaneously using the same matrix equation; outward centrality measures, however, are defined slightly different, using the transposed adjacency matrix A^T.

3.9.1 Degree Centrality

Degree centrality is synonymous with the measure degree mentioned in Section 3.7 and is considered the most fundamental centrality measure, with the degree of a node being equal to the number of edges incident to that node, with in-degree defining the number of edges coming into a node, and out-degree centrality being the number of edges coming from a node. The matrix equations for in-degree (degree) and out-degree are written as

$$x = A1 \tag{3.34}$$

and

$$x = A^T1 \tag{3.35}$$

respectively, with 1 being the unitary vector of length N, which equates to taking the sum of the rows of the adjacency matrix A for in-degree (degree) and sum of the columns of A for out-degree.

3.9.2 Eigenvector Centrality

Eigenvector centrality measures a node's importance in the network by accounting for the importance of the nodes to which the given node is connected. The equation for eigenvector centrality is the exact same equation used to determine eigenvalues and eigenvectors associated with a given matrix where

$$Ax = \lambda x, \tag{3.36}$$

where A is the adjacency matrix, x is the vector estimating the eigenvector centrality of each node, and λ is the largest dominant (magnitude) eigenvalue associated with its given eigenvector. For undirected networks, a node has high eigenvector centrality if it is connected to many other nodes or is connected to a few nodes that are themselves connected to many nodes. Similarly, in directed networks, a node has high inward (outward) eigenvector centrality if it has edges coming from (going to) nodes with high inward (outward) eigenvector centrality. In other words, the eigenvector centrality of a given node is proportional to the eigenvector centrality of the nodes to which it connects. Like out-degree centrality, outward eigenvector centrality is found by transposing the adjacency matrix A and solving the equation $A^T x = \lambda x$ for x using the largest magnitude eigenvalue λ.

3.9.3 Katz Centrality

Katz centrality, developed by Leo Katz in 1953 for social network analysis, measures node importance based on the total number of possible walks across the graph in which the given node initiates or terminates, and typically provides results that are similar to eigenvector centrality. The main idea of the measure is that the number of possible walks of length k that exists between two nodes in the network is related to how

much those two nodes interact, but longer walks should occur with lower probability.

This creates a type of "communication matrix" C that describes the interrelatedness of

two nodes such that

$$C = I + \sum_{k=1}^{\infty} \alpha^k A^k = (I - \alpha A)^{-1}. \tag{3.37}$$

Therefore, the Katz centrality of the nodes x for the adjacency matrix A is defined

as

$$x = (I - \alpha A)^{-1} \mathbf{1} \tag{3.38}$$

where I is an identity matrix, $\mathbf{1}$ is a unitary vector, and α is an attenuation factor

arbitrarily chosen such that $\alpha < \left(\frac{1}{\lambda}\right)$, where λ is the largest dominant eigenvector of A.

Hence, the Katz centrality of node i is found by summing the elements in row i of the

communication matrix C.

3.9.4 PageRank Centrality

Among all of the centrality measures used in this research, PageRank centrality is

the most recently developed. The centrality measure is used by Google for their web

ranking technology, and considers user behavior when traversing web pages, assuming

that a user may reach a web page via hyperlinks (edge traversals) or by entering a URL

(random leaps to different nodes). The equation for PageRank centrality is

$$x = (I - \alpha A D^{-1})^{-1} \mathbf{1} = D(D - \alpha A)^{-1} \mathbf{1} \tag{3.39}$$

where I, A, and $\mathbf{1}$ are defined as in Katz Centrality, D is a diagonal matrix with diagonal

elements $D_{ii} = \max(k_i^{out}, 1)$ where k_i^{out} is the out-degree of node i, and the attenuation

factor α is chosen to be less than the largest eigenvalue of $A D^{-1}$. Note that a typically

used value for the attenuation factor is $\alpha = 0.85$.

3.9.5 The Hyperlink Induced Topic
Search (HITS) Algorithm

When applied to directed networks, all of the previous centrality metrics consider

a given node to have high centrality under similar logical reasoning. That is, a node has

high inward (outward) centrality if it either has many edges to (from) that node or that

node has connections from (to) a few nodes which have high inward (outward) centrality.

However, another way to consider node having high inward centrality is if it points to a

node with high outward centrality, and vice-versa. In this manner, two nodes can have

distinct roles in the network, defined by a different (inward/outward) directional

centrality characteristic, but their mutual interaction increases their given centrality. This

centrality was first implemented by the Hyperlink Induced Topic Search (HITS)

algorithm where the two types of central nodes were denoted authorities and hubs. Here,

authorities have many connections from nodes with high hub scores and hubs have many

connections to nodes with high authority scores. A citation matrix, for example. has

papers as nodes and the references to other papers as edges. In this network review papers

would have a high hub score since they reference many papers which are authoritative on

a given subject matter. From this, nodes with high authority scores are related to nodes

with high inward centrality, and hubs are nodes with high outward centrality. The

authority scores and hub scores for nodes are defined by the vectors x and y,

respectively, from the equations

$$AA^T x = \lambda x \tag{3.40}$$

$$A^T A y = \lambda y \tag{3.41}$$

where λ is the dominant eigenvalue of each equation. We note that hubs and authorities

do not exist in undirected networks where no directional relationship between nodes

exists.

3.9.6 Harmonic Centrality

Harmonic centrality is a measure that considers node importance relative to the

length of the paths going to or coming from that node. The measure uses the shortest path

length, or geodesic distance, between nodes to determine node importance. Let d_{ij} denote

the shortest path length between nodes i and j (for undirected networks) or from node j to

node i (for directed networks), where $d_{ij} = \infty$ if no path (undirected or directed) exists.

Then, the inward (or undirected) harmonic centrality x_i for node i is

$$x_i = \frac{1}{n-1} \sum_{j(\neq i)} \frac{1}{d_{ij}}, \tag{3.42}$$

and the outward harmonic centrality y_j for node j is

$$y_j = \frac{1}{n-1} \sum_{i(\neq j)} \frac{1}{d_{ij}} \tag{3.43}$$

where n is the number of nodes in the network.

3.9.7 Betweenness Centrality

Like harmonic centrality, betweenness centrality utilizes the shortest path lengths

that exist between nodes but in a different manner. Conceptually, betweenness centrality

estimates centrality of a given node by counting the number of shortest paths that pass

through that node. In this way, nodes with higher betweenness centrality are very

important in efficiently traversing the network. Unlike the other centrality measures

utilized in this study, betweenness centrality by construction cannot be estimated from

the perspective of directed inward and outward connections since this measure is concerned with the number of paths traveling through a node and not the direction of said paths. However, directed and undirected versions of this measure can be considered since directed and undirected networks may have different shortest paths between nodes. Let n_{st}^i be the number of unique shortest paths between nodes s and t that pass through node i, and let p_{st} be the total number of shortest paths between nodes s and t. Then the betweenness centrality x_i for node i is

$$x_i = \sum_{st} \frac{n_{st}^i}{p_{st}} \tag{3.44}$$

where $n_{st}^i / p_{st} = 0$ if both n_{st}^i and p_{st} are zero. In this form, if multiple shortest paths exist between nodes s and t, then the number of paths passing through node i is proportional to the total number of shortest paths.

3.10 Centrality Feature Processing

As mentioned, these networks are derived using significant connections found via GPDC, from epochs taken from the ictal, or seizure event, recorded using iEEG in patients with temporal lobe epilepsy. For a given ictal event, GPDC values were estimated from three second non-overlapping windows (epochs) for discrete frequencies from 0 to 50Hz. Networks were then derived for each frequency and epoch using surrogate data analysis, and each of the previously mentioned centralities was estimated for each node. Because of the large number of centralities that are estimated, averaging was utilized in order to summarize the behavior of each node over given time frames and frequencies. Once the centralities were averaged, two selection criteria were tested in

order to determine which centrality metric would be associated with the epileptogenic

focus: maximum averaged value and absolute majority voting.

3.11 Averaging Strategy

The centrality values per recording site over sets of time epochs and frequencies

within seizures was averaged, as well as across seizures per patient. Let $C_{*,s}(f, t) =$

$[c_{*,s}^1(f, t), \dots, c_{*,s}^N(f, t)]'$ be the vector of the $c_{*,s}^i$ centrality metric's values estimated for

frequency f and time epoch t for seizure s at brain site $i = \{1, \dots, N\}$. If $\Omega =$

$\{f_1, f_2, \dots, f_m\}$ is a set of discrete frequencies within a frequency band, and $T =$

$\{t_1, t_2, \dots, t_n\}$ is a set of epochs within a given seizure, then

$$c_{*,s}^i(\Omega, T) = \frac{1}{m * n} \sum_{\omega \in \Omega} \sum_{\tau \in T} c_{*,s}(\omega, \tau) \tag{3.45}$$

represents the mean centrality values for each node i of the given seizure s over a set of

frequencies Ω and set of epochs T, which values from each node can be written as the

vector $c_{*,s}(\Omega, T)$. Then, for a given patient P with w recorded seizures $(s = 1, \dots, w)$

$$C_{*,P}^i(\Omega, T) = \frac{1}{w} \sum_{s=1}^{w} c_{*,s}^i(\Omega, T) \tag{3.46}$$

is the grand average of the estimated centrality over a specified frequency band Ω and

epoch T over all seizures for a given patient at brain site i, creating a vector $C_{*,P}(\Omega, T)$.

Estimation of $C_*^i(\Omega, T)$ was performed for Ω being any of the traditional EEG

frequency bands and for two epochs: early ictal and total ictal period, where early ictal

consisted of the first three epochs of the ictal event and total ictal was all three second

epochs within the ictal period. The thus derived grand average centrality values at

different brain sites were then studied in an attempt to detect discernable centrality values at the epileptogenic focal region versus the rest of brain regions.

3.11.1 Absolute Majority Voting

Absolute majority voting is a selection criterion choosing an alternative if it obtains more than half of the 'votes'. In the case of this research, absolute majority voting was used to determine if certain centrality metrics were associated with the epileptogenic focus in the majority of seizures for a given patient. For the selection criteria, let

$$\left\{ \hat{\imath} \,\middle|\, \hat{\imath} \in \{1, \dots, N\} \text{ and } c_{\hat{\imath}} = \max\left(c_{*,s}(\Omega, \mathrm{T})\right) \right\}$$ be the index of the component of $c_{*,s}(\Omega, \mathrm{T})$

having the maximum averaged centrality value for seizure s of a given patient. Let $G = \{g_1, \dots, g_N\}$ be the nodes of the network, and $V(G') \subset V(G)$ represent the nodes that are in the region declared by the physician as being the epileptogenic focus for the given patient. If $g_{\hat{\imath}} \in V(G')$, then $c_{*,s}(\Omega, \mathrm{T})$ is a centrality metric that successfully localizes the focal region for seizure s at frequency band Ω. If $c_{*,s}(\Omega, \mathrm{T})$ successfully localized the focal region in more than half of the seizures in the given patient, then that centrality metric was deemed successful in localizing the epileptogenic focus in patient P at frequency band Ω using epoch set T.

3.11.2 Maximum Average Centrality

The maximum value of the averaged centrality values across seizures was tested for association with the epileptogenic focus in each patient. For the selection criteria, let

$$\left\{ \hat{\imath} \,\middle|\, \hat{\imath} \in \{1, \dots, N\} \text{ and } c_{\hat{\imath}} = \max\left(C_{*,P}(\Omega, \mathrm{T})\right) \right\}$$ be the index of the component of

$C_{*,P}(\Omega, \mathrm{T})$ having the maximum averaged centrality value across all seizures for a patient P. Let $G = \{g_1, \dots, g_N\}$ be the nodes of the network, and $V(G') \subset V(G)$ represent the

nodes that are in the region declared by the physician as being the epileptogenic focus for the given patient. If $g_l \in V(G')$, then $C_{*,P}(\Omega, T)$ is a centrality metric that successfully localizes the focal region for patient P at frequency band Ω using epoch set T.

3.12 Methodological Considerations

In order to create networks accurately representing brain activity, several factors had to be considered, particularly, the connectivity measure to use, the window size of the multivariate time series data, and the frequencies which to analyze. Once the networks were derived and centralities are estimated, averaging was utilized for centrality metrics to summarize the results.

3.12.1 Measuring Brain Connectivity

Generalized Partial Directed Coherence is one of a multitude of measures for characterizing brain connectivity, and GPDC was chosen for this research after considering three general criteria of brain connectivity measures. First, like many connectivity measures, GPDC is a linear function. Linear functions are typically preferred in this type of research due to their computational efficiency. However, one hindrance of linear connectivity measures is that they capture linear relationships in systems that may operate in a nonlinear fashion. GPDC is measured using a vector autoregressive process, a linear set of relations, and the observed linear relationship between brain regions at each considered frequency may lack some important qualities that tie more closely to actual nonlinear brain behavior. Nonlinear measures may provide more insight as to how the brain behaves over time, but these methods are computationally prohibited to apply in a meaningful way.

Second, GPDC creates a connectivity network of directed edges, meaning that the connectivity measured from site i to site j may not be equal to the connectivity measures from site j to site i. Common frequency-based connectivity measures such as coherence and partial coherence observe the general relationship between signals based on the power spectra and inverse power spectra, which are symmetric matrices where directionality cannot be seen. However, as seen in the methodology, these power spectra can be decomposed in a manner that allows for underlying directionality to be observed. From a physiological perspective, this closely follows the behavior of neurons that send signals to other neurons via unidirectional synaptic clefts. By considering directionality, a better picture of the connections arising in the brain can be found.

Third, GPDC is a multivariate connectivity measure, meaning that the relationships between all signals is considered prior to measuring the connectivity relationship between two given signals. The advantage of using a multivariate method is that the values of the measured connections represent solely the connectivity between the two given regions by accounting for the connectivity that arises from other brain regions. Other popular measures, such as Directed Transfer Function, tend to fail in this task, as the values of connectivity they provide are in fact an amalgamation of direct connectivity between the two brain regions and indirect connectivity arising from a secondary connection generating a cascade effect.

GPDC measures not only the strength of the direct connection between two brain sites but also considers the direction in which the connection occurs, GPDC could be considered a pure distillation of the underlying brain network as seen from the perspective of the linear relationships between signals at a given frequency.

3.12.2 Window Sampling Size

The selection of window size for this research followed two important criteria. First, the window size had to be sufficiently large to allow the dataset to be considered stationary over its entire duration. This would allow for the creation of a stable vector autoregressive model to estimate GPDC values. Second, a window size was desired that provided the highest possible temporal resolution, thus providing enough epochs over the seizure event so that dynamic behavior could be observed. Sliding non-overlapping windows of three seconds were chosen and VAR models of order $p = 7$ were used, which were in agreement with model orders used in previous analyses of brain dynamics [52], [53]. For this data, the selection of three seconds also satisfied the requirements described in [54] such that

$$cd \gg c^2 p, \tag{3.47}$$

where c is the number of channels, d is the number of data points in each channel, and p is the model order. Each three second iEEG epoch contained 600 data points per channel for all 28 or 40 channels, both of which satisfy the above condition when using a VAR model of order $p = 7$. Thus, this epoch duration was sufficiently long for the model to be reliably constructed from the EEG, and sufficiently short to maximize temporal resolution and abide with possible nonstationarities of the EEG in epilepsy [53].

3.12.3 Frequencies Estimated

The selection of the frequencies used for estimation of GPDC was the integer values from 0Hz to 50Hz, based on four criteria. First, based on the Nyquist Theorem, which states that the theoretical maximum frequency that could be considered must be less than half the sampling frequency of the data, the highest frequencies for

which GPDC values could be considered would be at 100Hz since the sampling

frequency of the iEEG data was 200Hz (although two patients (P1 and P2) had iEEG data

sampled at 400Hz, these datasets were downsampled to 200Hz to keep them consistent

with the remaining seven patients). Second, electrophysiological sampling data often

suffer from noise generated at 60Hz since electrical lines in the United States transmit

power at this frequency. If the data are unfiltered, GPDC estimates near this frequency

are inaccurate due to a significant line noise artifact, while filtering out the noise around

this frequency can lead to overfitting of the VAR process generating the GPDC values.

Therefore, in practice, estimations near the power line frequency are avoided. Note that in

Europe, line noise occurs at 50Hz, which can lead to issues in estimating the higher γ

frequencies. Third, the frequencies chosen for estimation coincided with the traditional

EEG frequency bands used in clinical practice. Of course, this is not a requirement of

selecting EEG frequencies, but the traditional bands are standard in clinical practice, and

therefore, our averaging technique would be easily adopted in the clinical setting.

Last, only integer frequencies were used because of the gradual change in

networks which were derived from GPDC. However, using integer frequencies over

traditional EEG frequency bands raises one other concern that should be addressed: EEG

frequency bands are not the same length. While the lower δ, θ, and α frequency bands use

four different integer frequencies, the β and γ frequency bands use 18 and 20 integer

frequencies, respectively. Therefore, different sample sizes could potentially affect the

outcome of the final results. This is not the case as seen in our results with the gradual

changes of centralities over frequencies. In fact, if more frequencies were used to

estimate the lower frequency bands, it is more likely that over-fitting would occur in the

final results. In the same manner, using fewer frequencies to estimate the β and γ frequency bands would likely lead to under-fitting of these results. Therefore, although non-integer frequencies could have been utilized as well, no additional information would likely be derived.

3.12.4 Averaging Epochs

Once centrality estimation was completed, averaging over specified epoch sets and frequency bands helped summarize the data. For frequencies, it has been established that averaging frequency bands was the most reasonable approach. The choice of epoch sets, however, needs to be discussed further. The use of total ictal averaging was the first approach considered in this research. Considering every epoch set for each seizure seemed to be the simplest approach. Furthermore, the number of epochs in each seizure varies widely from a minimum of three epochs to a maximum of 107 epochs. Because of the dynamic centrality behavior found in some seizures, averaging longer seizures reduces the centrality values of nodes associated with the epileptogenic focus found near the beginning of the seizure. The initial decision to use three epochs was based on the fact that the shortest seizure had only three epochs.

CHAPTER 4

RESULTS

4.1 Epileptogenic Network and Centrality Metrics

An example of the results obtained using the given methodology from a directed

binary graph is shown in Figure 4-1. The adjacency matrix was constructed from the first

3-second iEEG epoch after the onset of a secondarily generalized seizure in patient P7

(electrode setup A) on the basis of GPDC values estimated at the frequency value of

30Hz. As we have observed, the network structures, and the underlying centrality

characteristics, do not change much for nearby frequencies. Only statistically significant

directed edges following surrogate data analysis are shown here. The nodes of the

network that are colored red correspond to electrode sites within the epileptogenic focus,

determined by a physician to be the left hippocampus (LTD) and left subtemporal (LST)

region in patient P7. It is apparent that the network is quite intricate with a large number

of directed edges representing the interactions between electrode sites at seizure onset.

Because of this intricacy, elucidating any significant information is difficult, which

explains the need for centrality metrics, so that the interactions between nodes and the

relative importance of each node in the network can be better understood.
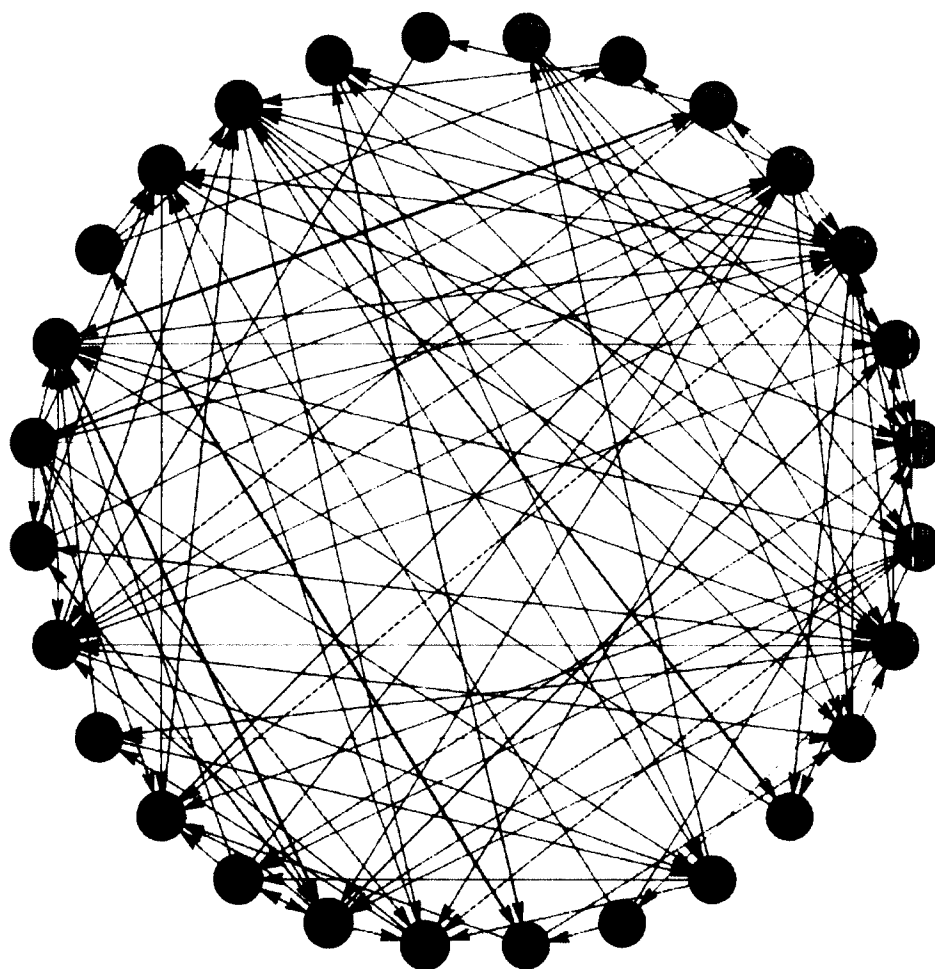
Figure 4-1: Example network of binary directed connections obtained from the 3-second epoch immediately after initiation of a secondarily generalized seizure in patient P7. This network is derived from GPDC values measured at a frequency of 30Hz. Nodes colored in red indicate the electrodes located within the region of the epileptogenic focus.

In Figure 4-2, the estimated centrality measures from the network shown in

Figure 4-1 are estimated and shown as bar graphs with the left column being the inward

directed centrality measures (along with betweenness centrality) and the right column

showing the outward directed centrality values from the network. Red bars indicate the

electrodes associated with the epileptogenic focus (LTD and LST), and the bar with green

stripes indicates the node having maximum value for that centrality metric. For these

results, we first note that the scale of each bar graph is not the same, showing that each

measure actually produces different values. Regardless, the relative centrality values between nodes was the most important consideration when looking at importance of each node in the network; the actual values of the centrality metrics were not of interest in this research. By focusing on relative node importance, it is revealed that certain centrality metrics may behave similarly for a given network, as seen by comparing degree, eigenvector, and Katz centralities for both the inward and outward cases. Each of these centralities has the maximum value associated with the same electrode within the epileptogenic focus (LTD4) for inward connections, and for the outward centralities, the same electrode (RST1) is shown to have maximum centrality in all three metrics. Although the authority and hub scores and harmonic centralities did not have quite the same relative node centrality behavior as was seen in degree, eigenvector, and Katz centralities, they also showed the maximum value associated with the same electrode within the epileptogenic focus (LTD4) for inward connections and the same electrode (RST1) for outward connections. For this network, only PageRank centrality was revealed to have the maximum value associated with an electrode found within the epileptogenic focus for both inward and outward centralities, though the nodes were associated with different recording electrodes. Overall, all inward-based centralities, as well as betweenness centrality and the outward directed PageRank centrality, exhibited maximum values at electrode sites within the region of the epileptogenic focus, even though these sites were not the same across seizures in the same patient. From Figure 4-2 its apparent that the rest of the outward centrality measures failed to identify any characteristic quality of the focus, showing maximum centrality values at an electrode contralateral to the focal region (RST1).
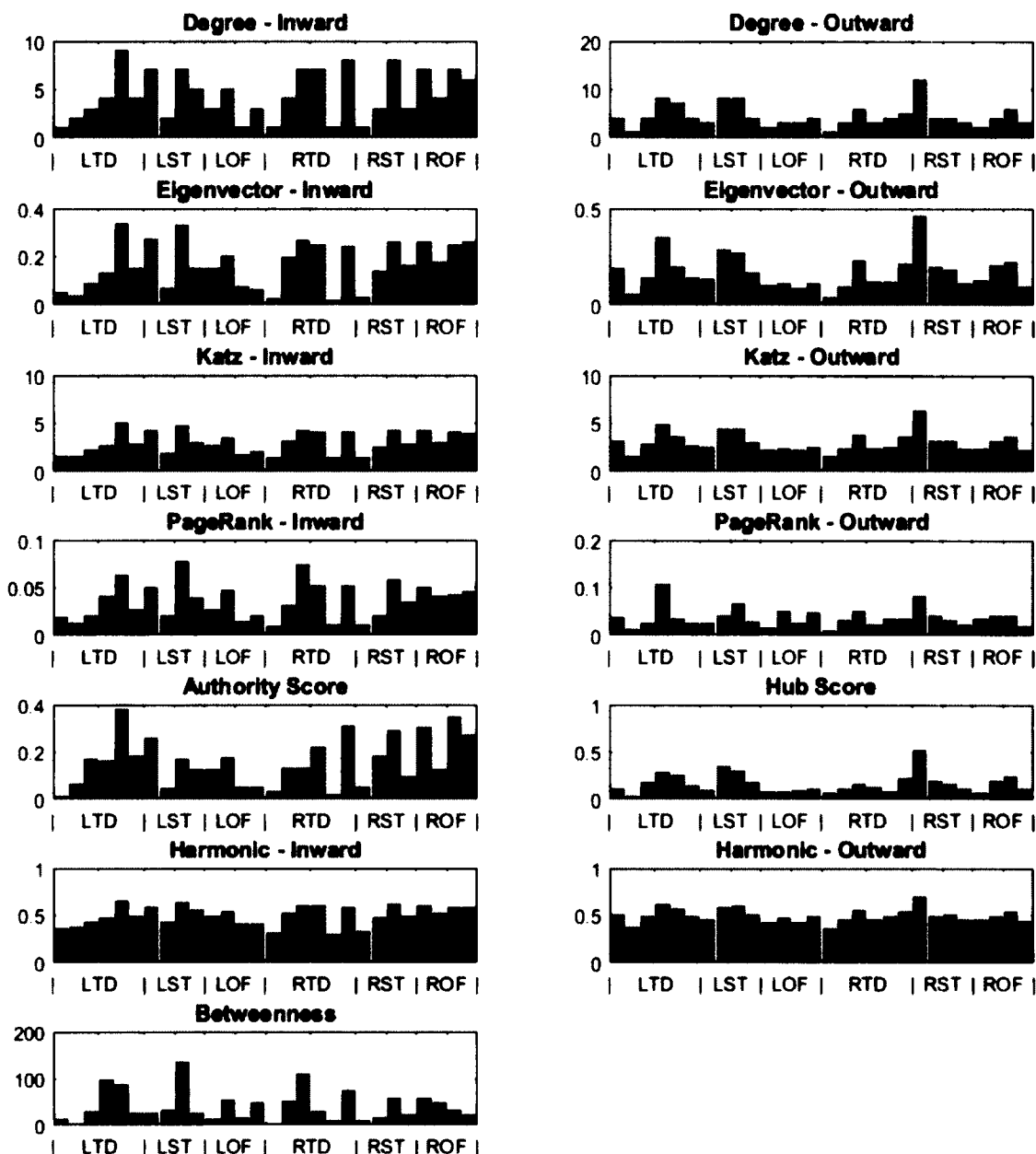
Figure 4-2: Bar graphs of the values of different directed centrality measures per electrode site estimated from the network in Figure 4-1. Red bars indicate the electrodes associated with the clinically assessed epileptogenic focus. Bars with green stripes indicate the nodes that exhibit maximum centrality value in the network.

4.2 Centrality Dynamics within Ictal Periods and across Patients

Centrality values at brain sites change over time as expected since brain networks are dynamic. The results from this research support this notion, showing wide variations

in network centrality values over time within individual seizures and across patients.

Primary findings of this nature are seen in Figure 4-3 showing three representative

examples using both inward and outward degree centralities. In particular, the degree

centralities were estimated at 30Hz from sequential three second EEG epochs over the

entire ictal period of three clinical seizures, one seizure from each of three of our patients.

Each panel was normalized between 0 and 1 with the x-axis representing time epochs and

the y-axis representing the electrodes. The color of the square intersecting a time epoch

and electrode represents the relative centrality value of that node in the network at the

given time epoch with red color being associated with larger/maximum centrality values

and blue colors indicating low relative centrality for the node. Red arrows to the left of

each panel indicate which electrode sets are associated with the epileptogenic focus.
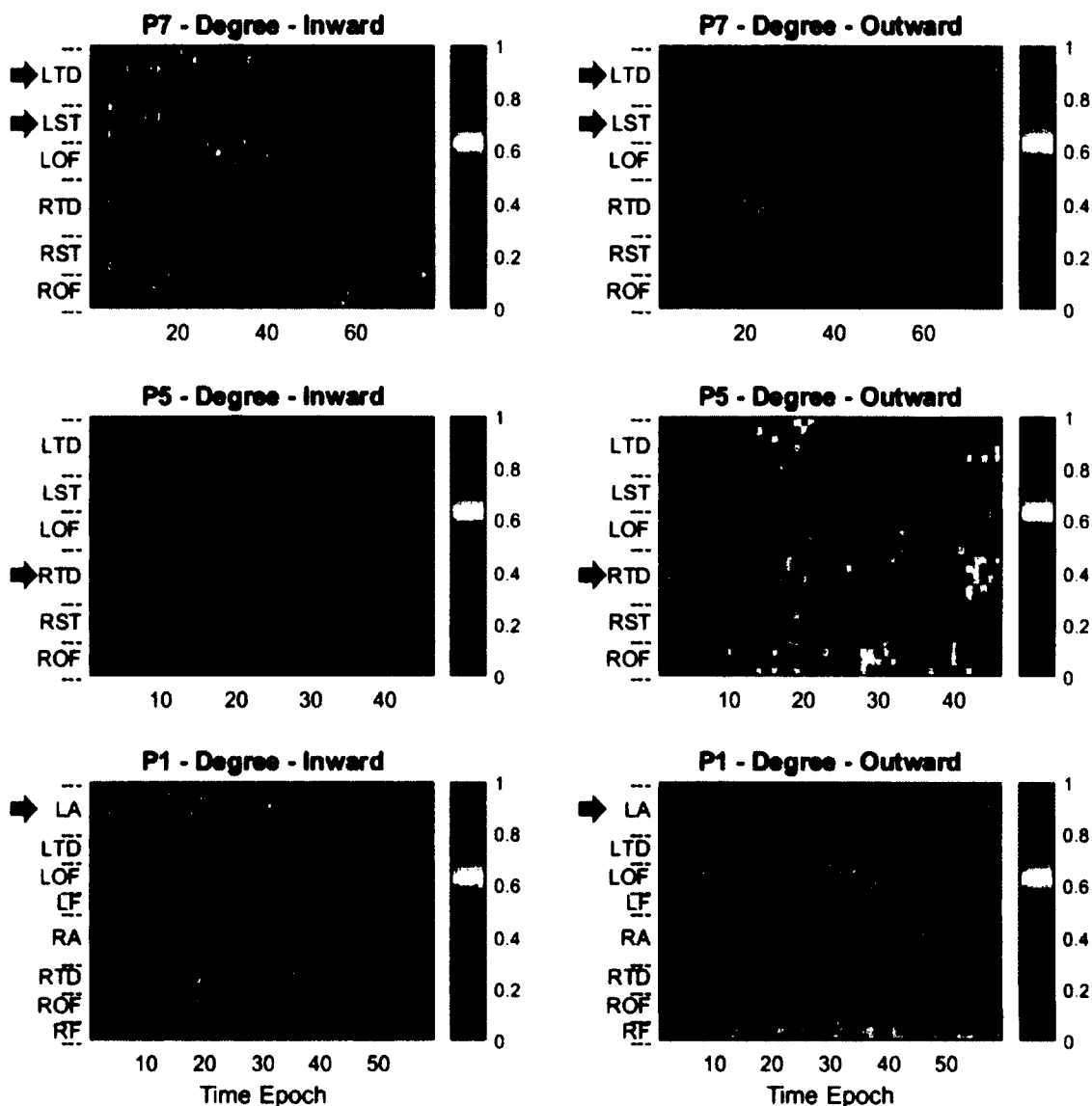
Figure 4-3: Directed degree centrality values estimated over the full ictal periods in clinical seizures from (Top Panels) patient P7 seizure #21, (Middle Panels) patient P5 seizure #7, and (Bottom Panels) patient P1 seizure #22. The respective brain networks were created from GPDC values estimated at the discrete frequency of 30 Hz over three second non-overlapping EEG epochs throughout the ictal period of the seizures. Illustrated values of centralities were normalized with respect to their maximum per seizure for visualization purposes.

In the top panels of Figure 4-3, inward and outward degree centralities come from

a secondarily generalized seizure in patient P7 (focus in LST/LTD). At the ictal onset,

determined by the physicians, higher values of the inward degree centrality are observed

at the left depth hippocampal (LTD) electrodes, that quickly spread over time to other

electrodes (LST and LOF) within the left hemisphere. Midway through this seizure,

inward degree centrality in the left hemisphere dramatically drops, with a slight increase

observed in the right hemisphere that intensifies to almost all brain areas except the focal

area at seizure's end. In the same seizure, outward degree centrality (top right panel)

shows nearly complementary behavior to its inward degree counterpart, with higher

outward degree centrality presenting right hippocampus (RTD) and right subtemporal

(RST) regions, dropping around the same time as seen in inward degree centrality (time

epoch #38) with an increase outward centrality spreading to left hemisphere contacts near

the end of the seizure (time epoch #61).

The middle panels of Figure 4-3 show a different behavior for inward and

outward centrality values during a seizure from patient P5 (focus in RTD). In the left

panel, inward degree values for all electrodes remain relatively low at the seizure onset

and increase across all electrodes around the 13th epoch. After, the electrodes with the

highest inward degree at each epoch seem random. For outward degree centrality (middle

right panel), increased values are observed in the right hippocampal electrodes during

seizure onset and remain elevated throughout the event. Similar to the activity seen in the

middle left panel, outward centrality values increase in all electrodes around the 13th

epoch and decay around the 25th epoch. However, increased outward centrality is seen in

the right orbitofrontal (ROF) brain region during the 10th epoch and remains elevated

until seizure termination. Furthermore, near the end of the seizure event, increased

outward centrality is observed in both regions near the hippocampus (LTD/RTD) with

more prominence in the right hippocampal electrodes.

Patient P1 (bottom panels) shows again different behavior of degree centralities over the duration of a complex partial (focal) seizure (focus in LA). Inward degree values are shown to gradually increase in both the left amygdala (LA) and right hippocampal (RTD) regions, peaking in the left amygdala (LA) at the 23rd epoch and shortly after the 25th epoch in the right hippocampus (RTD). Like the seizure presented in the top panels, the inward and outward centralities of this seizure behave in a complementary fashion, with elevated outward degree values in all regions, excluding the left amygdala and right hippocampus, for the duration of the seizure.

To study further the differences and similarities of centrality metrics, Figure 4-4 shows the dynamic behavior of the authority and hub scores for the same seizures taken from GPDC estimates at the same frequency (30Hz). The behavior of authority and hubs scores is very similar to their degree centrality counterparts shown in Figure 4-3 with the exception of the seizure presented in patient P5 (middle panels) which does not show the increase in centrality over all electrodes that was seen in both inward and outward degree centralities.
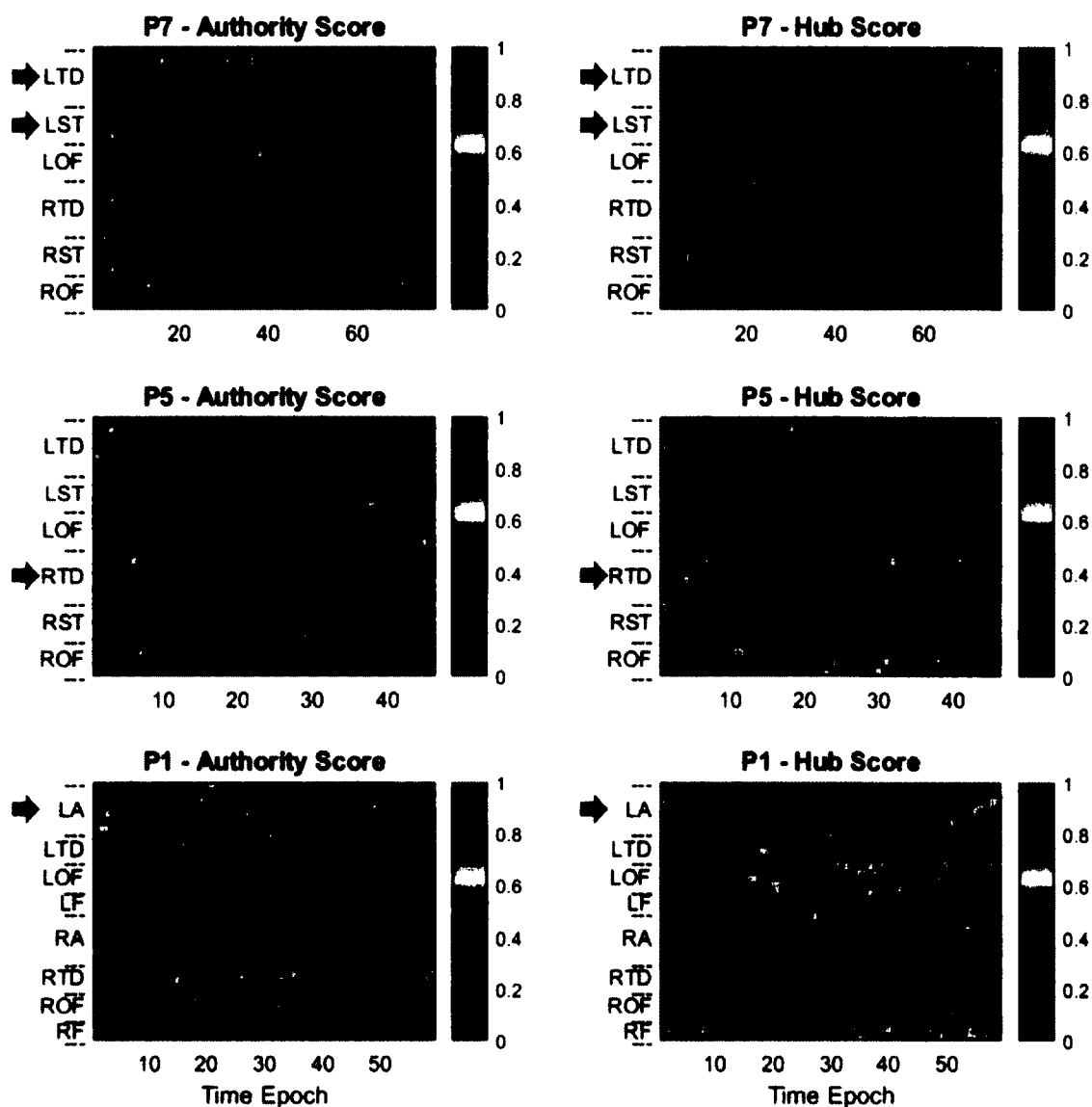
Figure 4-4: Authority and Hub scores estimated over the full ictal periods in clinical seizures from (Top Panels) patient P7 seizure #21, (Middle Panels) patient P5 seizure #7, and (Bottom Panels) patient P1 seizure #22.

From these simple examples some important general results can be derived. First, the behavior of seizures across patients can be highly dissimilar. This is particularly troublesome since all patients studied herein have been diagnosed with some form of temporal lobe epilepsy leading one to assume that the behavior of the seizures should be similar, which is obviously not the case. Second, inward and outward centrality metrics

can behave in either a complementary fashion or present similar behaviors. Lastly, the dynamics of seizures are highly varied with some seizures presenting highly dynamic changes arising throughout the seizure event and other seizures presenting behavior the remains relatively constant as the event transpires. This evidence leads to two different temporal cases to be considered for determining the epileptogenic focus: the centrality behavior during the seizure onset period (early ictal) and the centrality behavior across the entire seizure event (total ictal).

4.3 Centrality Dependence on EEG Frequencies

Centrality is estimated from the network reconstructed by GPDC, where GPDC quantifies the effect of the activity at a source node on the activity of a receiver node in the frequency domain. Hence, another important observation is how networks and the centralities produced from those networks change with respect to frequency. Figure 4-5 shows the dependence of the degree centrality values on the frequency content of the EEG from the first epoch of the seizures (previously presented in Figure 4-3).
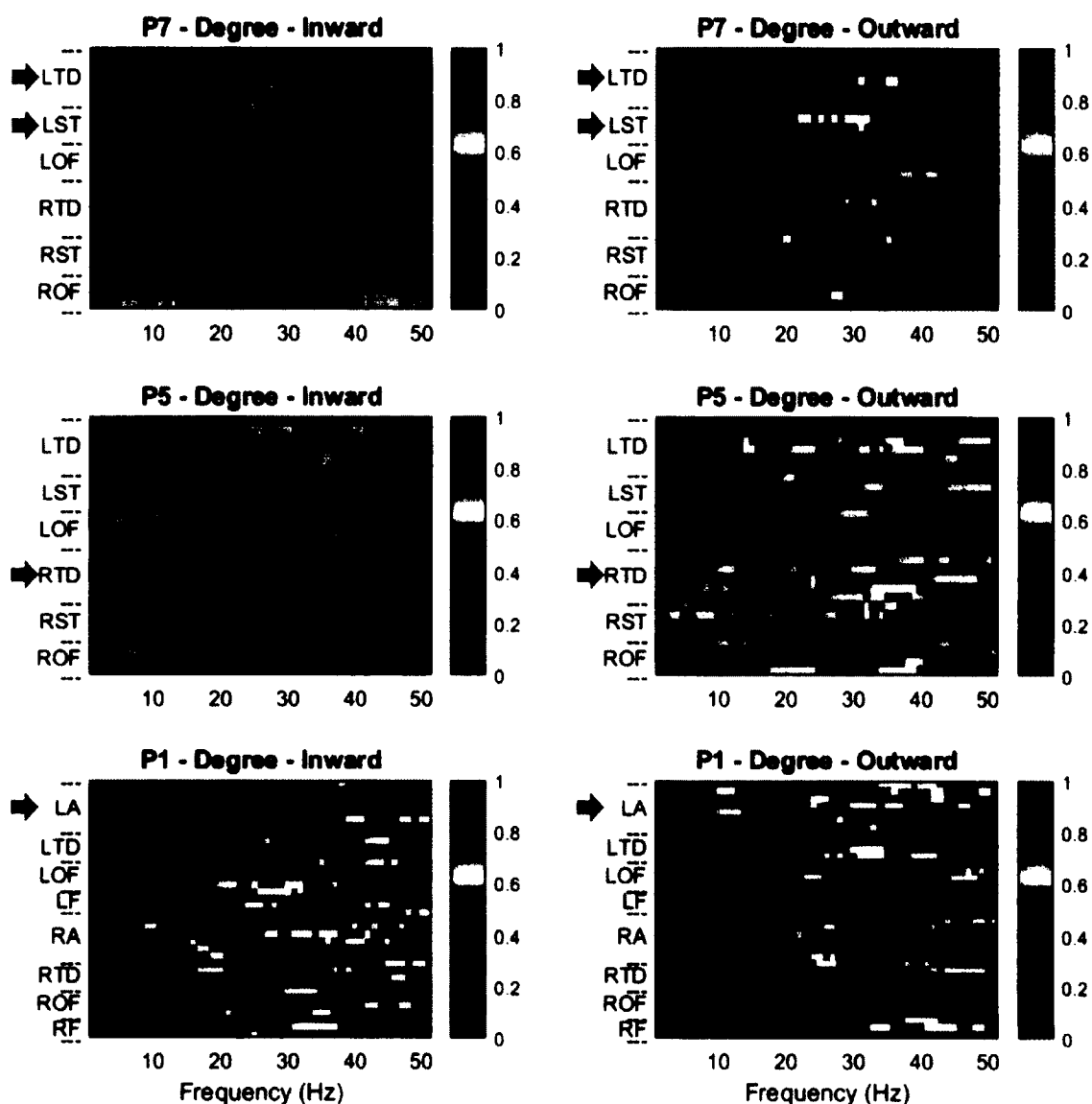
Figure 4-5: Degree centrality values estimated over all analyzed frequencies for clinical seizures from (Top Panels) patient P7 seizure #21, (Middle Panels) patient P5 seizure #7, and (Bottom Panels) patient P1 seizure #22. The respective brain networks were created from GPDC values estimated the first three second non-overlapping EEG epochs of each ictal event. Illustrated values of centralities were normalized with respect to their maximum over all frequencies for visualization purposes.

For patient P7 (top panels), high inward degree centralities are observed for lower frequencies in the right orbitofrontal region (ROF), and as frequency increases, inward degree values increase in multiple EEG electrodes, many originating in the epileptogenic focus. For outward degree centrality, increased values arise in electrodes within the focal

region and one electrode contralateral to the focus (RST1) starting at 18Hz. For electrodes LTD5, LST3, and RST1, these centrality values peak in the higher frequencies at around 48Hz, 37Hz, and 30Hz, respectively.

The middle panels of Figure 4-5 (patient P5), show very different behavior, with high inward degree centrality arising at lower frequencies in the two electrodes in contralateral positions (LTD1 and RTD1), with higher values appearing in the non-focal electrode (LTD1), and high outward degree centrality values are also seen on other electrodes in LTD, peaking in two different ranges, 18Hz to 28Hz and 44Hz to 48Hz. Lastly, patient P1 (bottom panels) show another example of the differing behavior over frequencies. Here elevated inward degree centralities arise in both high and low frequencies in electrodes located in the right hemisphere, opposite of the focal region (LTD), and inward degree values increase in a focal electrode (LTD1) from 25Hz and likely continues to increase past 50Hz. For outward degree, centrality values seem to increase in most electrodes in the left hemisphere and a few electrodes in the right hemisphere as frequency increases.

To compare the similarities and differences of centrality values, authority and hub scores for the same seizures at the first epoch are presented in Figure 4-6. Although the authority scores (left panels) behave similarly to their inward degree centrality counterparts (Figure 4-6: left panels), the images are much less saturated with elevated centrality scores. The same is observed for the hub scores; however, patients P7 (top right panel) and P1 (bottom right panel) present elevated activity in multiple electrodes seemingly unrelated to the focal region in lower frequency ranges.
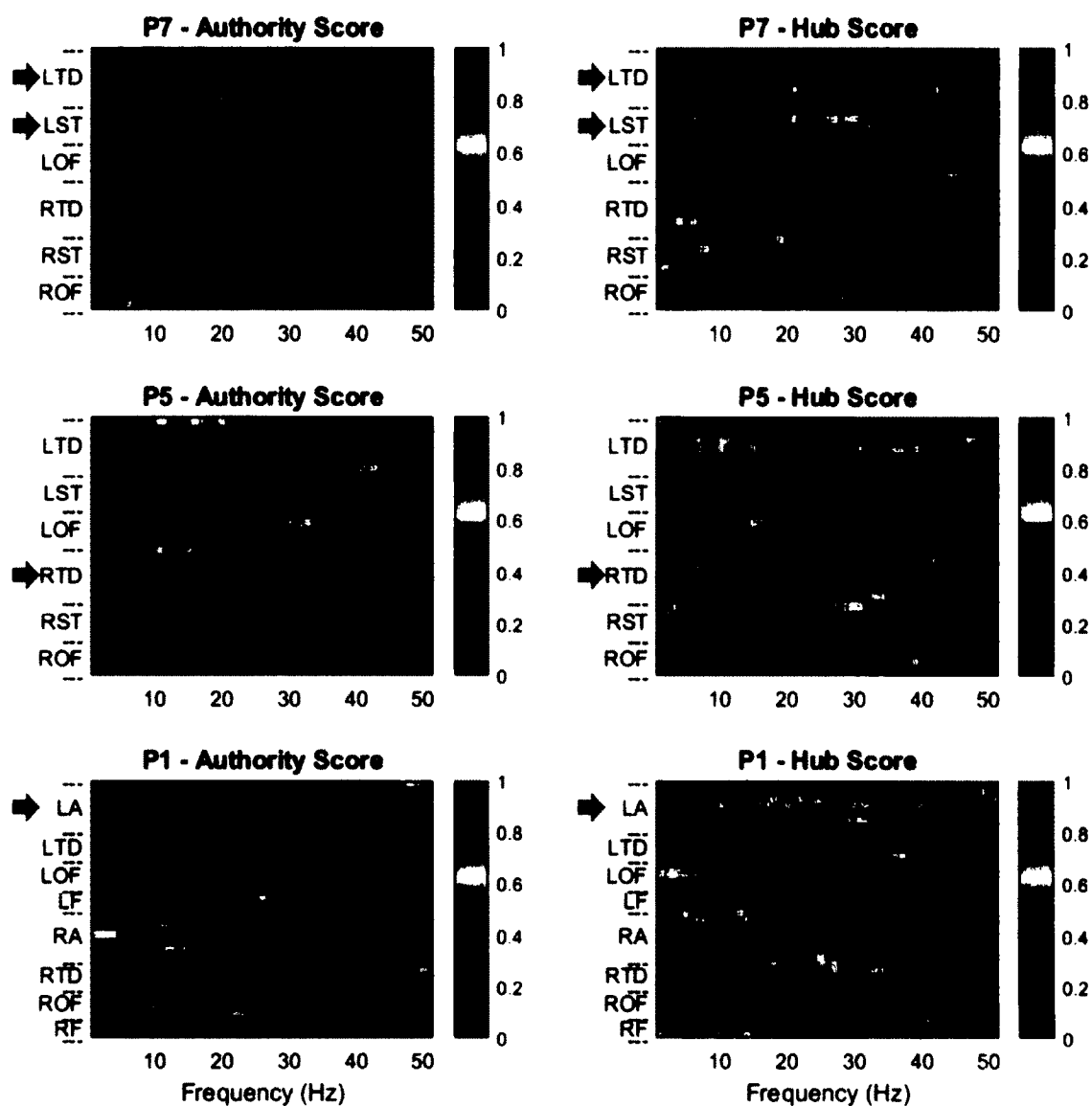
Figure 4-6: Authority and hub scores estimated over all measured frequencies (0-50Hz) from the first epoch in clinical seizures from (Top Panels) patient P7 seizure #21, (Middle Panels) patient P5 seizure #7, and (Bottom Panels) patient P1 seizure #22.

Overall, the centrality values, and the underlying networks, do seem to depend heavily on the frequencies used to generate the network. Lastly, considering the inward centrality metrics (inward degree and authority scores), both show lower centrality values at lower frequency ranges.

4.4 Average Centrality of Clinical Seizures for Epileptogenic Focus Localization

Due to the observed variability of centrality values across time epochs and frequencies of clinical seizures, and the large number of clinical seizures that needed to be studied in each patient, averaging centrality values over traditional EEG frequency bands and certain sets of epochs helped to determine associations between nodes in the network and the electrodes within the epileptogenic focus. Figure 4-7 shows the averaging process as done over frequencies for the first epoch from seizure #20 of patient P1 when using authority scores. In the left panel, authority scores for discrete frequencies are presented with horizontal red line separating the traditional EEG frequency bands (δ: 1-4Hz, θ: 5-8Hz, α: 9-12Hz, β: 13-30Hz, γ: 31-50Hz). The top right panel illustrates the authority score at all brain areas averaged over the δ frequency band ($1 - 4$Hz). Centrality assumes its highest value at one of the electrodes contralateral to the focal region (right hippocampus – RTD). The same electrode exhibits the highest centrality in the θ frequency band ($5 - 8$Hz). In the α ($9 - 12$Hz) and β ($13 - 30$Hz) frequency bands, the authority score is maximum at one of the focal electrodes (left amygdala - LA). The electrode that exhibits highest centrality in the γ ($31 - 50$Hz) frequency band is different from the one in the α and β bands but it is still within the epileptogenic focus (LA). In summary, centrality values clearly change across frequencies, the biggest difference being obtained between low and high frequency bands, with higher frequency bands exhibiting higher focus localization potential.
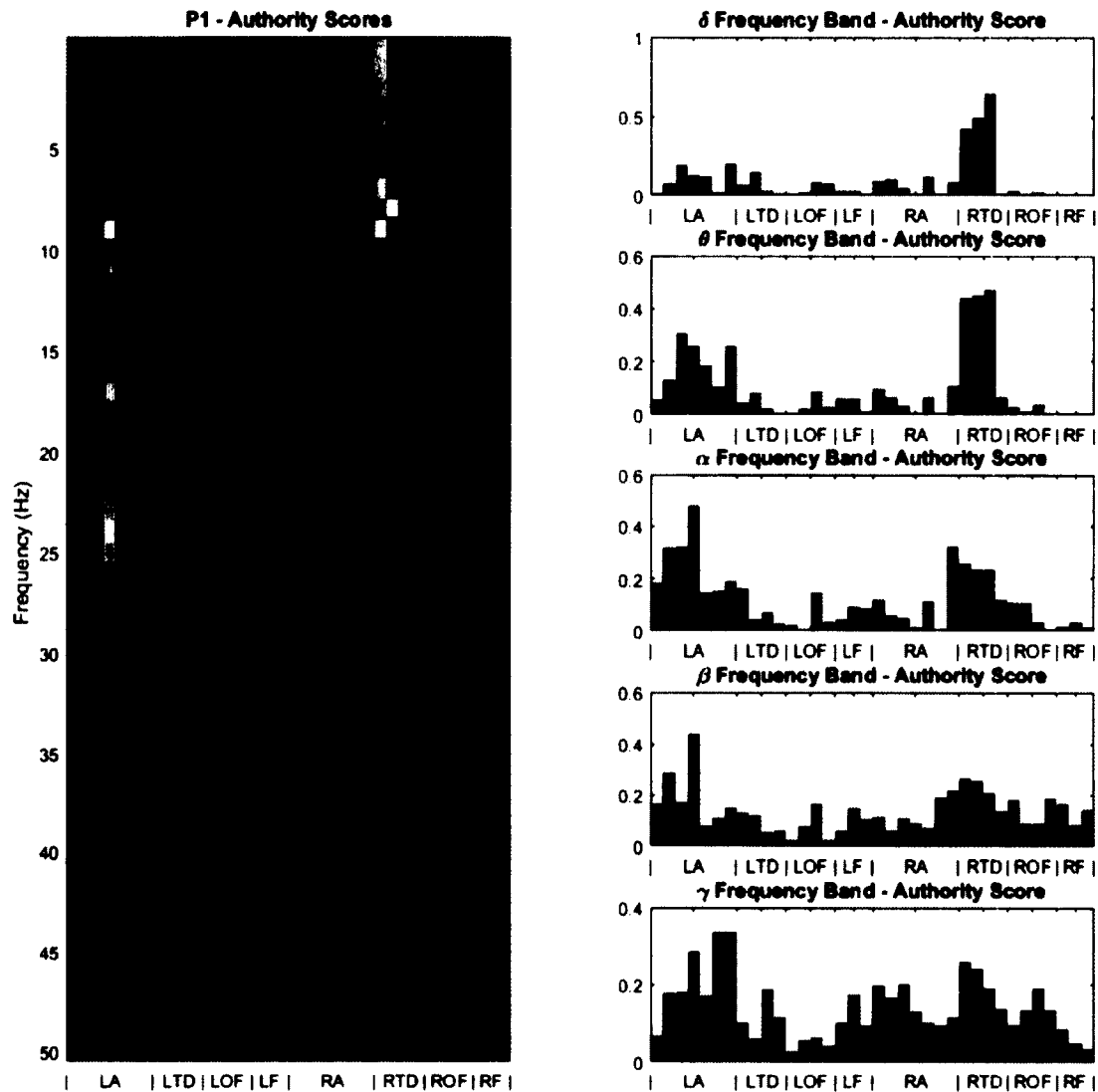
Figure 4-7: Centrality dependence on frequency. (Left Panel) Authority scores over EEG frequency bands per electrode site estimated from the EEG epoch right after the onset of clinical seizure #20 from patient P1. Frequency bands are separated by horizontal red lines. (Right Panels) Authority values at individual frequencies were averaged over the respective frequency bands. Red bars indicate the electrodes associated with the clinically assessed epileptogenic focus. Bars with green stripes indicate node(s) having maximum value in each authority score profile. It is observed that maximum authority scores of electrode sites within the clinically assessed focus are ones estimated from the higher frequency bands.

Figure 4-8 provides an example of two averaging schemes performed on the authority scores derived from the networks created using the $25Hz$ GPDC values from the sixth clinical seizure from patient P1. Seizure 6 of patient P1 behaves similarly to

other presented seizures from this patient with elevated authority scores present in the epileptogenic focus (the left amygdala - LA), and in the contralateral electrodes found in the right hippocampus (RTD). For this seizure, averaging over the first three epochs (early ictal period, bottom left panel) gave elevated average authority scores for multiple electrodes with maximum values presenting in the epileptogenic focus (left amygdala – LA) of patient P1. Averaging over the entire seizure event (total ictal, bottom right panel) provided elevated average authority scores for the epileptogenic focus and the right hippocampus and orbitofrontal brain regions, but the maximum averaged authority score appeared contralateral to the focal region. Although this seizure showed that averaging over epochs present in the beginning of the seizure event provided a maximum value located in the focus, there exists seizure events where the early ictal averaging fails to localize the focus and/or averaging over the entire ictal period presents a maximum value within the focus.
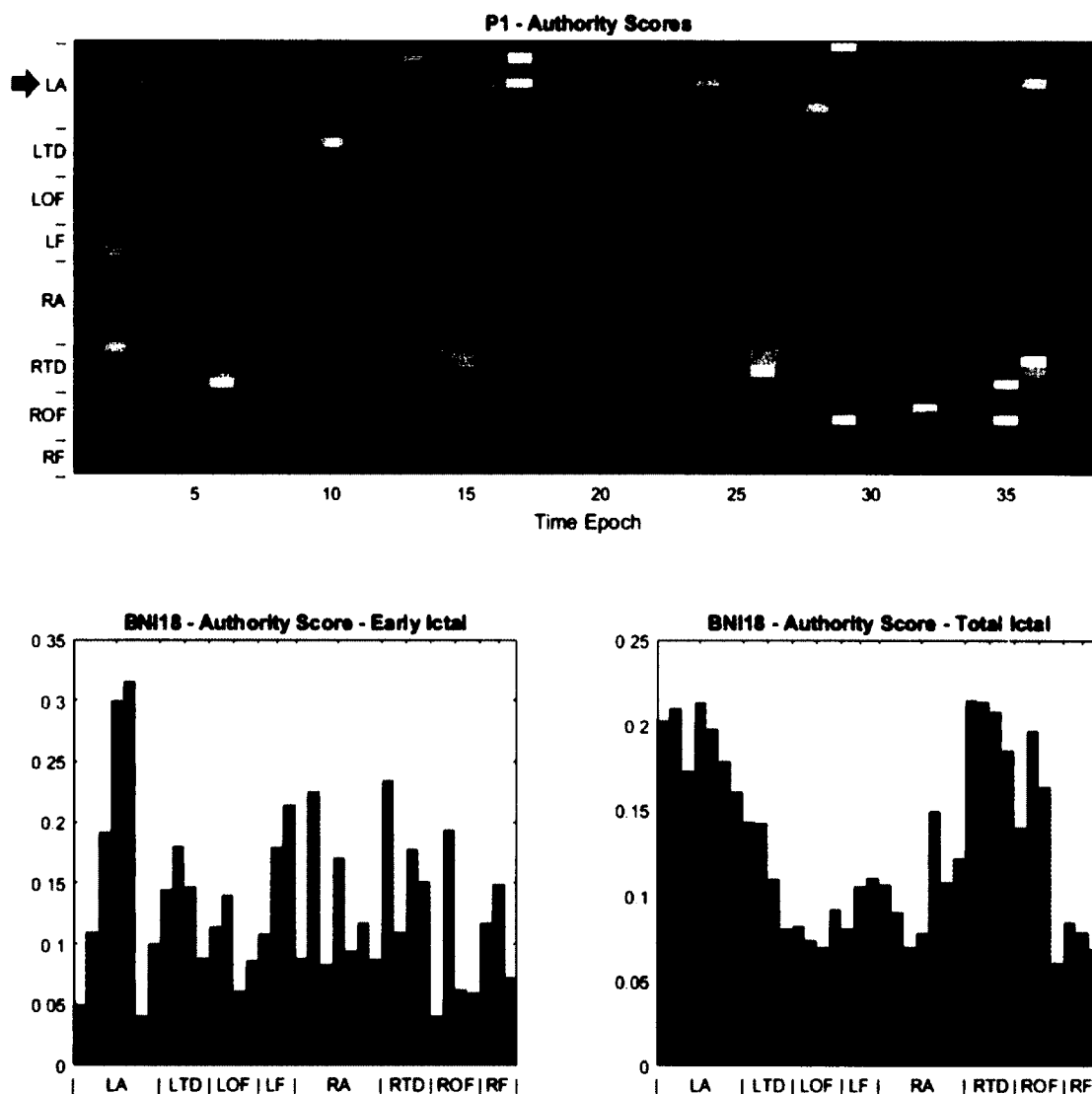
Figure 4-8: Centrality dependence over time. (Top Panel) Authority scores over time epochs per electrode site estimated from the EEG frequency of 25Hz over seizure #6 from patient P1. (Bottom Left Panel) Authority values averaged over the first three time epochs (early ictal). (Bottom Right Panel) Authority values averaged over the all estimated time epochs (total ictal).

As shown, a given centrality can be averaged over the time or frequency domains, but further summarization can be done by averaging over the two ranges simultaneously. For example, Figure 4-9 shows the authority score averaged first over the γ frequency band per epoch and then over the first three epochs (9 sec) of the ictal periods for each of

all six clinical seizures recorded from patient P3 (focus RTD – right hippocampus). It is

noted that, although high centrality values were obtained within the epileptogenic area,

the maximum centrality value corresponds to electrodes in the focal area in only three out

of the six seizures in this patient.
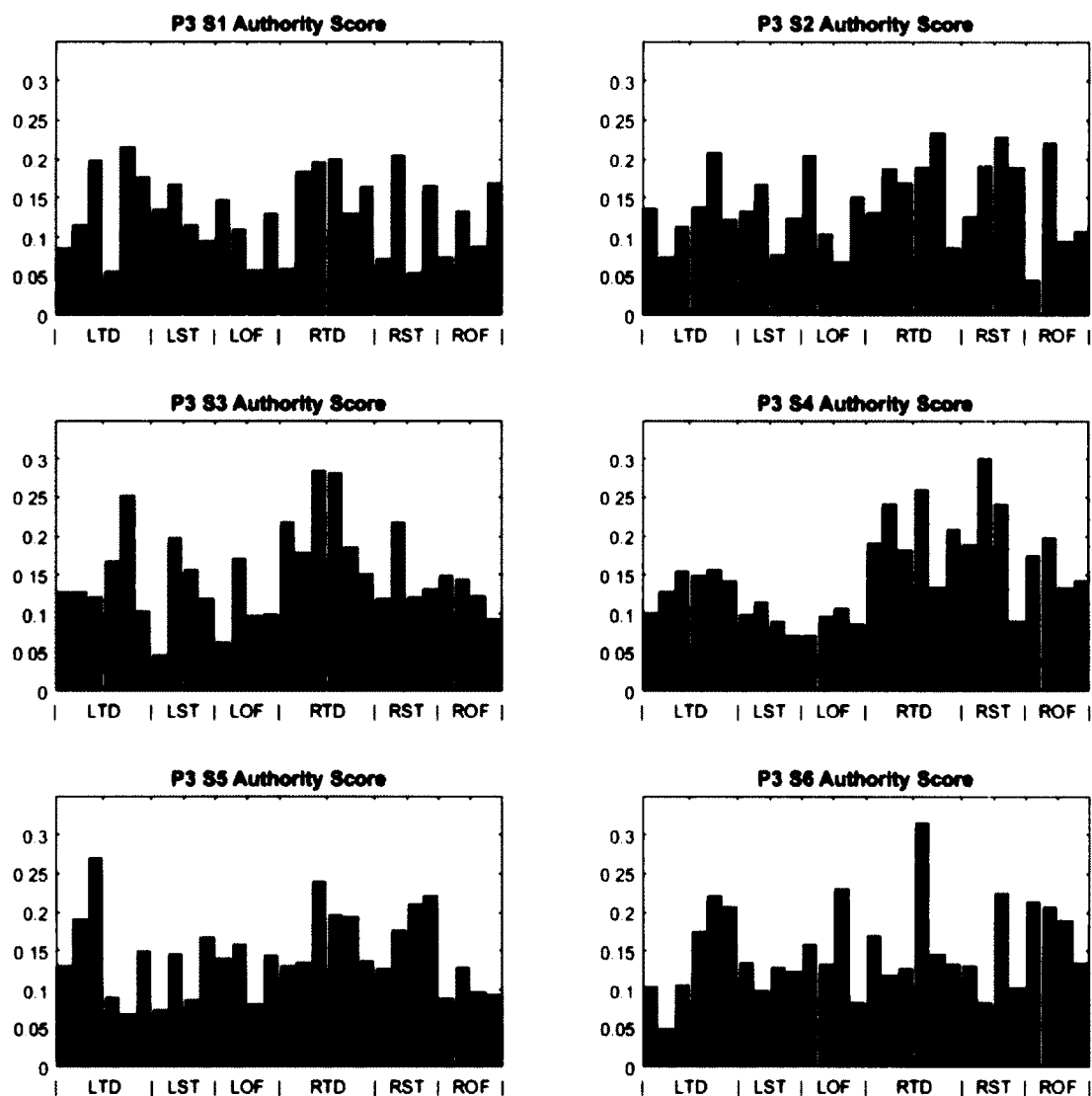
Figure 4-9: Authority scores averaged over the γ frequency band over the first three epochs for the six seizures analyzed for patient P3. Red bars represent the electrodes located within the epileptogenic focus, and the bar with green stripes is the electrode have maximum authority score.

Since only three of the six seizures had maximum values located within the focal

region of patient P3, challenges arise when using absolute majority voting as described in

Subsection 3.11.1. Using this approach, more than half of the seizures must have the

maximum value within the focal region. Therefore, for patient P3, authority score using

early ictal epochs at the γ frequency band would fail to localize the focus. However, if

the authority scores for each seizure are averaged (i.e. $C_{Auth,3}(\gamma, T_{start})$), as seen in

Figure 4-10, the maximum value occurs on one of the focal electrodes, and, in this case,

the focus would be localized under the given parameters for patient P3.
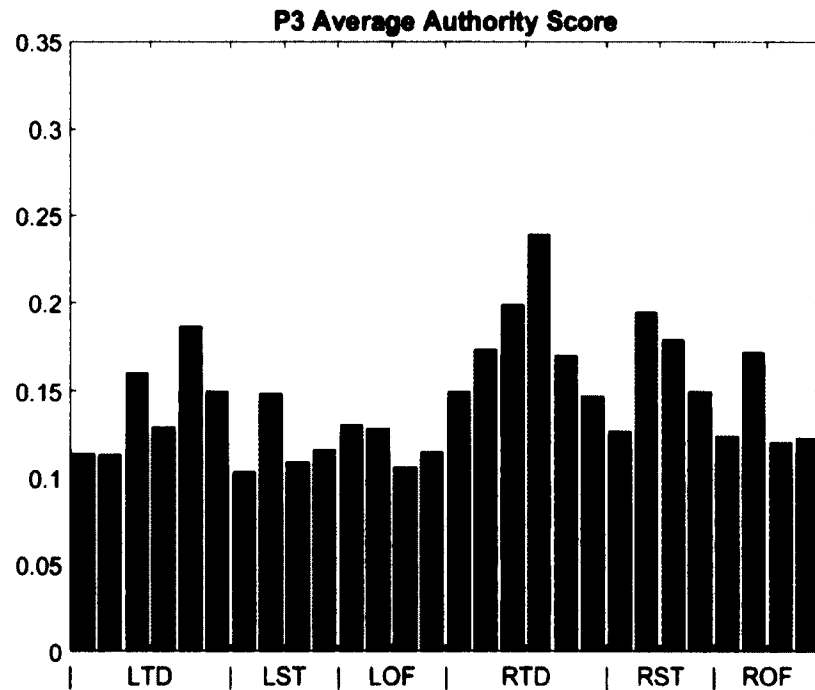
Figure 4-10: Authority score averaged for each seizure of patient P3 where the authority score of each seizure is averaged for the γ frequency band over the first three epochs of each seizure.

4.5 Undirected Networks

All of the centrality measures observed until this point come from directed

networks, but undirected networks were also considered during this research, because of

the complementary behavior between inward and outward degree seen in seizures shown

in Figure 4-3, Figure 4-11 shows the (undirected) degree centrality over time for the same

set of seizures used in Figure 4-3 (P7 seizure #21, P5 seizure #7, and P1 seizure #22) at

an EEG frequency of 30Hz. Using degree centrality, the seizure from patient P7 (top

panel) still shows changes in centrality behavior over time. However, this change in

behavior seems to occur over all electrodes simultaneously, so deciphering unique

qualities of the focal electrodes is unlikely. Like patient P7, the seizure from P5 also

shows dynamic changes, but the change occurs again over all electrodes simultaneously,

so focus localization from these results is difficult. Lastly, the seizure presented for

patient P1 shows no relevant changes in behavior over time or electrode. Each of these

images is in essence a combination of the inward and outward degree centralities shown

in Figure 4-3, and therefore no characteristic qualities over time are found that could

reveal the epileptogenic focus from these seizures.
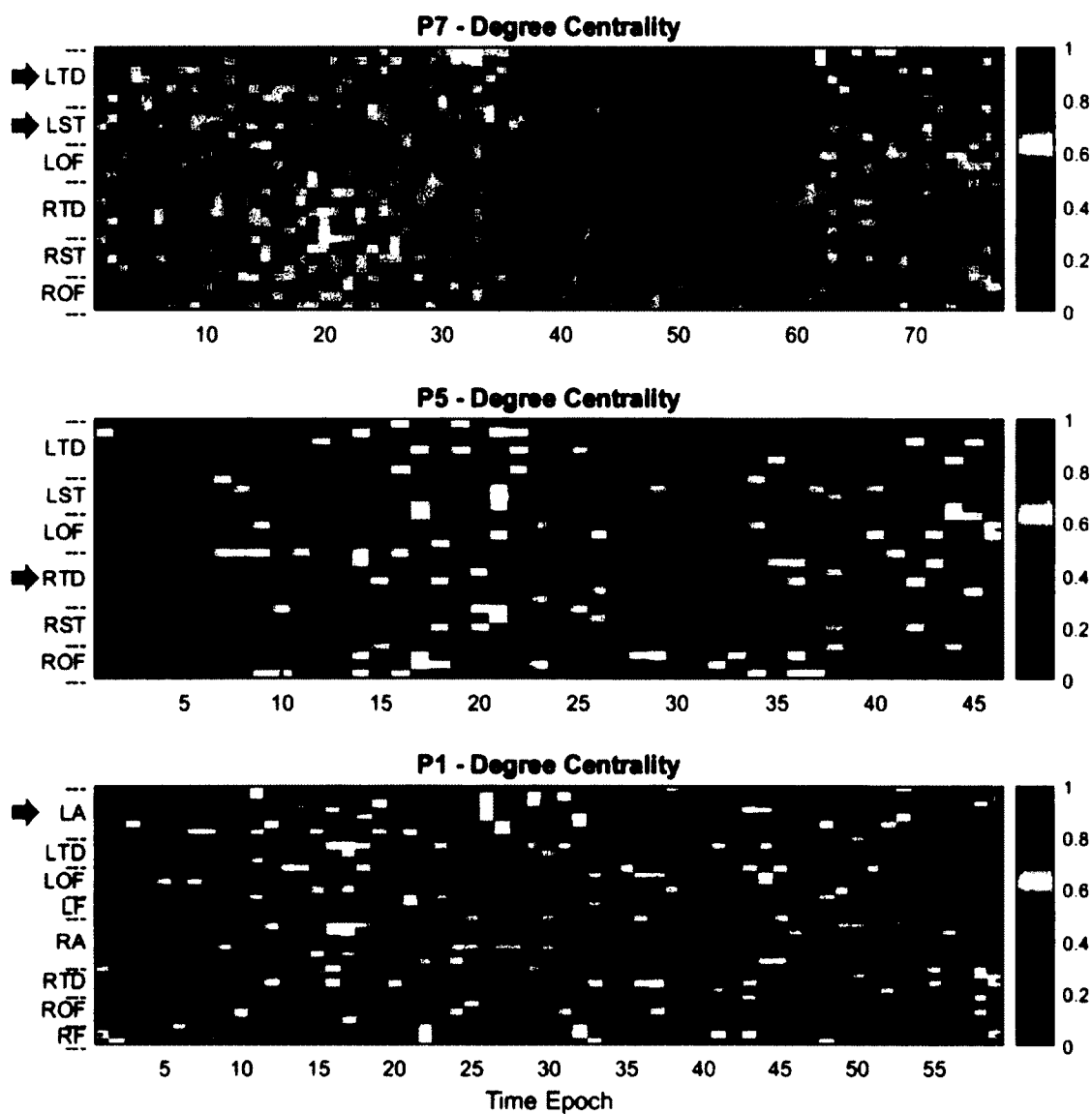
Figure 4-11: Degree centrality values estimated over the full ictal periods in clinical seizures from (Top Panels) patient P7 seizure #21, (Middle Panels) patient P5 seizure #7, and (Bottom Panels) patient P1 seizure #22. Illustrated values of centralities were normalized with respect to their maximum per seizure for visualization purposes.

Figure 4-12 shows the degree centrality of the networks over all analyzed frequencies taken from the first epoch of the seizures used in Figure 4-11. When observing the degree centrality over frequencies, higher centrality values seem more associated with the focal electrodes at higher frequencies, as seen in the seizures from patient P7 and P1 but not in P5.
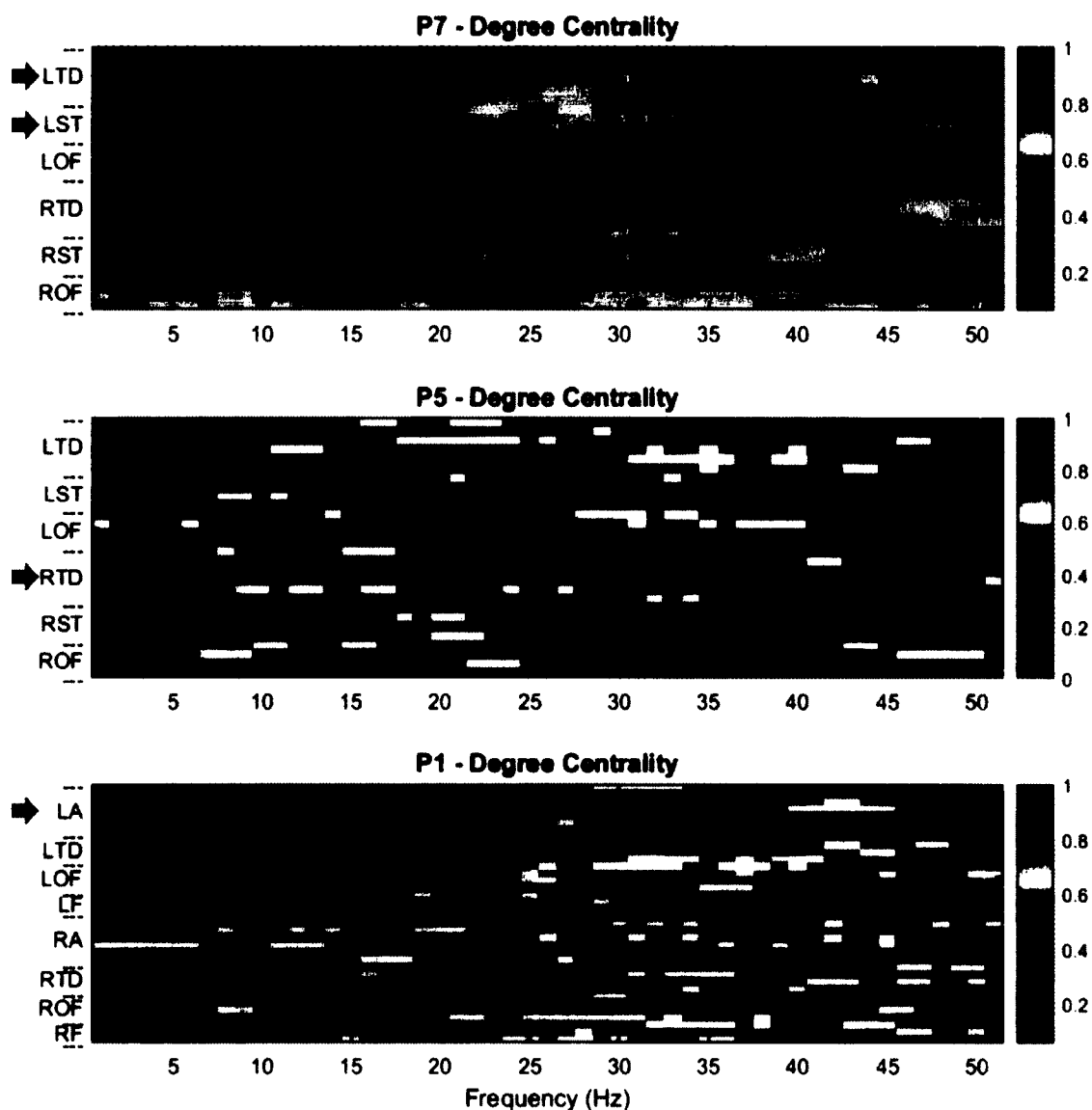
Figure 4-12: Degree centrality values estimated over frequencies 0Hz to 50Hz from the first epoch of recorded in clinical seizures from (Top Panels) patient P7 seizure #21, (Middle Panels) patient P5 seizure #7, and (Bottom Panels) patient P1 seizure #22. Illustrated values of centralities were normalized with respect to their maximum per seizure for visualization purposes.

To summarize the undirected centralities and determine how successful an undirected centrality metric is at localizing the focus, centrality values were estimated per epoch and averaged over all epochs for the duration of each seizure (total ictal) and all frequencies within the traditional EEG frequency bands (δ: 1-4Hz, θ: 5-8Hz, α: 9-12Hz,

β: 13-30Hz, γ: 31-50Hz). Using the majority voting approach for selection and all 127

seizures, if more than 50% of the seizures from a given patient had the maximum average

centrality value in a frequency band associated with the clinically assessed focus, that

centrality metric was declared to have successfully localized the epileptogenic focus for

that patient at that frequency band. Table 4-1 shows the number of patients (out of nine)

with foci associated with maximum centrality values for each frequency band for the

degree (DC), eigenvector (EVC), Katz (KC), PageRank (PRC), and betweeenness (BC)

centrality metrics. The best results were obtained for Katz Centrality in the θ band, where

eight out of nine patients had their clinically assessed foci corresponding to the nodes

having maximum Katz centrality in more than half of their seizures. The second best was

degree centrality in the γ band and eigenvector centrality in the θ band (agreement with

the focus in seven out of the nine patients). PageRank and betweenness centrality showed

at most six out of nine patients having an association between the region with maximum

centrality values and the clinically assessed focus.

TABLE 4-1: NUMBER OF PATIENT (OUT OF NINE) WHOSE FOCI EXHIBITED
MAXIMUM VALUE OF CENTRALITY IN MORE THAN 50% OF THEIR SEIZURES
USING UNDIRECTED CENTRALITY MEASURES

Frequency Bands	Undirected Centrality Measures				
	DC	EVC	KC	PRC	BC
Delta	6	6	6	6	6
Theta	6	7	8	6	6
Alpha	5	4	4	4	3
Beta	5	3	6	5	4
Gamma	7	6	6	6	6

To compare to the success of directed centrality measures, Table 4-2 shows the

success of directed centrality measures under the same parameters. The best results

shown in this table come from betweenness centrality averaged over the δ frequency band where eight out of nine patients had more than 50% of seizures exhibiting maximum value on one of the focal electrodes. For inward based degree, eigenvector, Katz and betweenness centrality, five instances occurred where seven out of nine patients had maximum centrality associated with the epileptogenic focus.

TABLE 4-2: NUMBER OF PATIENTS (OUT OF NINE) WHOSE FOCI EXHIBITED MAXIMUM VALUE OF CENTRALITY IN MORE THAN 50% OF THEIR SEIZURES USING DIRECTED CENTRALITY MEASURES

Frequency Bands	Directed Centrality Measures								
	DC		EVC		KC		PRC		BC
	In	Out	In	Out	In	Out	In	Out	
Delta	5	6	6	5	4	3	3	5	8
Theta	5	5	6	5	7	5	4	3	7
Alpha	6	3	6	3	6	3	4	4	5
Beta	5	2	5	1	4	1	6	1	5
Gamma	7	4	7	3	7	3	6	3	5

Compared to undirected centrality measures, the results of directed measures do not seem to improve the success of centrality measures for localizing the focus. However, it is important to note that the success of inward and outward centrality measures is mutually exclusive, meaning that for a given patient at a given frequency band, either one, both, or neither directional centrality may localize the focus. Therefore, directed centralities may work better than undirected centralities if both inward and outward measures are considered simultaneously, something that is shown in Table 4-3 using the same parameters as the two previous tables (betweenness centrality was included for consistency). Here, results are vastly improved over undirected centrality measures with maximum success (nine out of nine patients) occurring using directed degree centralities

over the δ frequency band. However, combining both inward and outward centralities

create new problems which must be solved before reasonable implementation could

occur. In particular, more research must be focused on a technique for selecting which

directional metric should be used per patient. This is important because, in practice,

inward and outward centrality metrics may determine that the focus exists in two

different brain regions, and without a technique for selecting which directional centrality

to use, the focal region will remain undetermined. Therefore, although the results of

Table 4-3 are promising for using centralities for focus localization, here they are to

support the idea that directed centralities outperform undirected centralities for focus

localization.

TABLE 4-3: NUMBER OF PATIENTS (OUT OF NINE) WHOSE FOCI EXHIBITED
MAXIMUM VALUE OF CENTRALITY IN MORE THAN 50% OF THEIR SEIZURES
USING COMBINED DIRECTED CENTRALITY MEASURES

Frequency Bands	Combined Directed Centrality Measures				
	DC	EVC	KC	PRC	BC
Delta	9	8	6	6	8
Theta	7	7	8	5	7
Alpha	8	7	8	8	5
Beta	6	6	5	7	5
Gamma	8	8	8	8	5

4.6 Subclinical Seizures

In the previous section, the success of undirected networks was determined based

on all 127 analyzed seizures. However, among these 127 seizures there exists a class of

seizures, known as subclinical seizures, that present clear epileptiform activity recorded

onto the EEG but the patient shows no clinical change in behavior. Also, not all patients

exhibit subclinical seizures, so localization of the epileptogenic focus is primarily

determined using their clinical seizures. Because 35 of the 127 analyzed seizures were deemed subclinical events (see Table 3-1), it was important to determine whether subclinical seizures will help localize the epileptogenic focus using the techniques presented herein.

Figure 4-13 provides examples of the inward and outward degree centrality measures, taken from an EEG frequency of 30Hz, from three subclinical seizures coming from patients P2, P5, and P8. Patient P2 (top panels) has an epileptogenic focus covering electrodes in both the right amygdala (RA) and hippocampal (RTD) regions. Here, inward degree centrality is elevated briefly in the focal region during the middle of the event, and outward degree centrality remains elevated over the whole event with maximum values occurring sporadically for the majority of electrodes. Patient P5 (middle panel; focus RTD) presents no elevated or particularly interesting values for any electrode in either inward or outward degree centralities. For patient P8 (bottom panel), slightly more elevated inward degree centrality is present in the right hemisphere electrodes, ipsilateral to the focus (right hippocampus – RTD), and outward degree values remain consistently elevated in the right subtemporal (RST) electrodes, but neither measure provides sufficient evidence of the focal region. Overall, subclinical seizures do not have the same dynamic behavior as observed in clinical seizures, tending to behave consistently for the duration of the event.
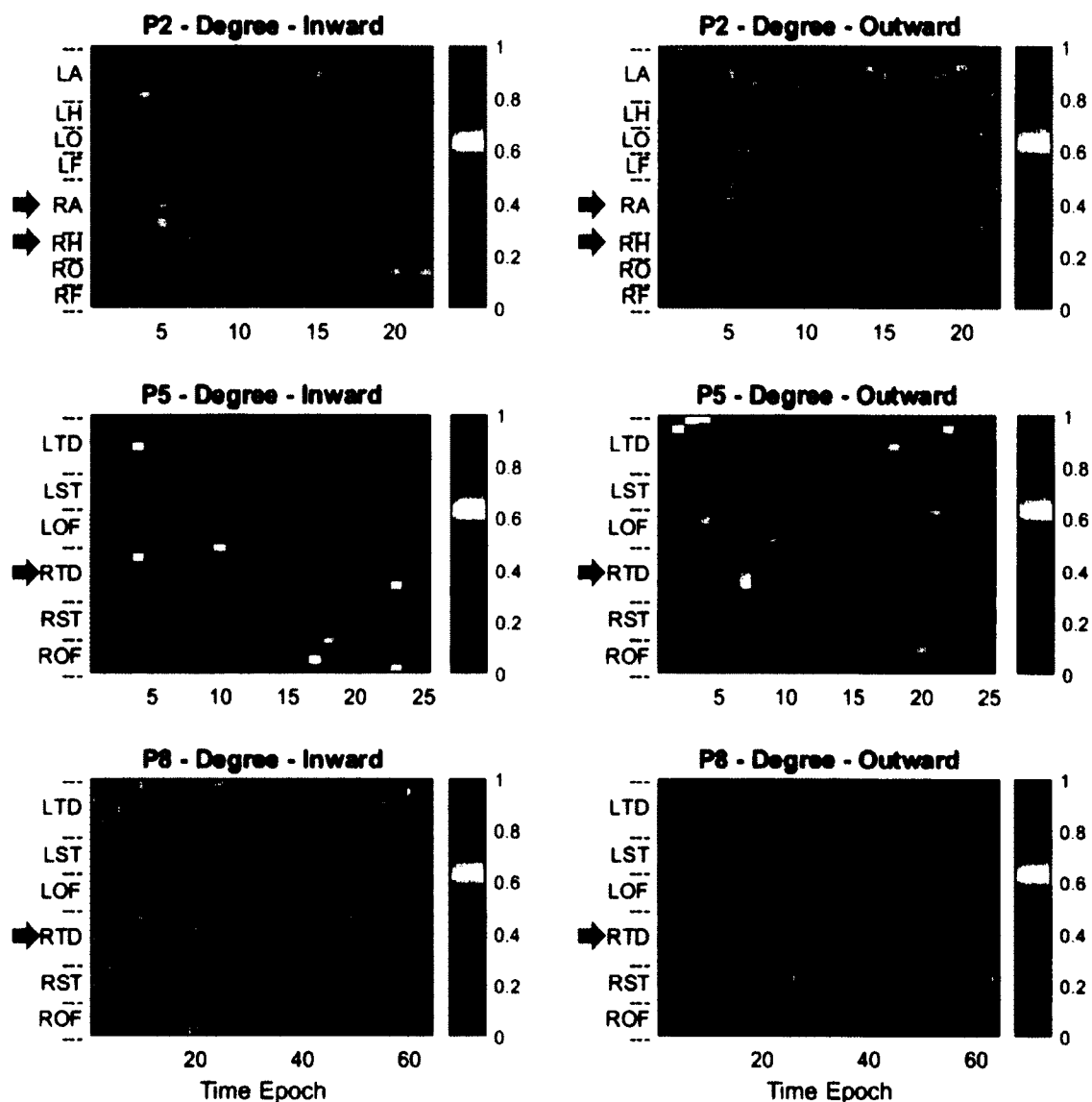
Figure 4-13: Degree centrality values estimated over the full ictal periods in subclinical seizures from (Top Panels) patient P2 seizure #3, (Middle Panels) patient P5 seizure #8, and (Bottom Panels) patient P8 seizure #15. The respective brain networks were created from GPDC values estimated at the discrete frequency of 30 Hz over three second non-overlapping EEG epochs throughout the ictal period of the seizures. Illustrated values of centralities were normalized with respect to their maximum per seizure for visualization purposes.

To observe the behavior of subclinical seizures for different frequencies, Figure 4-14 shows the behavior of the seizures seen in Figure 4-13 as observed from the first epoch of each ictal events. Patient P2 shows increasing inward and outward centrality

values as frequency increases; patient P5 has sporadic increases in both inward and

outward degree centrality across frequencies; and, patient P8 shows elevated inward

degree centrality values present across frequencies in the left hemisphere and high

outward degree centrality seen in the right subtemporal (RST) brain region for higher

frequencies (β and γ frequencies). Again, using these research methodology, subclinical

seizures do not seem to provide supporting evidence of the location of the epileptogenic

focus.
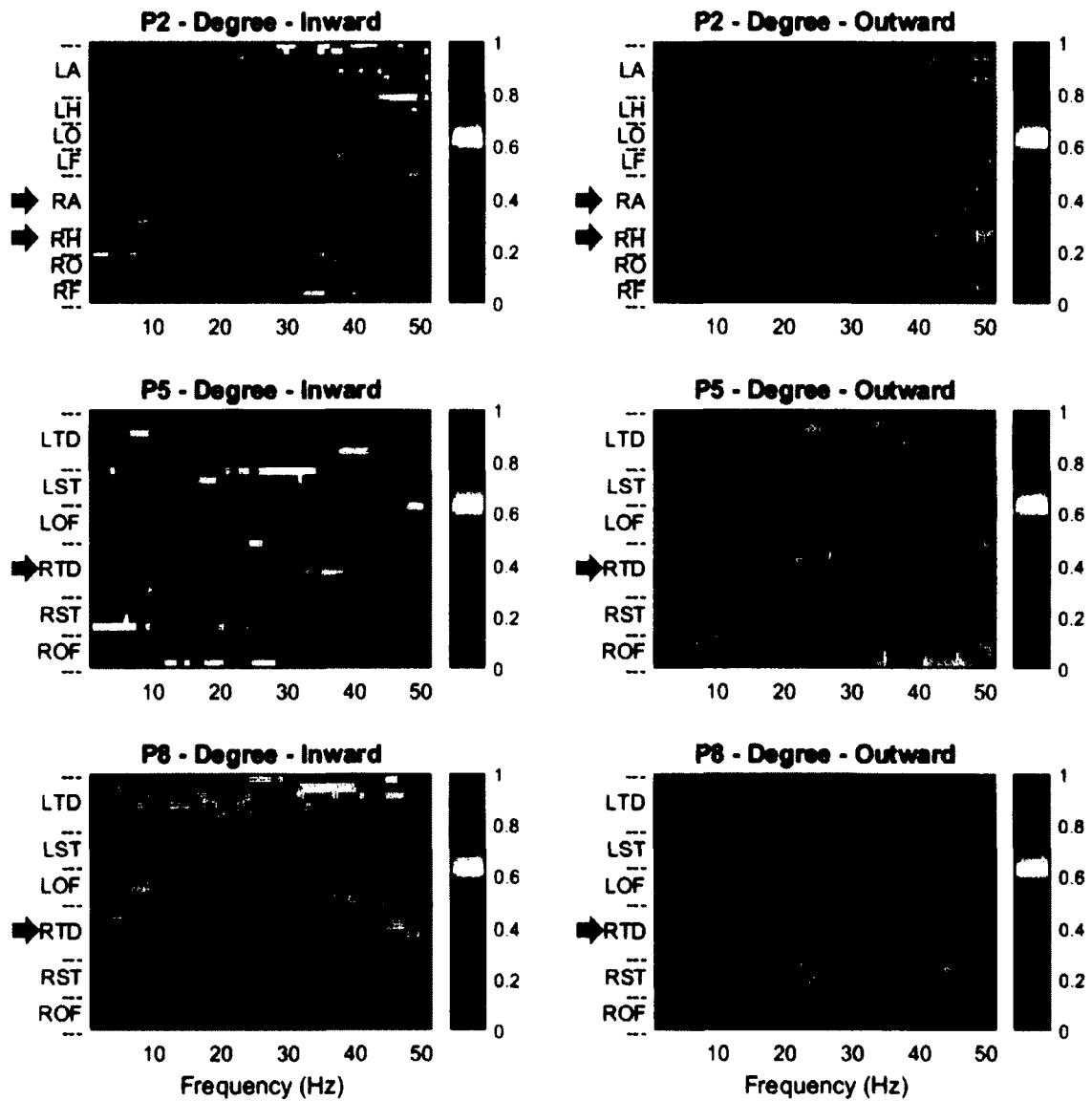
Figure 4-14: Degree centrality values estimated over all analyzed frequencies for subclinical seizures from (Top Panels) patient P2 seizure #3, (Middle Panels) patient P5 seizure #8, and (Bottom Panels) patient P8 seizure #15. The respective brain networks were created from GPDC values estimated on the first three second non-overlapping EEG epochs of each ictal event. Illustrated values of centralities were normalized with respect to their maximum over all frequencies for visualization purposes.

Lastly, to show that not only do subclinical seizures provide no supporting evidence as to the location of the epileptogenic focus but also hinder focus localization, Table 4-4 and Table 4-5 were generated. To create these tables, directed centrality metrics were estimated for the total ictal period as well as for the traditional EEG

frequency bands. Then, for each patient, the average centrality for each seizure was averaged over all seizures of a given patient to provide a grand average centrality for that patient. If the maximum value of this grand average centrality was observed for one of the electrodes within the epileptogenic focus for a given patient, that measure, for the given frequency band, was considered to successfully localize that patient's focus. Hence, these tables provide the number of patients whose focus was successfully localized. Table 4-4 shows the success of each centrality when all seizure events, clinical and subclinical, are averaged in each patient. Table 4-5 is the success of each centrality when only clinical events are considered.

In Table 4-4, eight out of nine patients had maximum averaged centrality in a focal electrode with Katz Centrality (KC) in the γ band, authority score (Auth) in the α band, and betweenness centrality (BC) in the δ band. The next best results (seven out of nine) came from using the inward forms of degree (DC), eigenvector (EVC), PageRank (PRC), HITS, and harmonic (HC) centralities. For outward directed centralities, the best results came from degree centrality in the θ frequency band (5Hz to 8Hz).

TABLE 4-4: NUMBER OF PATIENTS (OUT OF NINE) WHOSE FOCI EXHIBITED MAXIMUM VALUE AFTER AVERAGING CENTRALITIES ACROSS ALL SEIZURES OF EACH PATIENT FOR THE TOTAL ICTAL PERIOD

	Directed Centrality Measures											
Frequency	DC		EVC		KC		PRC		HITS		HC		BC
Bands	In	Out	In	Out	In	Out	In	Out	Auth	Hub	In	Out	
Delta	6	5	7	5	3	2	7	5	6	5	7	5	8
Theta	6	6	6	5	4	2	7	5	6	4	7	3	6
Alpha	7	3	7	3	5	1	6	3	8	4	6	3	6
Beta	6	2	7	2	6	1	4	3	6	2	6	2	6
Gamma	7	3	7	4	8	4	6	3	7	4	7	3	6

Table 4-5 contained the first result where all nine patients had a focal electrode

associated with maximum centrality value, which occurred using betweenness centrality

over the δ frequency band (1Hz to 4Hz). This was an encouraging result as it supported

the idea that centrality metrics may be useful for accurately and objectively localizing the

epileptogenic focus. When using only clinical seizures 18 different measures showed

improved results compared to when all seizures were used. In 11 instances, using all

seizures lead to improved results, however, 9 of the 11 results only lead to a maximum of

six patients with accurately localized foci; the remaining two were from the measures

where eight of nine foci were accurately localized (inward Katz and Authority scores).

TABLE 4-5: NUMBER OF PATIENTS (OUT OF NINE) WHOSE FOCI EXHIBITED
MAXIMUM VALUE AFTER AVERAGING CENTRALITIES USING ONLY THE
CLINICAL SEIZURES OF EACH PATIENT FOR THE TOTAL ICTAL PERIOD.

	Directed Centrality Measures											
Frequency	DC		EVC		KC		PRC		HITS		HC		BC
Bands	In	Out	In	Out	In	Out	In	Out	Auth	Hub	In	Out	
Delta	6	5	7	4	4	2	7	5	6	5	7	5	9
Theta	6	5	6	4	4	2	7	4	5	4	7	3	8
Alpha	7	3	7	3	6	1	6	3	7	2	6	3	6
Beta	7	2	7	2	7	1	6	2	5	2	7	2	7
Gamma	7	5	8	5	7	3	7	5	8	5	7	4	7

Overall, it seems that using only clinical seizures improved the success of inward

based centralities for localizing the epileptogenic focus. Furthermore, removal of

subclinical seizures resulted in the first instance where a given centrality measure

successfully localized the epileptogenic focus in all nine patients, ultimately leading to

the removal of subclinical seizures when trying to determine the epileptogenic focus.

4.7 Final Results

In the previous subsection, overall results have only been shown where centralities were averaged across the entire ictal period. For each seizure this duration can vary, and as seen in previous results, dynamic behavior across the seizure can lead to averaging data that may not be related to the actual activity of epileptogenic focus. The second averaging scheme, denoted "early ictal" or T_{start}, uses only the first three epochs of each seizure, equivalent to nine seconds of seizure data, to localize the focus.

Figure 4-15 shows the $C_{Auth,P}(\gamma, T_{start})$ grand average authority score per electrode for all patients P1-P9 where individual centralities estimated over the γ frequency band per epoch were averaged over the first three epochs of each seizure and across clinical seizures per patient. We observe that for each patient, the site with the highest grand average of authority score was located within the clinically assessed focus. Appendix B provides similar figures for each centrality measure at each frequency band.
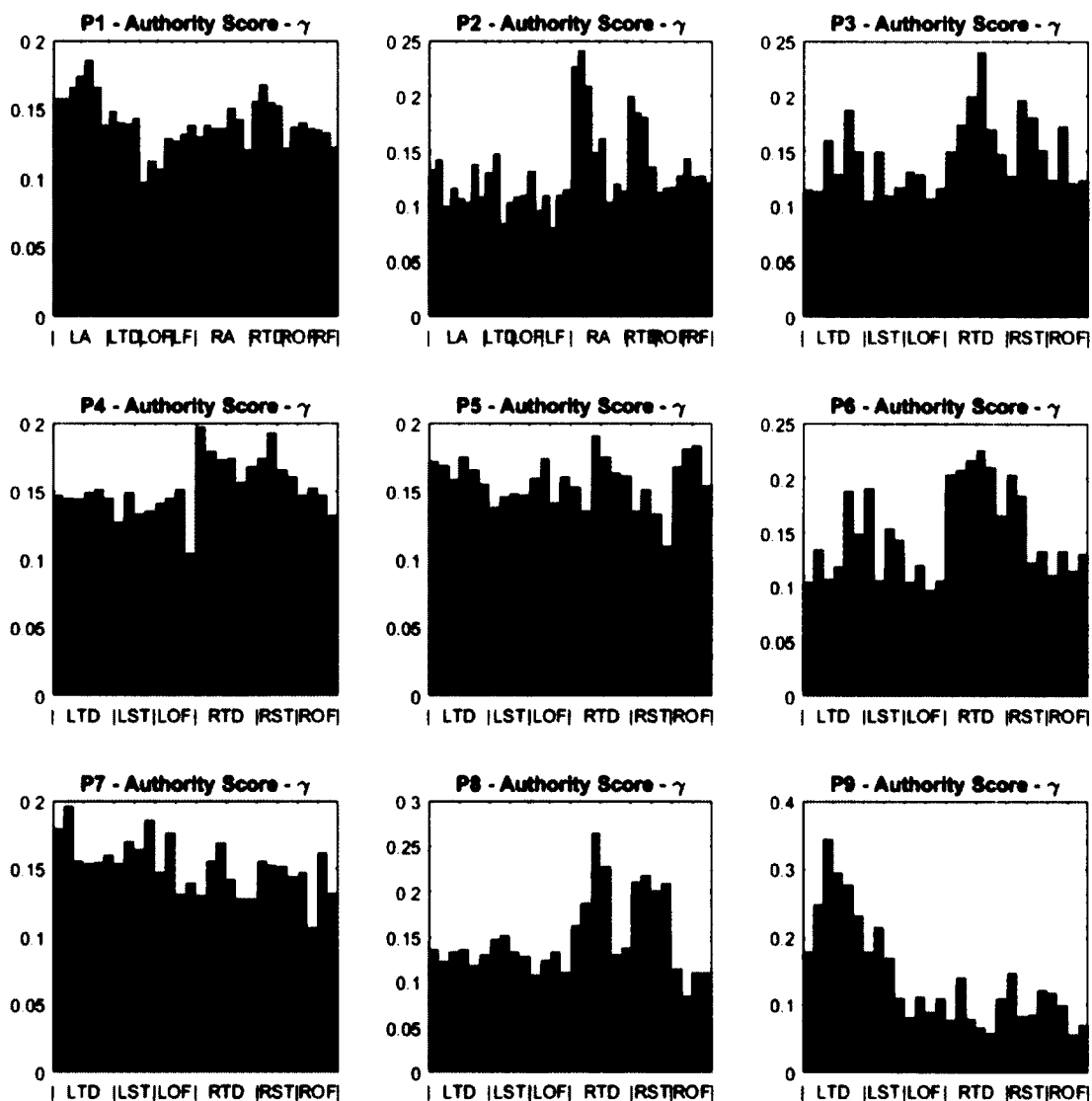
Figure 4-15: Authority scores estimated from all clinical seizures for each of nine patients with temporal lobe epilepsy.

The results of the above analysis for all different inward and outward centrality measures employed per EEG frequency band and per patient are summarized in Table 4-6. For all patients, all inward-based centrality metrics, except for the inward degree and PageRank centralities, estimated in the γ band had the brain site that exhibited maximum grand average centrality value located within the clinically assessed epileptogenic focal region. The betweenness centrality metric had brain sites with maximum centrality value

associated with focal regions after averaging over θ and γ frequency bands in eight out of

nine patients. Inward degree in the γ band and hub scores in the α band provided the next

best results, having maximum grand average centrality values associated with the focal

region in seven of nine patients. Outward centrality metrics had maximum values found

within the epileptogenic focus in at most six of nine patients.

TABLE 4-6: NUMBER OF PATIENTS (OUT OF NINE) WHOSE FOCI EXHIBITED MAXIMUM VALUE AFTER AVERAGING CENTRALITIES USING ONLY THE CLINICAL SEIZURES OF EACH PATIENT FOR THE EARLY ICTAL PERIOD.

Frequency Bands	Directed Centrality Measures											
	DC		EVC		KC		PRC		HITS		HC		BC
	In	Out	In	Out	In	Out	In	Out	Auth	Hub	In	Out	
Delta	2	5	5	3	3	3	3	2	4	3	3	2	4
Theta	4	6	6	5	4	3	3	6	5	6	4	6	8
Alpha	5	6	6	6	5	6	6	3	6	7	4	5	4
Beta	5	4	5	2	5	4	5	4	5	4	6	2	4
Gamma	7	5	9	6	9	6	5	5	9	6	9	6	8

Considering a binomial distribution where a centrality metric either does or does

not localize the focus in a patient and given the number of analyzed electrodes used in each

setup, the probability of correctly localizing the focus purely by chance in all nine patients

is $p = 2.017 \times 10^{-6}$. This probability value was found by taking the product of the ratios

of the number of the clinically assessed focal electrodes over the number of total electrodes

analyzed per patient. Furthermore, the result of correctly identifying the focus in nine out

of nine patients corresponds to a Jeffrey's 95% confidence interval of $(76.2, 100)\%$. [55],

meaning that if this methodology was replicated under the same parameters, 95% of the

replications should have success rates of at least 76.2%.

CHAPTER 5

DISCUSSION

5.1 Conclusions

In this research investigation a novel framework for an objective and robust

analysis of the ictal iEEG for localization of the epileptogenic focus in patients with

epilepsy was developed. In particular, the measure of Generalized Partial Directed

Coherence was employed to estimate the strength of the directional interactions between

brain sites, selecting only the statistically significant interactions via surrogate data

analysis. Centrality metrics were then measured from the constructed epileptic networks

from a total of 127 epileptic seizures in nine patients with focal (temporal lobe) epilepsy.

From the results provided, several conclusions can be derived.

First, many clinical seizures present dynamic behavior over both time and

frequency domains per brain site, and different dynamic behaviors are seen across

seizures even in the same patient. To account for this dynamic behavior and reduce the

presented variability, centrality values per brain site were averaged over predetermined

time epochs and frequency bands for a given seizure, and focus localization results from

seizures for a given patient were either averaged or underwent a majority voting scheme

to evaluate the potential of a centrality metric to conclusively localize the focus in each

patient.

Second, both directed and undirected networks were derived from GPDC.

Although undirected networks did show dynamic behavior over time and frequency, they

did not provide clear centrality distinctions between focal and non-focal electrodes over time epochs but showed potential localization in certain frequency bands. When undirected centralities were compared to their directed centrality counterparts under the majority voting scheme, no individual directed centrality seemed to produce more promising results. However, when inward and outward centralities were taken together, directed centralities generally outpaced undirected centralities by a large margin.

Third, because 35 of the 127 seizures analyzed were subclinical seizures, it was important to determine if these seizures were also useful for focus localization. The centrality metrics taken over subclinical seizures did not present dynamic behavior over time, but centrality metrics per brain site did change over the frequency domain. However, the removal of subclinical seizures did markedly improve focus localization results.

Fourth, averaging schemes were considered over two sets of epochs, the entire set of epochs for each ictal event and the first three epochs from each ictal event. Considering only the early ictal epochs led to the best localization results where it was found that, during the early ictal period up to nine seconds after seizure onset, the epileptogenic focus in all patients exhibited inward-type centralities in the high frequency (γ) band.

5.2 Relationship to Clinical/Neurophysiological Evidence

It is widely accepted that the mechanism behind generation of seizures is related to intermittent hyperexcitation of the epileptogenic focus [56]. This hyperexcitation may be due to increased excitation from excitatory neurons, reduction in the activation of inhibitory neurons, or reduced activation of intermediate excitatory/inhibitory neurons

that control inhibitory/excitatory neurons, respectively [57], [58]. The focal region, being unstable, responds abnormally to excessive input activity from other brain regions, and may then manifest erratic behavior (seizures, interictal epileptiform activity, etc.). If the epileptogenic focus is "over-reacting" to input activity from other brain regions or, in other words, if inputs from other brain sites have a great (destabilizing) effect on the focus, its inward centrality will be elevated with respect to the one of other brain sites, especially at seizure onset. Alternatively, and given that focal seizures are believed to not occur abruptly but typically after a prolonged preictal period of minutes to hours [59], [60], the observed high values of inward centrality at the beginning of seizures in the focus area may be due to the last "effort" of its "surrounding at large" area to keep it under control in a similar scheme described in [61]–[64]. Furthermore, the presence of enhanced activity in the frequency ranges above 20Hz at the time of seizure onset has been previously documented [58], [65], [66]. Our findings of elevated inward centrality values in the focal region, especially in the high frequency band and the beginning of seizures, are in agreement with the above scenarios and those prior frequency-related findings.

5.3 Comparison to Other Epilepsy Research using Brain Connectivity Analysis

Studying epilepsy using brain connectivity analysis has been a major focus in the last decade, approaching the problem from many directions. For example, in order to understand the connectivity of the brain in patients with temporal lobe epilepsy having epileptogenic foci in either the left or right hemisphere, James et al. [67] studied fMRI data from 23 control participants, seven patients with left-sided epileptogenic foci, and eight patients with right-sided epileptogenic foci. In this study, voxels of fMRI data taken

from participants in a wakeful resting state were subdivided into anatomical brain regions

of interest (ROI) to determine any differences present in the default mode network

(DMN) of each test group, using the ROI as the nodes of the generated DMN. Through

this process it was found that left and right focal patients had lower connectivity between

regions of interest compared to healthy participants. In particular, they found that patients

had reduced connectivity between the hippocampus and parahippocampus in the

hemisphere associated with the epileptogenic focus. Although this approach allowed for

the focus to be lateralized to a single hemisphere with some degree of certainty, our

method successfully not only lateralized but localized the focus.

In 2012, Tang et al. analyzed iEEG data using visibility graphs [68] and graph

index complexity (GIC) [69] and found that GIC values were comparatively higher in

signals associated with the epileptogenic focus [70]. This research took a different

approach to the problem, treating each data point of a signal as a node in a graph, with the

GIC measuring connectivity complexity of each signal to itself, ignoring interactions

between multiple signals. Although this nonlinear approach did localize the focus in a

very limited pool of patients, this would not necessarily be considered brain connectivity

analysis in the classical definition since interactions between brain regions was not

considered, only the complexity at each brain site.

In an article published in 2014 by Burns et al. the dynamic behavior of seizure

events were closely studied using graph theoretic techniques on iEEG data taken before,

during, and after seizure events [32]. Using modifications to the coherence measure,

weighted-undirected networks were generated over three second epochs, and the

eigenvector centrality of each node was estimated. Then, K-means clustering grouped the

centrality metrics over time, identifying multiple distinct brain states occurring over the entire seizure event. Through this research it was discovered that the brain undergoes a relatively consistent sequence of brain states and that a subset of nodes in the network associated with the epileptogenic focus are more isolated at the beginning of the seizure event and grow increasingly connected towards seizure termination, which is in agreement with part of our own findings concerning the dynamic behavior seen in several clinical seizures in our dataset.

Determining the network via a connectivity measure and then analyzing the network relative to the epileptogenic focus has been applied before. In 2009, Wilke et al. used the connectivity measure Directed Transfer Function (DTF) on multivariate iEEG data from two patients with neocortical-onset epilepsy and found a correlation between the out-degree measured over ictal data and the clinical foci [29]. In their research, DTF was used to produce weighted-directed networks from six-second epochs of the ictal data, and for both patients, only the 200 strongest connections were considered when finding the out-degree (commonly denoted the 'outward strength' when using weighted networks). Using the 200 strongest connections can be problematic. First, the two patients used in this study had different numbers of electrodes used in their analysis with one patient having 32 electrodes (992 possible connections) and the other 56 electrodes (3080 possible connections), meaning a larger percentage of connections are considered when calculating the out-degree in the first patient. Second, choosing the 200 strongest connections is an arbitrary approach to generate the network. Instead, using an adaptive thresholding technique such as the surrogate data analysis used in our research ensures that only significant connections are considered when analyzing the networks.

In 2011, Wilke et al. published results of their continued research into focus localization for patients with neocortical-onset epilepsy, expanding their data to 25 patients, but instead chose to analyze the estimated networks using betweenness centrality. Through this study, they found a decrease in betweenness centrality in the epileptogenic focus over the course of the seizure in frequency spectra above 3Hz [71]. Again, DTF estimated networks were used to generate weighted-directed networks, but here, the inverse of the DTF estimates were used to estimate betweenness centrality based on the notion that higher DTF connection strengths are associated with shorter path lengths. In that investigation, they chose to use the top 5% strongest connections produced from DTF estimation, which is an improvement over the arbitrary 200 strongest connections, but an adaptive thresholding technique could provide more accurate results. In our research, networks were generated from GPDC in the delta frequency band as well, which is where the maximum betweenness centrality averaged over the entire ictal period correlated to the epileptogenic focus.

In 2013, van Mierlo et al. published similar focus localization results, showing that out-degree estimated from brain networks generated from a modified DTF were highest in regions associated with the epileptogenic focus [31]. Spectrum-weighted adaptive directed transfer function (swADTF) was estimated using time-variant autoregressive (TVAR) models from epochs starting five seconds prior to seizure onset to 20 seconds into the seizure event. One advantage of their technique is that TVAR models allow networks to be generated for every time point. However, obtaining accurate results from this approach requires large amounts of data. Furthermore, this research chose to obtain swADTF values by averaging over frequencies from 3Hz to 40Hz, thus losing the

ability to study time and frequency domains simultaneously. Binary-directed networks

were created using an adaptive threshold by comparing the estimated seizure data to 10

randomly chosen 25 second interictal epochs estimated in the same manner. Adaptive

thresholding allows for only significant connections to be considered in the network, but

surrogate data analysis as used in our research determines significant connections using

the data that is to be analyzed, and, therefore, avoids the use of random or arbitrarily

chosen data for the sake of comparison. Similar to our research, correlations between

centrality estimates and the epileptogenic focus are primarily seen in earlier ictal stages.

For most of the above described approaches for focus localization, DTF was used

as the connectivity measure to create networks. Because DTF is a connectivity measure

that also includes both direct and indirect connections, centrality estimates from the

derived networks likely produce different outcomes, which may explain why these

researchers found the high outward directed centrality to be associated with the

epileptogenic focus. Furthermore, two of the above studies used patients with neocortical

epilepsy and the epileptogenic focus being close to the brain surface, whereas our patients

had mesial temporal lobe epilepsy with foci located in deeper brain structures, which

could be another explanation for the differences in results. Lastly, the patients used in our

research had electrodes placed symmetrically in both brain hemispheres, a more objective

measure for focus identification if lateralization is unknown, which was not the case in

the other studies. This could have significant impact on the networks that are generated.

5.4 Challenges of Research

5.4.1 Network Connectedness and Centrality Estimations

For many of the centrality metrics that are related to eigenvalue decomposition of the adjacency matrix used in this research, a structural characteristic known as graph connectedness can influence centrality estimation. This structural characteristic relates to walk traversals throughout the graph. From the perspective of nodes of the graph, node v is said to be reachable from node u if there exists a walk from u to v. For an undirected graph to have a connection, there must exist a walk between every pair of nodes within the graph, or every node must be reachable from any other node. For directed graphs, graph connectedness is divided into two types. A directed graph is weakly connected if the underlying undirected graph is connected, and a directed graph is strongly connected if every node is reachable from every other node in the directed graph; in other words, there exists at least one directed walk from every node u to node v. In matrix terms, the adjacency matrix of connected undirected graphs and strongly connected directed graphs correspond to irreducible matrices, and the eigenvector centrality of such graphs are clearly determined from the Perron-Frobenius Theorem. According to the Perron-Frobenius Theorem, an irreducible $n \times n$ matrix A with nonnegative elements has a real positive eigenvalue λ_1 with multiplicity one and positive corresponding eigenvector, meaning that the matrix has a unique dominant eigenvalue with all positive elements in the eigenvector. However, if the matrix is reducible, these qualities may not hold true. Challenges occur when the multiplicity of the dominant eigenvalue is greater than one, where the eigenvector does not possess the abovementioned qualities, and, therefore, the eigenvector centrality of the underlying network is then ambiguous.

For this research, network connectedness was an issue when measuring certain centralities in networks derived from lower frequencies (within the δ and θ frequency bands). These problems occurred because of a markedly lower edge density compared to higher frequency derived networks. In general, the edge density increased as the frequency used to generate the network was also increased, and, in some cases, networks generated from lower frequency GPDC estimations had too few significant connections to generate a connected network.

In order to solve these issues, a few possible approaches could be taken to alleviate estimation errors. First, a minimum number of connections could be added to the network to make it strongly connected. However, the inclusion of these connections would be artificial, and since each network is created from a methodical rule-set which is meant to represent the connectivity behavior of the brain for a given epoch, inclusion of too many artificial connections breaks down the integrity of what the network represents. Second, the threshold/critical value chosen for the test of significance for edges in the network could be lowered sufficiently such that enough edges arise that make the network strongly connected. However, the amount of reduction needed to bring the critical value low enough to make the network strongly connected is unknown and would be unique for each network, so a consistent critical value for each network would not be feasible. Furthermore, reducing the critical value leads to an increased significance level, therefore, an increase in Type I error would occur, meaning that newly added edges into the network could in fact be false positives from a statistical standpoint. One could argue, however, that determination of the critical value needed to make each network strongly connected could be a metric of brain behavior itself. With these issues arising from

possible solutions to this problem, it may be the case that certain centrality metrics just do not perform ideally under non-ideal connectivity circumstances, which may support the use of spectral centrality metrics such as PageRank centrality and the HITS algorithm which were designed to be used on directed networks. Lastly, with all the centrality estimation issues that may occur, and taking in consideration that the vast majority of generated networks from this methodology did not suffer from these issues, averaging the centralities for each network over time epochs and frequencies should minimize the overall effect of these errors per patient.

5.4.2 Possible Patient Issues

Although a centrality metric was discovered which localized the epileptogenic focus in all nine patients studied, it is a very real possibility that certain issues can occur that were not present in our dataset, particularly different electrode placements and different forms of epilepsy, both of which may drive the need for more patient-specific approaches.

For all nine available patient EEG data, the symmetrically positioned sets of electrodes produced networks with nodes symmetrically spaced throughout the brain. As mentioned in the prepossessing section, whenever one electrode produced signals with a low signal to noise ratio, that signal as well as the signal from the contralateral electrode were removed from our analysis. This was done to ensure that no subset of electrodes dominated the network and produced possible biases during centrality estimation.

One obvious but important requirement for this methodology to succeed is that electrodes must be placed so that at least one electrode is located near the epileptogenic focus. If no electrode is located near the focus, our method will still consider the node

having maximum centrality to be the epileptogenic focus, regardless. Unfortunately, if electrodes are placed away from the focus, our method will not localize the actual focus. Another issue relating to electrode placement, is the use of high density electrodes placed on a region of the brain. If this is the case, more than one spatially close electrodes would likely show higher connectivity. One possible solution could be to consider only a few sparsely distributed electrodes throughout the recorded regions to find the region to focus our attention. Then, the electrodes located in that specific area could be analyzed to gain an improved location of the focus.

All of the patients provided had some type of mesial temporal lobe epilepsy. Because all patients had similar forms of epilepsy, our results may not necessarily be similar if the methodology is applied to patients with other types of epilepsy. This may occur because (1) the neurophysiological behavior of the epileptogenic focus may behave differently when located in other brain regions or (2) since the general location of the epileptogenic focus in Phase I monitoring drives the placement of Phase II intracranial electrodes, electrode placement may be inadequate for our method to succeed. Furthermore, it was found that some patients in our dataset had a stronger tendency to associate the focus with outward centrality measures. This may point to a need to incorporate a patient specific element to our methodology, where the centrality metric used for each patient, or even for each seizure, is determined prior to connectivity analysis. Of course, such a selection process would require a much deeper understanding of the neurophysiological dynamics of each seizure and the type of epilepsy.

5.4.3 <u>The Gold Standard</u>

For epileptic focus localization, the current gold standard, as stated in the introduction, requires a registered EEGer and epileptologist specialist to visually inspect the recorded EEG data and determine which electrode first exhibits initiation of multiple typical seizures in a given patient. Using this information, the epileptologist forms a conclusion as to the location of the epileptogenic focus so that the affecting brain tissue can be resected. Even though our method was able to successfully localize the focus, the location of the focus had to be initially given by the specialist so that our method could be tested and fine-tuned. Therefore, as is currently stands, our method may be able to reach the success rate of the gold standard but cannot surpass it. To determine if this method could prove better than the standard, animal studies would need to be performed where animals are inflicted with some form of epilepsy that can be clearly defined and understood. Then, EEG data could be collected from these test animals, and the accuracy of our method could be compared to the accuracy of the gold standard by double blinded experiments.

5.5 <u>Further Research</u>

One of the most powerful aspects of brain connectivity analysis is its versatility. Making changes to a single part of the methodology or the type of data studied has the potential to produce new and interesting results. Herein, potential research directions will be discussed, including variations to the networks derivation process, different network analysis methods, and other potential techniques that could be applied to this research.

5.5.1 Data

As with any study, the type of data used has a major impact on the type of tools that can be utilized for analysis. Intracranial EEG data, with its high temporal resolution and low spatial resolution, has been thoroughly discussed for epileptic focus localization. However, epilepsy research also includes other aspects, such as seizure detection, seizure prediction, and ictogenesis, all of which could benefit from studies looking at the network structure of the brain. Furthermore, the same research could be tested on different types of epilepsy or even the similar types of epilepsy with different electrode setups.

Due to its noninvasive nature, studies using scalp EEG data could be implemented on larger populations on a wide array of topics. However, the lower signal to noise ratio present in EEG data promotes a big challenge to the researcher. Like scalp EEG data, fMRI data is noninvasive, and the high spatial resolution means that connectivity analysis studies with fMRI can study more precisely brain regions. However, fMRI's low temporal resolution limits certain aspects of brain connectivity research such as analysis in the high frequency domain.

Recently interest has risen for use of magnetoencephalography (MEG) in brain connectivity research since MEG has both high temporal and high spatial resolution. This increased level of resolution in both domains could provide deeper understanding of the dynamics of the brain over many types of functional characteristics. However, in addition to increased cost, movement artifacts are a major factor in MEG data quality, so our analysis within epochs with high quantity of movement artifacts, like a clinical seizure, may not be feasible without appropriate preprocessing of the data.

In principle, any research towards understanding the functional behavior of the brain can employ our techniques of measuring and analyzing brain connectivity,

including Alzheimer's disease, dementia, psychological disorders, or cognitive behaviors like learning and memory.

5.5.2 Network Derivation

To derive a connectivity network, many factors must be considered. In order to decide which connectivity measure to use, the researcher must decide on the use of a linear or nonlinear measure, to consider connections between signals (bivariate case) or all signals simultaneously, direct connections or allow the inclusion of indirect connections, and whether the measure should produce directed or undirected networks. GPDC, for example, is a linear measure considering multivariate connections of all signals to produce directional connectivity networks including only direct connections. DTF is similar to GPDC but also includes indirect connections between nodes. Furthermore, GPDC and DTF fall into a category of measures that require a model such as a multivariate autoregressive model to work, but other models, such as a time variant autoregressive model could be used to generate more networks over time. Nonlinear measures like mutual information, which produces undirected networks, or transfer entropy, which produces directed networks, are only able to consider bivariate interactions between signals, so cascade effects are typically included in these networks. Furthermore, those methods are computationally expensive. When computers and technology advance sufficiently to allow nonlinear methods to be applicable on large datasets and multiple signals, nonlinear connectivity measures may become the standard.

Lastly, more recently developed measures, such as cross frequency coupling (CFC), could be utilized to investigate how brain regions may connect/interact across frequencies.

Thresholding is also an important aspect of network reconstruction. Thresholding the connectivity matrix could be as simple as taking a percentage of the strongest connections or using an adaptive method such surrogate data analysis. Once thresholding is done the retained values of the connectivity matrix can be utilized to produce a weighted network or the retained edges can be simplified into an unweighted network. Of course, it's also possible to not threshold the connectivity matrix and analyze a fully connected weighted network, but this approach would ultimately disregard graph theory concepts.

5.5.3 Measures of a Network

Network analysis is a very large field of study, and many measures have been developed to understand the topological structure of any given network. The choice of network measure typically depends on what is being studied. For this research, centrality estimates were chosen since the desire was to locate a local brain region which is associated with the epileptogenic focus, and, of course, this set of research did not cover every existing centrality measure. A multitude of centrality metrics have been devised across a bevy of fields studying network science, and as these new metrics are defined, they can be embodied in our framework of analysis. Of course, each newly proposed centrality measure should be studied prior to its employment to determine if it makes sense in terms of each application. For example, percolation centrality is a good centrality metric for studying the spread of a disease through networks, but requires weights to be provided for each node in the network.

Centrality metrics measure node importance, but many other graph measures have been created that could study brain networks from different perspectives. For example,

characteristic path length and global efficiency when applied to brain networks will measure brain's integration, and have been used to study how anatomically different brain regions interact to process information. Measures of brain segregation, such as modularity, clustering coefficient, and transitivity, are used to study the clustering behavior that occurs within separate brain regions. Together, the measures of integration and segregation help create an image of the global functional behavior of the brain. Combining the clustering coefficient and characteristic path length of the network provides a measure of the small-world behavior of the brain, providing information about its global topological structure. For epilepsy research, such measures have been used to study the diagnosis of epilepsy, and how the dynamics of global topological behavior can be utilized for seizure detection or prediction. Even for focus localization this approach could be tried. For example, sets of spatially local electrodes could be treated as modules or subsets of the network, and inter-regional and intra-regional behavior of the modules could be studied.

5.5.4 Other Techniques

Additional techniques that one could use to improve or better automate the analytical process also exist. Change detection, or change point analysis, is a technique from time series analysis that locates the points in time where a dynamic system undergoes changes. These methods are commonly used in industrial applications to ensure that the manufacturing process continues to run smoothly. Many papers have been published on this concept for general purposes [72]–[74] as well as specifically for EEG data [75], by extracting specific features from time series data and pinpointing when those features undergo drastic changes using a technique such as cumulative sum

(CUSUM) [76]. In a future extension of our research, change detection could be an effective means of determining the different brain states that occur throughout the seizure event, much like the work performed in [32], however, instead of clustering a given feature of the network over time, these techniques point out the time in which changes occur. With such a method, selection of time windows for averaging relevant subsections of seizure events could be automated and possibly improve the accuracy and recue the variance of focus localization. Furthermore, the actual dynamic behavior of individual seizures per patient could then be more deeply studied.

In recent years, another growing field of network research is temporal network centrality, which considers the importance of network evolution and dynamics of the behavior of a given system [77]-[79]. Although our research allowed for the study of network dynamics, the generation and analysis of network behavior only within specified EEG epochs (e.g. beginning of seizures) constitutes a snapshot of the behavior of the network. The goal of temporal network analysis is to minimize the intrinsic separation that arises between snapshots and, in doing so, provides a more accurate and continuous perspective of the dynamic behavior of the network being studied. With the growing interest in temporal networks, metrics have been devised to better analyze networks under this perspective, and many of which have been adapted from the traditional perspective of networks [80]-[83]. For example, broadcast and receiver centralities are evolutions of the classic Katz centrality modified to consider the importance of a node as its connections change over successive networks, thus measuring node importance through time, a centrality metric that may work for epileptogenic focus localization [81]. In general, many metrics currently use successive snapshots of the network over time but,

as this field of study grows, more connectivity measures will be developed to close the

gap between successive networks, which could potentially lead to a new set of techniques

for the study of seizure dynamics and epileptogenic focus localization.

APPENDIX A

FREQUENCY DEPENDENCE OF FOCAL
LOCALIZATION USING GPDC

Although the majority of this research involved estimations from the ictal events

presented in the EEG datasets, one study was performed that took the entire EEG dataset

into account. In this study, the iEEG recordings from four of the nine patients were

measured using GPDC. Table A-1 provides relevant patient information for this study.

For consistency, the patient labels have remained the same as was in the rest of this

research.

TABLE A-1: PATIENT INFORMATION

Patient	Electrode Setup	Total EEG Recording Duration (hours)	Number of Electrodes Utilized	Clinically Determined Focus/Foci
P1	B	47	40	Left Amygdala (LA)
P2	B	34	40	Right Amygdala (RA) Right Hippocampus (RTD)
P6	A	49	28	Right Hippocampus (RTD)
P7	A	156	28	Left Subtemporal (LST) Left Hippocampus (LTD)

Using 10 second iEEG windows, a VAR model of order $p = 7$ was estimated

using the Vierra-Morf algorithm and GPDC values were estimated for integer frequencies

from 0Hz to 50Hz in the same manner as shown in the methodology. Following

117

estimation of GPDC values between all possible pairs of sites at each frequency, the sum

of inflows (*IF*) from the rest of the sites into a brain site i for successive epochs T of 10

second duration each was estimated per epoch T and frequency f as:

$$IF_i(T, f) = \sum_{j=1, j \neq i}^{n} GPDC_{j \to i}(T, f)$$

where $GPDC_{j \to i}(T, f)$ is the inflow into site i from site j at epoch T and frequency f.

Then, the brain site with the maximum inflow for each epoch T and frequency f was

found. Finally, histograms HIF_i (f) of the percentage of time that each site manifests the

maximum inflow over all epochs T were constructed per frequency f. In previous work

[52], by taking in consideration the full frequency band (i.e. HIF_i not as a function of f),

the brain region that exhibited the most frequent maximum average inflow across the full

frequency band related well with the clinically determined epileptogenic focus.

To ensure the statistical significance of the derived HIF_i (f), the Grubb's test for

outliers [84] was used. Defined under the hypotheses H_0: *no outliers* vs.

H_1: *at least one outlier*, the one-sided test was performed at each frequency across sites

to determine at which particular frequencies a site could be considered as the location of

the epileptogenic focus using a significance level of $\alpha = 0.01$.

The results of our study are presented in Figure A-1 (results normalized to $0 - 1$).

Patient P1 (first row, left panel) shows increase in occurrence of maximum inflows

beginning at 5Hz at the focus (left amygdala - LA) that continually increases in

prevalence as frequency increases beyond 5Hz. This is also observed in the left

hippocampus (LH) beyond 25Hz. Statistically significant occurrence of maximum

inflows to LA (first row, right panel) begins at 10Hz with a gap between 17Hz and 23Hz.

Significant occurrence of maximum inflow is observed in the left hippocampus (LH) at 32-33Hz.

Patient P2 clinical foci were in the right amygdala (RA) and right hippocampus (RH) (Table 1) and did show increased occurrence of maximum inflow (second row, left panel): in the right amygdala at low frequencies up to 20Hz and the right hippocampus beyond 20Hz. Statistically significant occurrence of maximum inflows (second row, right panel) occurs in the right amygdala for frequencies up to 18Hz and in the right hippocampus for frequencies greater than 28Hz.

Patient P6 (third row, left panel), an increase in the occurrences of maximum inflow begin at 5Hz at the clinically determined focus (RTD). This increase in the occurrences of maximum inflow continues at higher than 5Hz frequencies. Gradual increase of occurrence of maximum inflow with frequency also occurs at one site of the contralateral hippocampus (LTD), peaks at around 35Hz and then decreases. Statistically significant higher occurrence of maximum inflows (third row, right panel) are first detected at 10Hz at the focus. Detection of statistically significant outliers is found intermittently as frequency increases. Gaps in significance occur when multiple brain sites show frequent maximum inflow.

For patient P7 (forth row, left panel), high occurrence of maximum inflow values was found in LST, LTD, and RTD. However, statistically (forth row, right panel), these were not deemed outliers, implying inability of the algorithm to localize to one focal region at confidence level $\alpha = 0.01$ (due to the fact that LTD and RTD are both highly active). Although the clinically defined focus for patient P7 was defined to be the left subtemporal (LST) and left hippocampus (LTD) areas, patient P7 was the only patient of

these four patients who presented with clinical and subclinical seizures in the right

hippocampus (RTD) as well.

In summary, in all patients, increased occurrence of maximum inflow was

observed at the clinically assessed foci at frequencies greater than 10Hz. For three of four

patients, significant occurrence of maximum inflows was also found at the clinically

assessed foci at frequencies greater than 10Hz.
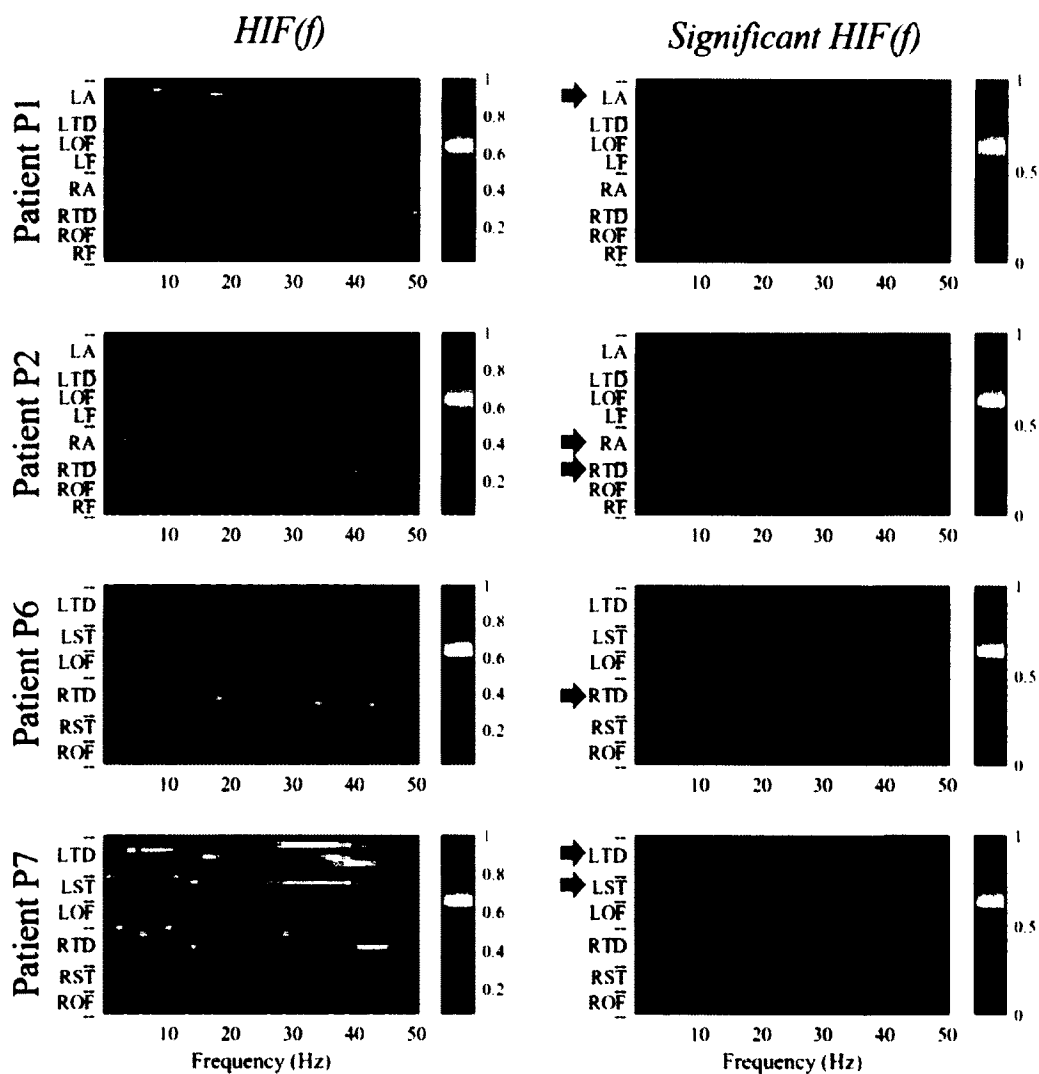
Figure A-1: Left panels: Percentage of time over the duration of the whole EEG recording (HIFi (f) values) that each brain site i exhibits maximum information inflow from the rest of brain sites as a function of EEG frequencies f. Blue color denotes infrequent and red color most frequent maximum inflow. Right panels: Illustration with red color of only the sites with statistically significant percentages of time with maximum inflow (HIFi (f)) as a function of EEG frequencies f. Red arrows in right panels denote the clinically determined focus (foci) for each patient.

APPENDIX B

FINAL METHODOLOGICAL RESULTS FOR EACH
CENTRALITY METRIC

Figures B-1 through B-5 show the show the grand average inward degree

centrality per electrode for all patients P1-P9 where individual centralities were estimated

over the $\delta, \theta, \alpha, \beta$, and γ frequency bands, respectively. The first three epochs of each

clinical seizure were averaged per patient. In patient P9, inward degree centrality worked

for all frequency bands, and for many patients, higher frequency bands provided higher

centrality values in the epileptogenic focus compared to non-focal brain regions.
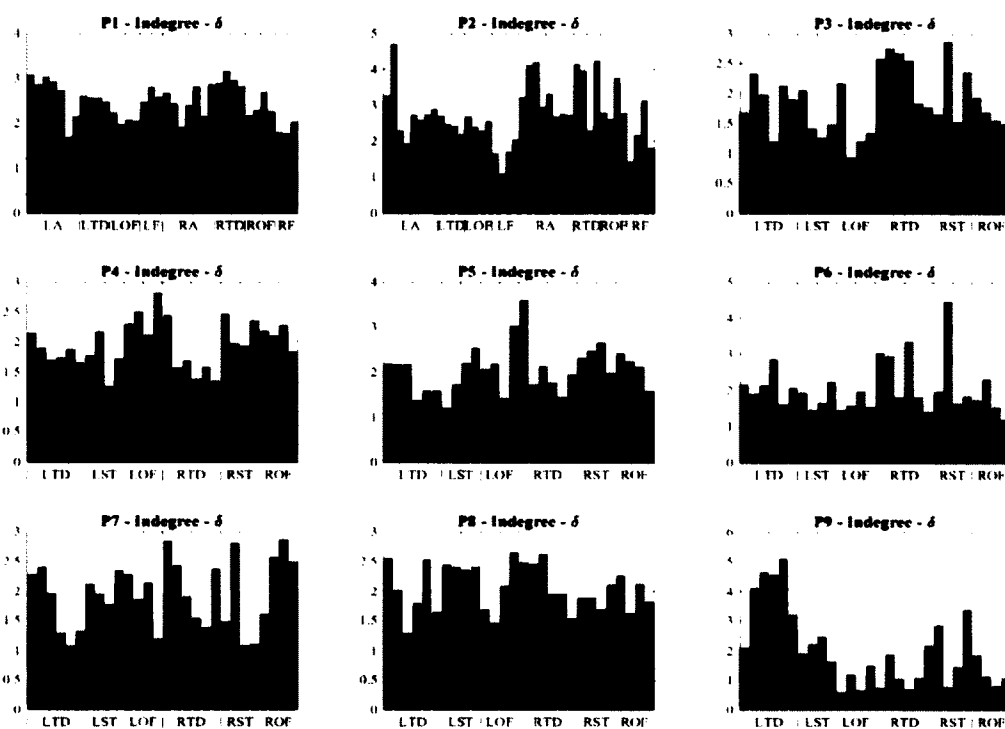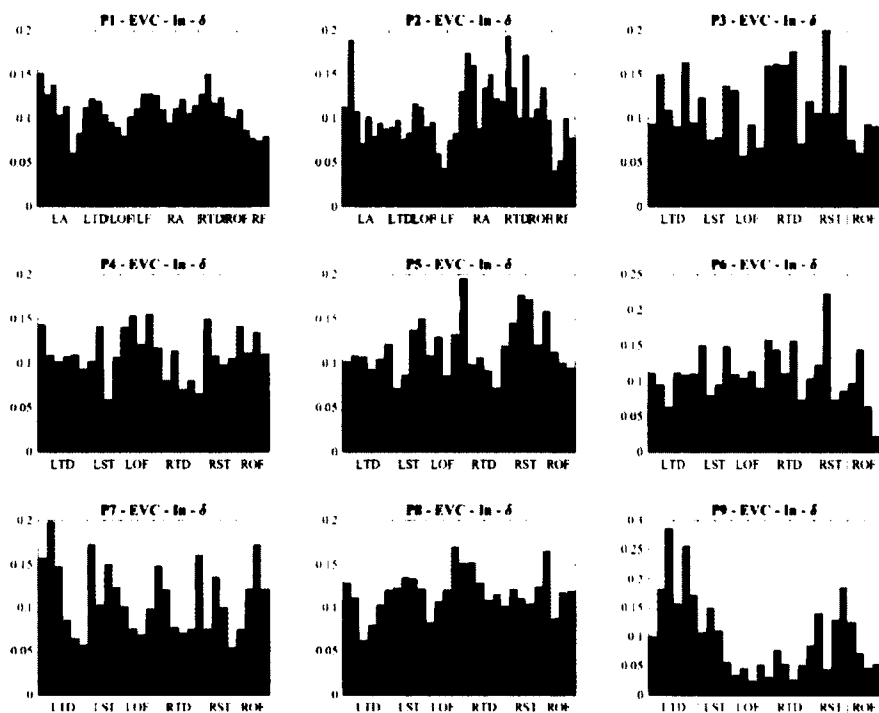

Figure B-1: In-degree centrality averaged for delta frequencies (1-4Hz) over early ictal epochs for each patient.
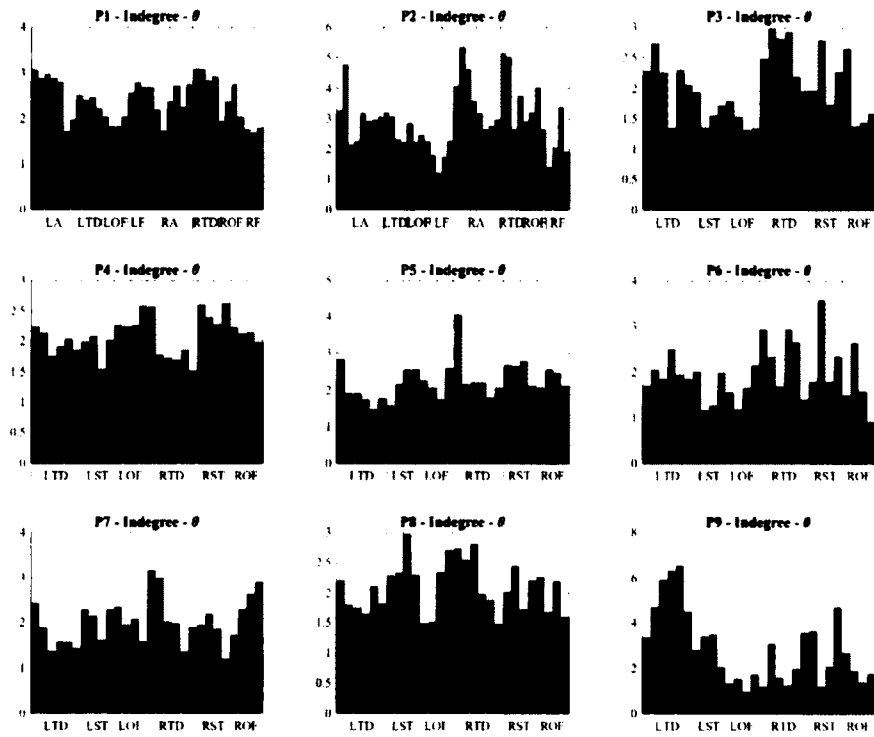
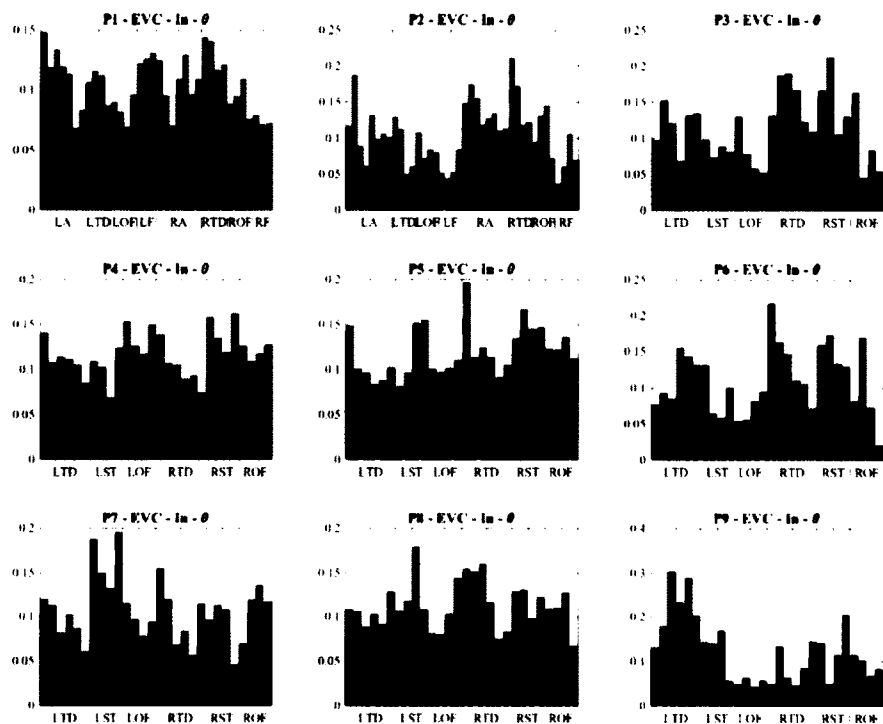Figure B-2: In-degree centrality averaged for theta frequencies (5-8Hz) over early ictal epochs for each patient.
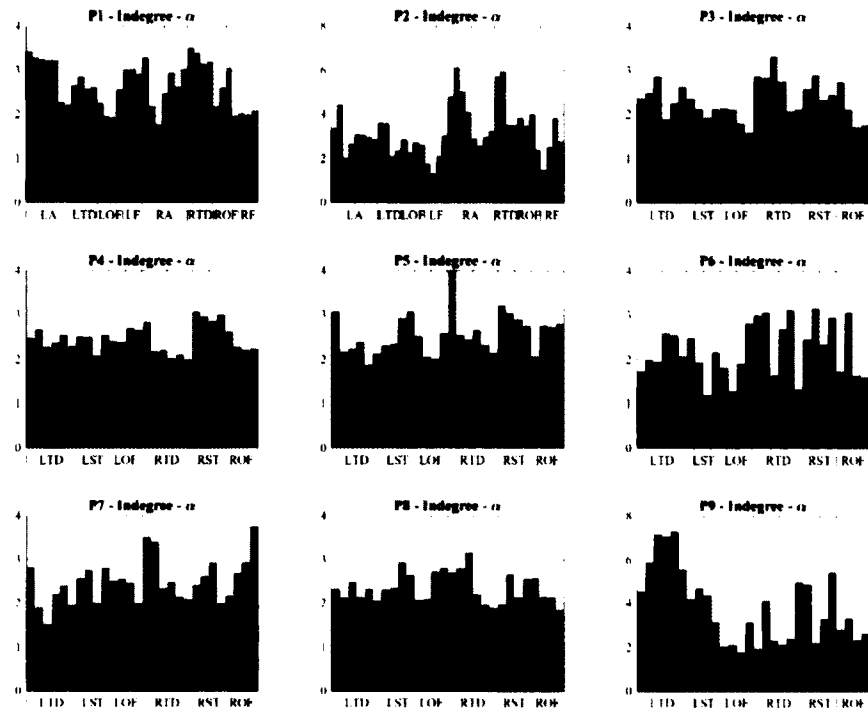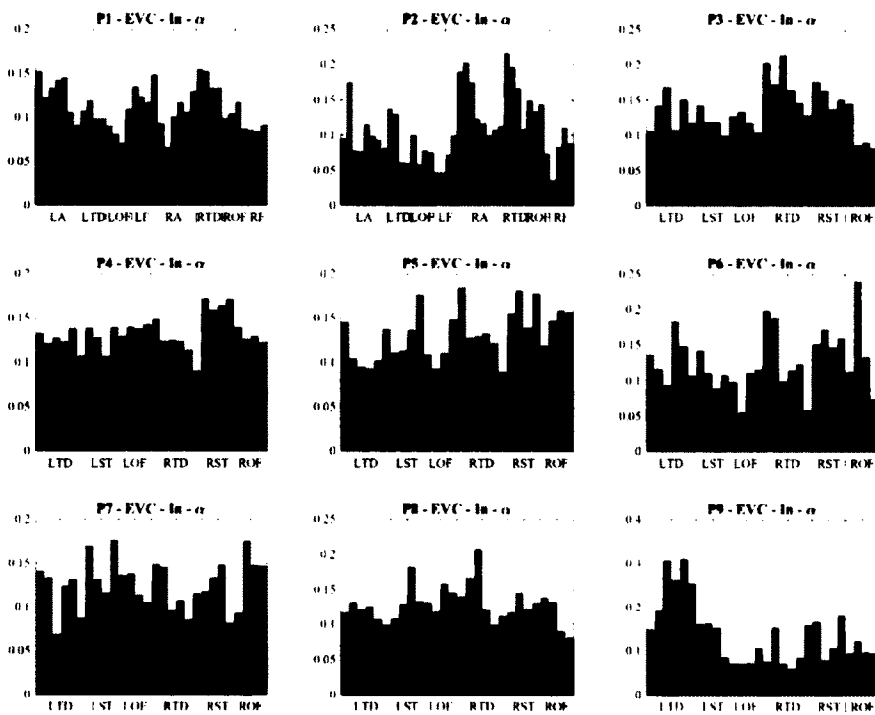

Figure B-3: In-degree centrality averaged for alpha frequencies (9-12Hz) over early ictal epochs for each patient.
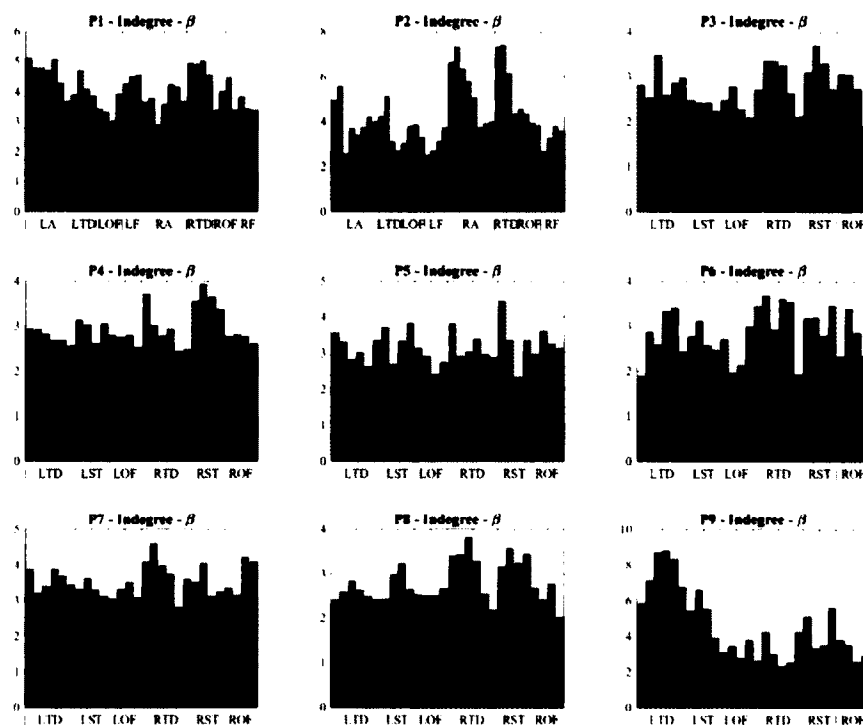
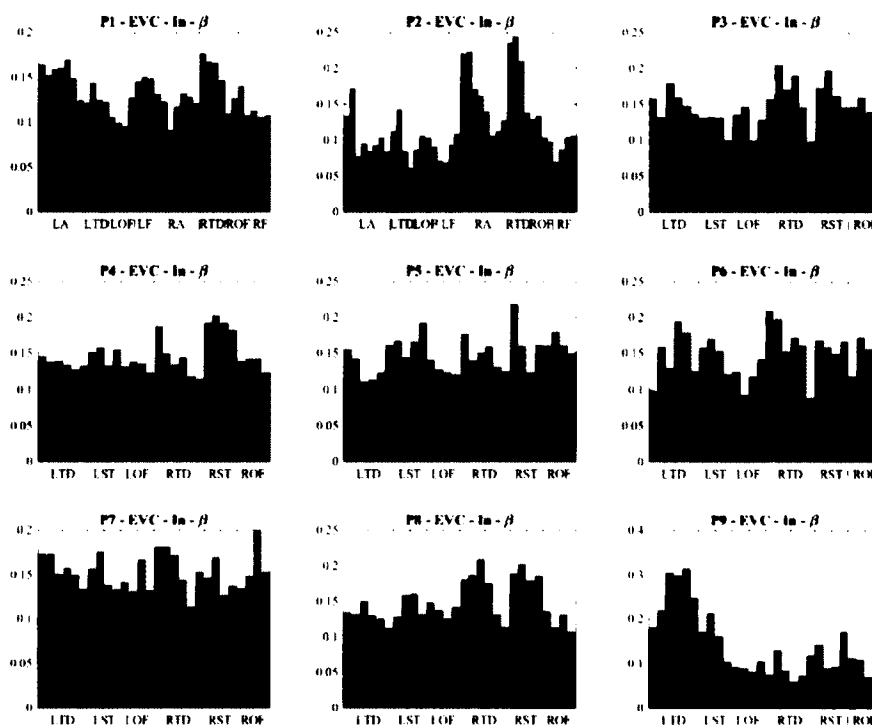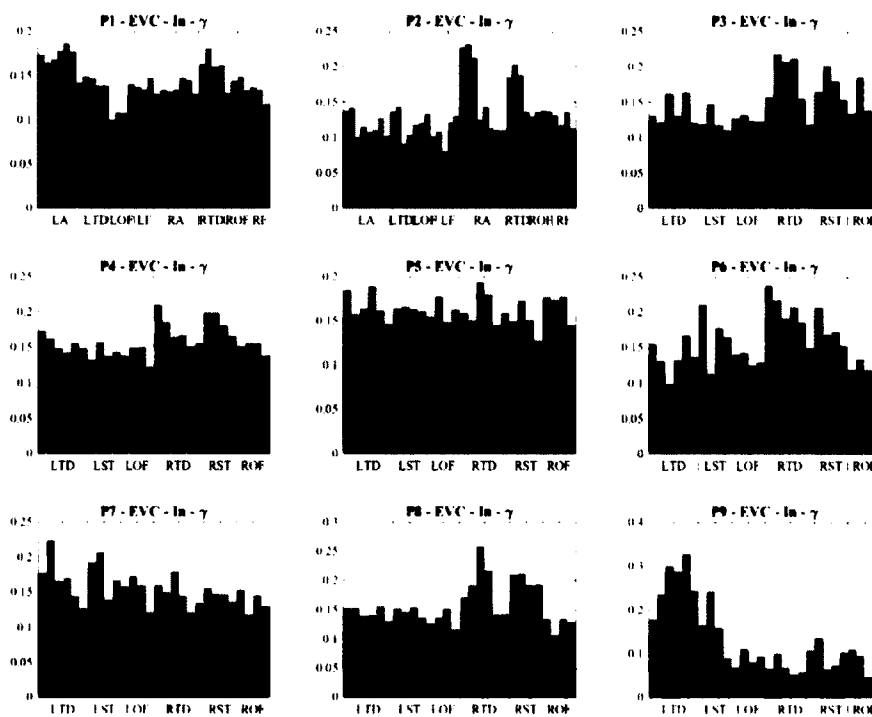Figure B-4: In-degree centrality averaged for beta frequencies (13-30Hz) over early ictal epochs for each patient.
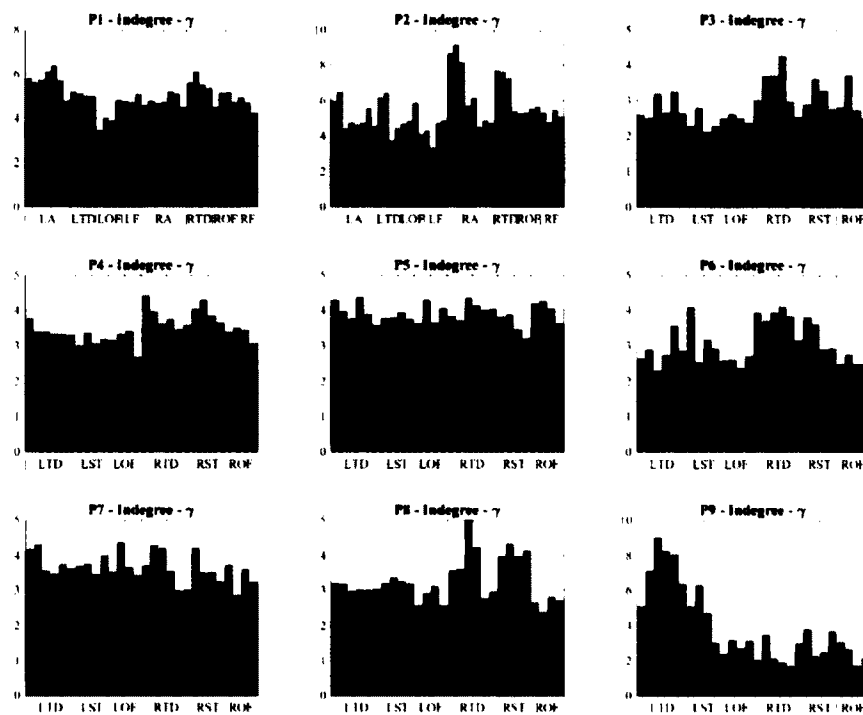
Figure B-5: In-degree centrality averaged for gamma frequencies (31-50Hz) over early ictal epochs for each patient.

Figures B-6 through B-10 show the show the grand average outward degree

centrality per electrode for all patients P1-P9 where individual centralities were estimated

over the $\delta, \theta, \alpha, \beta$, and γ frequency bands, respectively. The first three epochs of each

clinical seizure were averaged per patient. As frequency increases, we see the focal

electrodes for patients P2 through P7 have markedly higher centrality. However, in

patient P3, non-focal electrodes are higher, causing our selection process to fail to

localize the focus in this patient. In patient P8, centrality values in the high frequency

regions are dominated by the right subtemporal electrodes which are relatively close to

the focal region (right hippocampus), and in patient P9, outward degree centrality is

generally lower in the focal electrodes compared to the non-focal electrodes in each

frequency band.
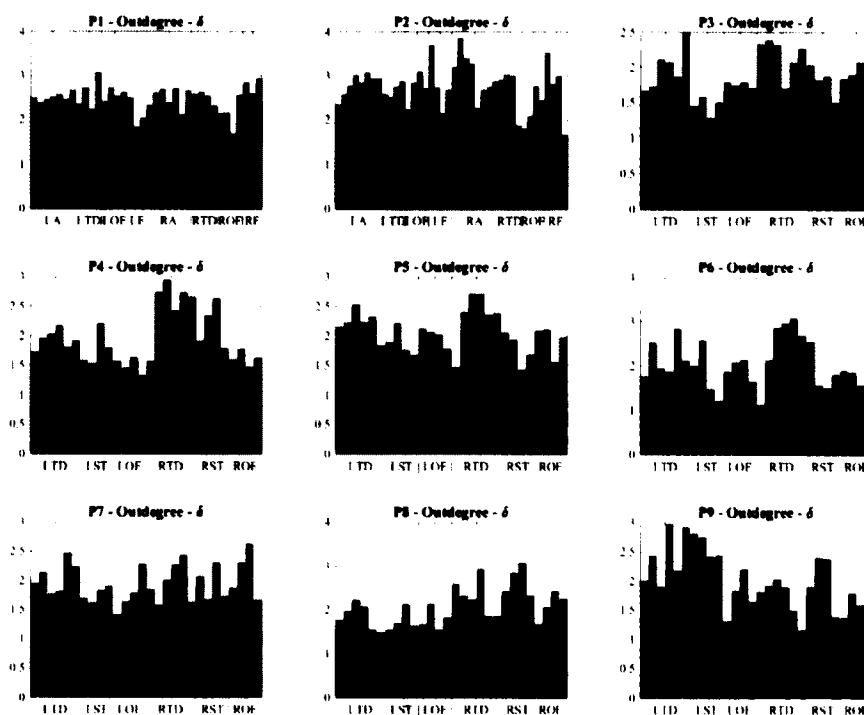
Figure B-6: Out-degree centrality averaged for delta frequencies (1-4Hz) over early ictal epochs for each patient.
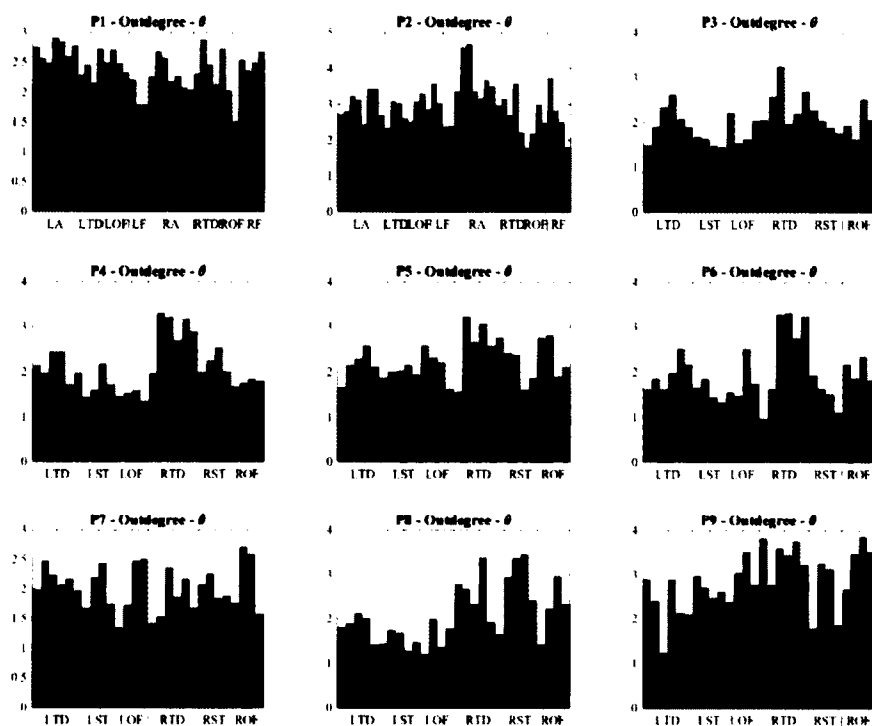
Figure B-7: Out-degree centrality averaged for theta frequencies (5-8Hz) over early ictal epochs for each patient.
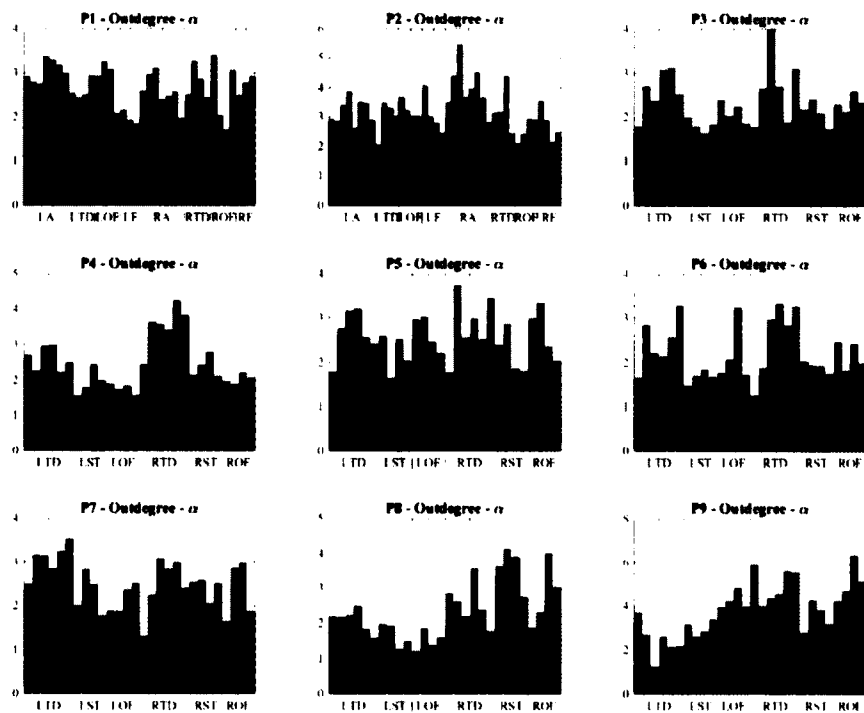
Figure B-8: Out-degree centrality averaged for alpha frequencies (9-12Hz) over early ictal epochs for each patient.
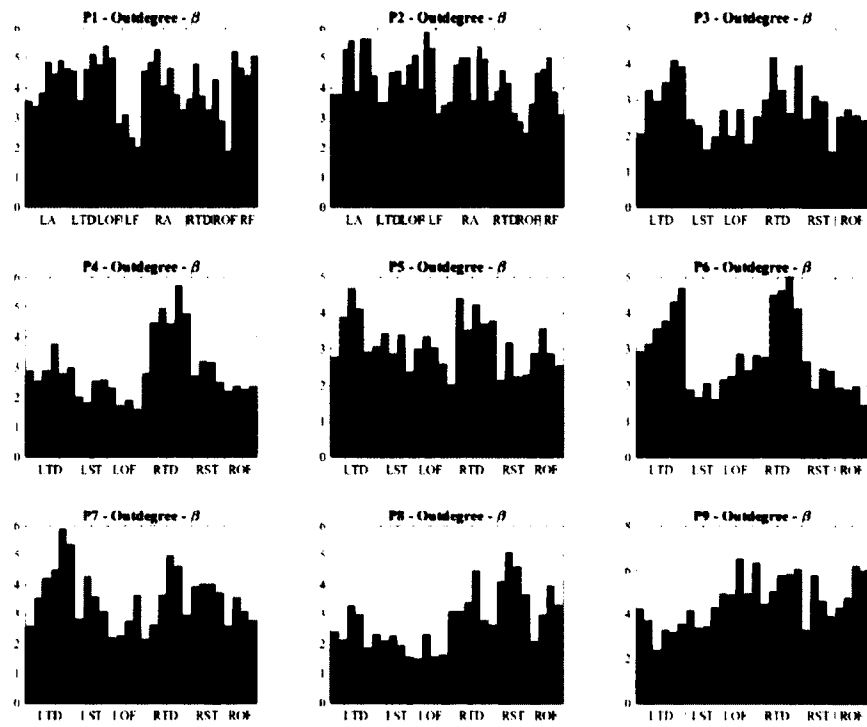
Figure B-9: Out-degree centrality averaged for beta frequencies (13-30Hz) over early ictal epochs for each patient.
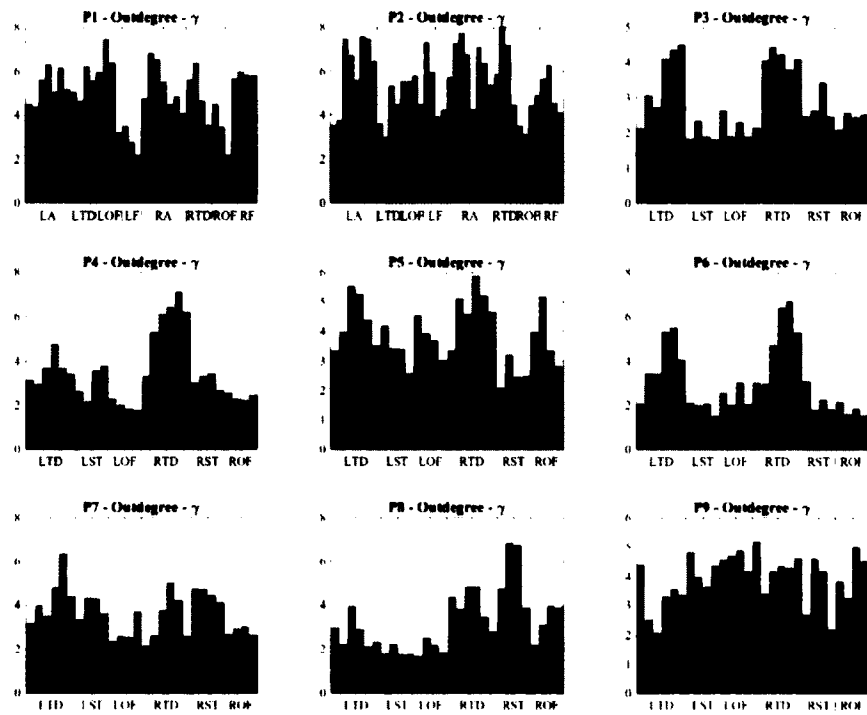
Figure B-10: Out-degree centrality averaged for gamma frequencies (31-50Hz) over early ictal epochs for each patient.

Figures B-11 through B-15 show the show the grand average inward eigenvector centrality per electrode for all patients P1-P9 where individual centralities were estimated over the $\delta, \theta, \alpha, \beta$, and γ frequency bands, respectively. The first three epochs of each clinical seizure were averaged per patient. In lower frequency bands, the centrality within each set of electrodes is sporadic. However, for many of these patients the electrodes within the focal region are in general elevated compared to non-focal electrodes, but the fact remains that one non-focal electrode has maximum centrality, causing focus localization to fail. For higher frequency bands, the electrodes within the focus remain elevated compared to non-focal electrodes, and fewer non-focal electrodes are markedly higher than others in their electrode set. This trend continues in the gamma frequencies (Figure B-15) where all patients have maximum centrality at one of the focal electrodes.

Figure B-11: Inward eigenvector centrality averaged for delta frequencies (1-4Hz) over early ictal epochs for each patient.
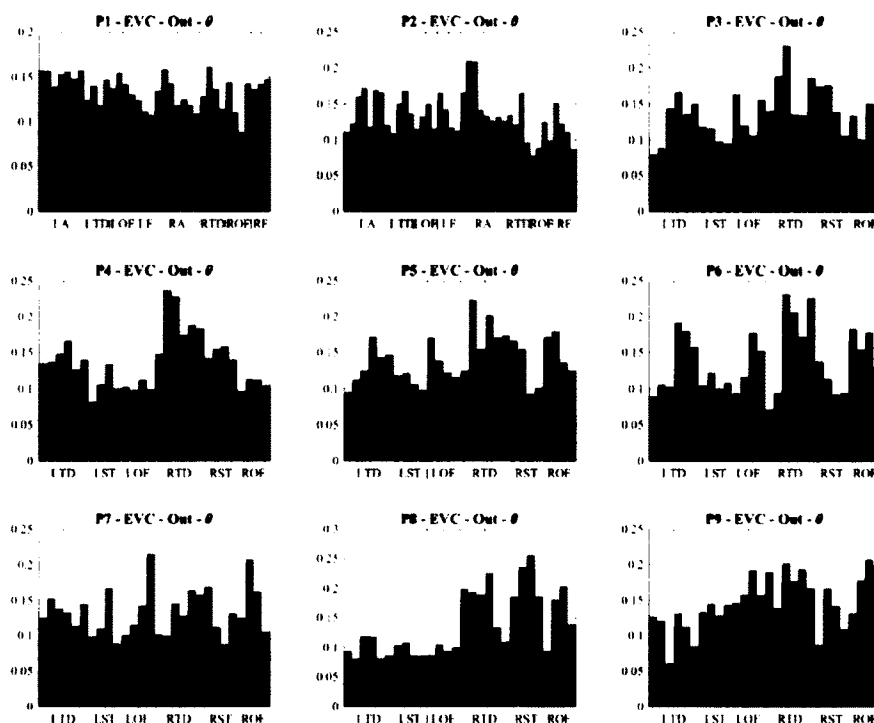
Figure B-12: Inward eigenvector centrality averaged for theta frequencies (5-8Hz) over early ictal epochs for each patient.
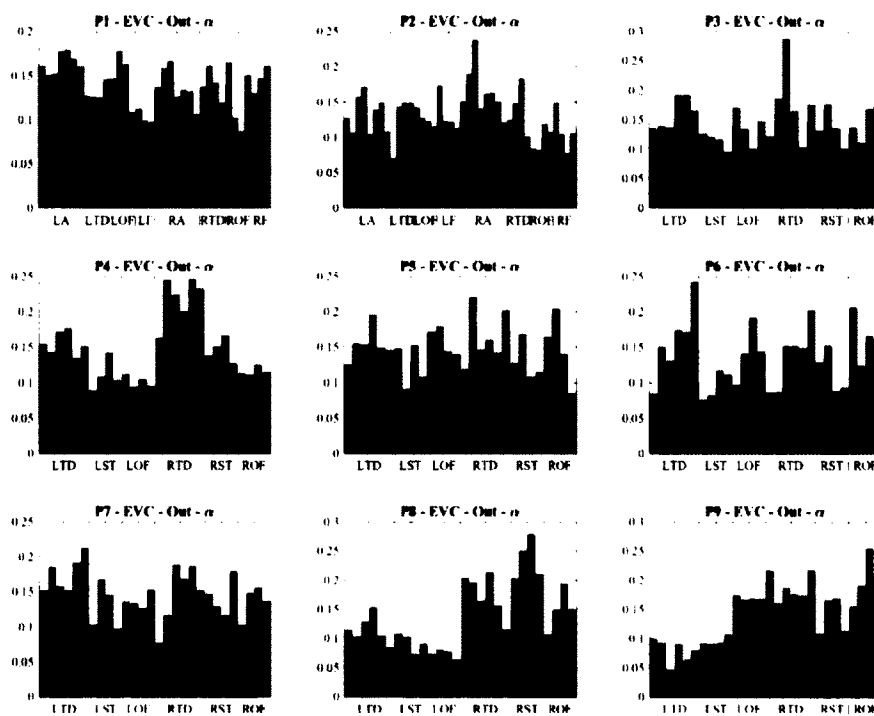

Figure B-13: Inward eigenvector centrality averaged for alpha frequencies (9-12Hz) over early ictal epochs for each patient.
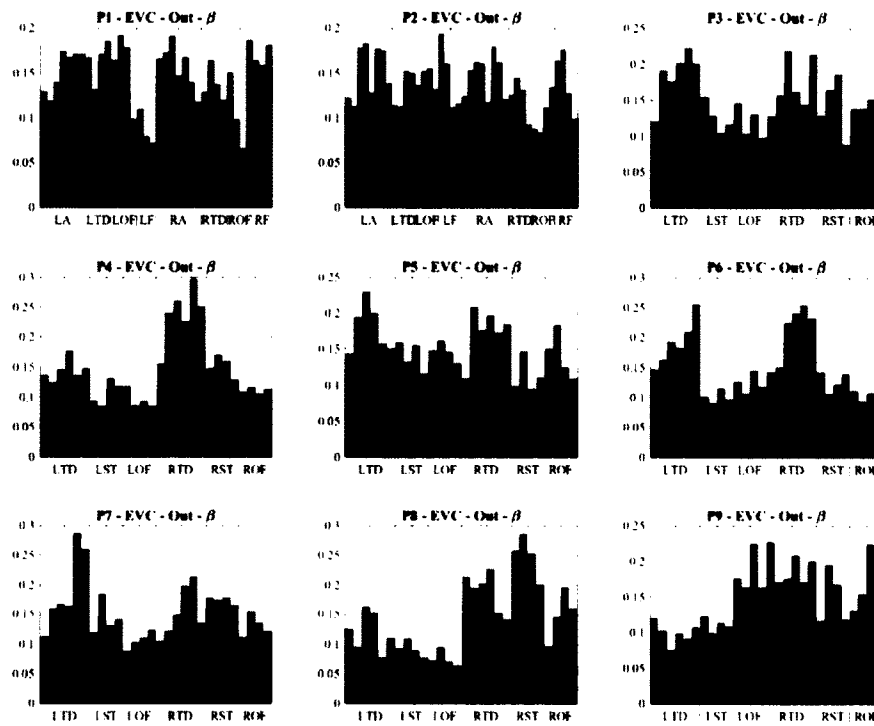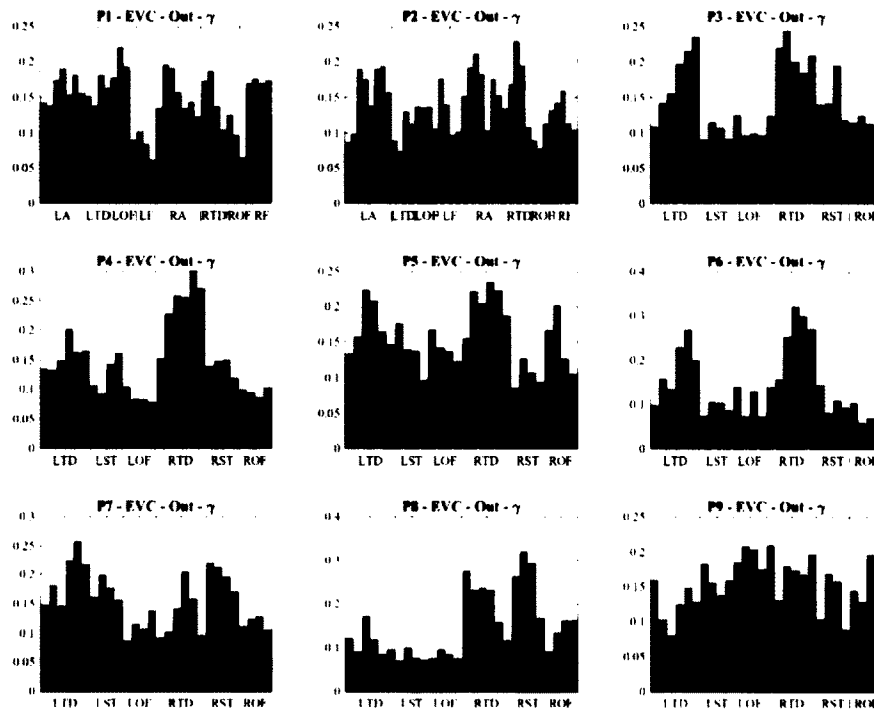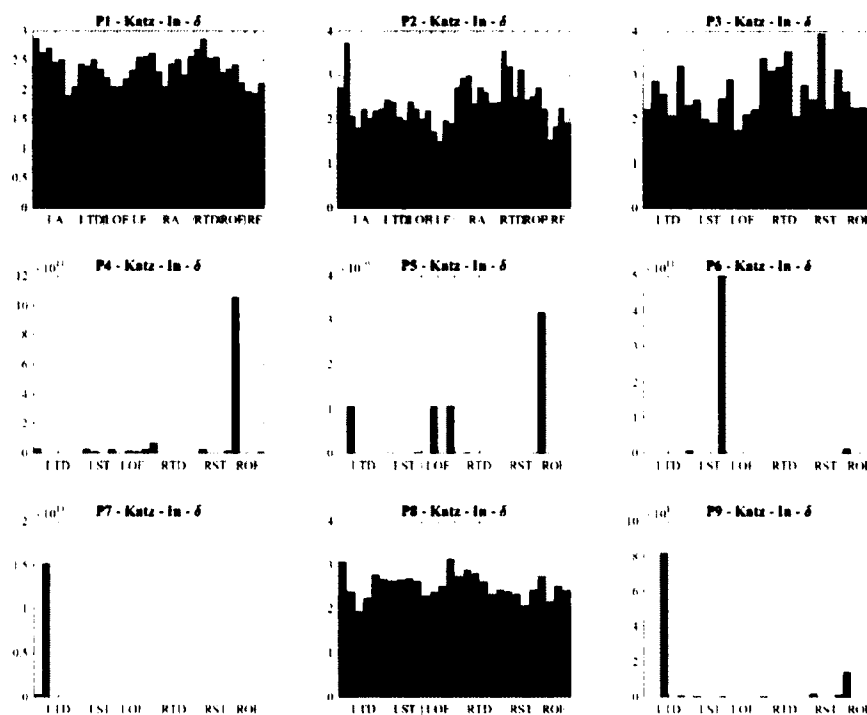
Figure B-14: Inward eigenvector centrality averaged for beta frequencies (13-30Hz) over early ictal epochs for each patient.

Figure B-15: Inward eigenvector centrality averaged for gamma frequencies (31-50Hz) over early ictal epochs for each patient.

Figures B-16 through B-20 show the show the grand average outward eigenvector centrality per electrode for all patients P1-P9 where individual centralities were estimated over the $\delta, \theta, \alpha, \beta$, and γ frequency bands, respectively. The first three epochs of each clinical seizure were averaged per patient. For outward eigenvector centralities at lower frequencies, no set of electrodes seems markedly higher than other sets. In higher frequencies, the focal electrodes do become elevated, with maximum outward eigenvector centrality located at the focal electrodes in patients P2 through P7. In patients P1 and P8, the centrality of the focal electrodes is generally outpaced by other nearby electrode sets in the gamma frequency band, and for patient P9, centrality for focal electrodes seems markedly lower than most other electrodes.
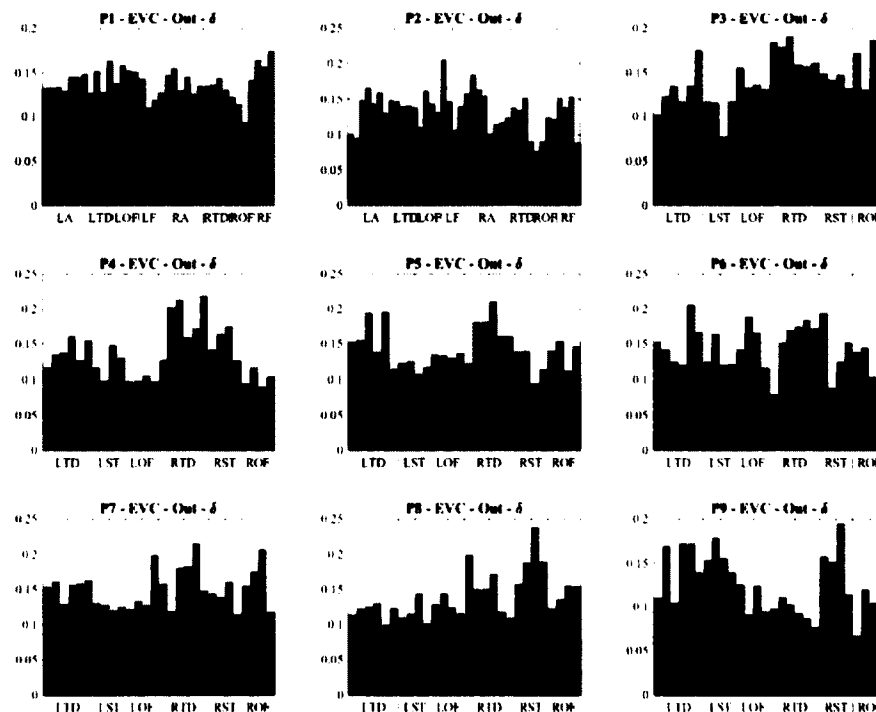
Figure B-16: Outward eigenvector centrality averaged for delta frequencies (1-4Hz) over early ictal epochs for each patient.
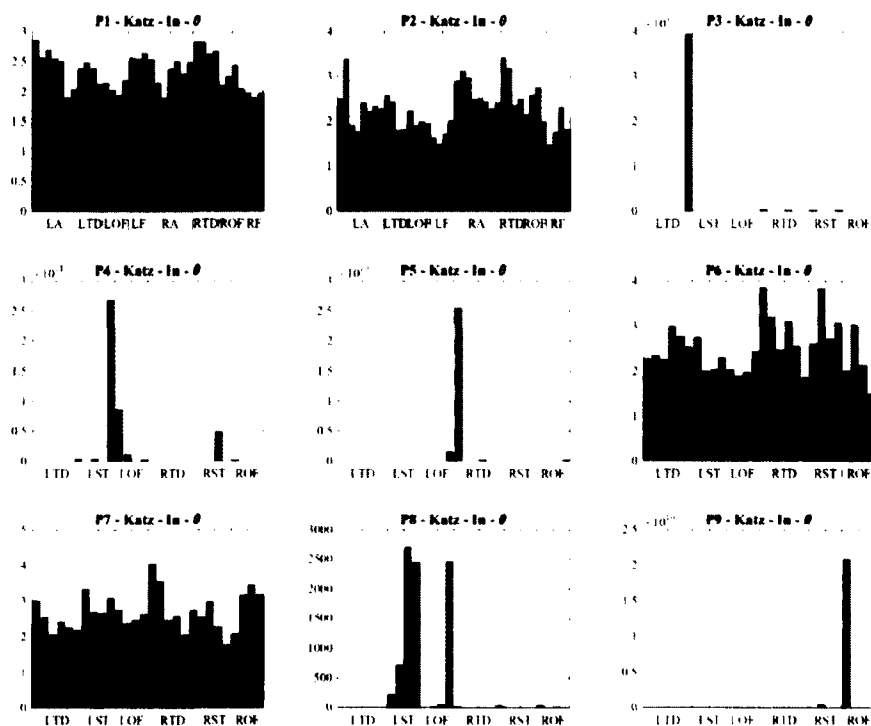
Figure B-17: Outward eigenvector centrality averaged for theta frequencies (5-8Hz) over early ictal epochs for each patient.
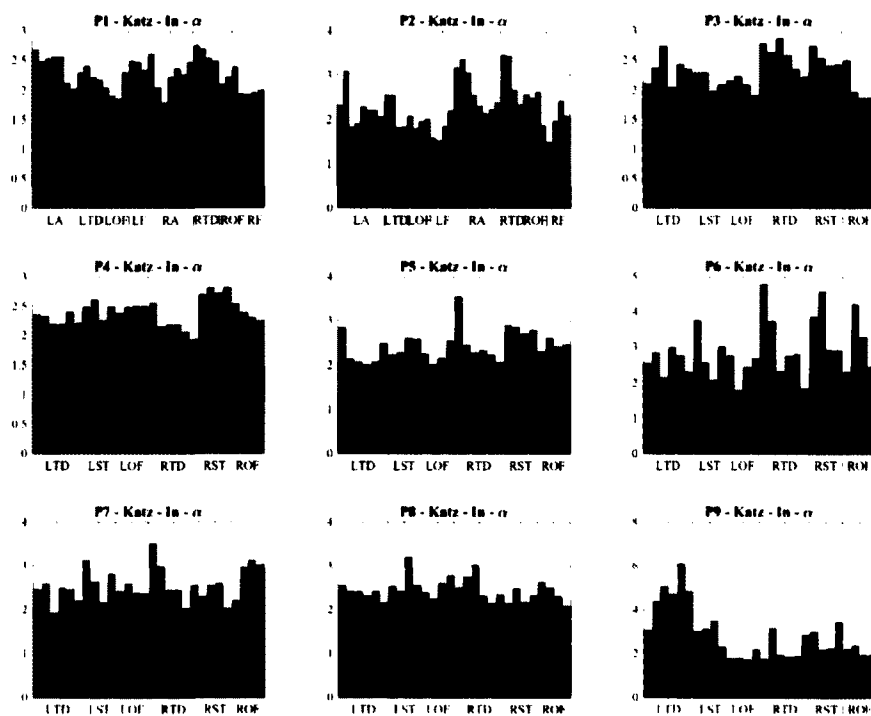

Figure B-18: Outward eigenvector centrality averaged for alpha frequencies (9-12Hz) over early ictal epochs for each patient.
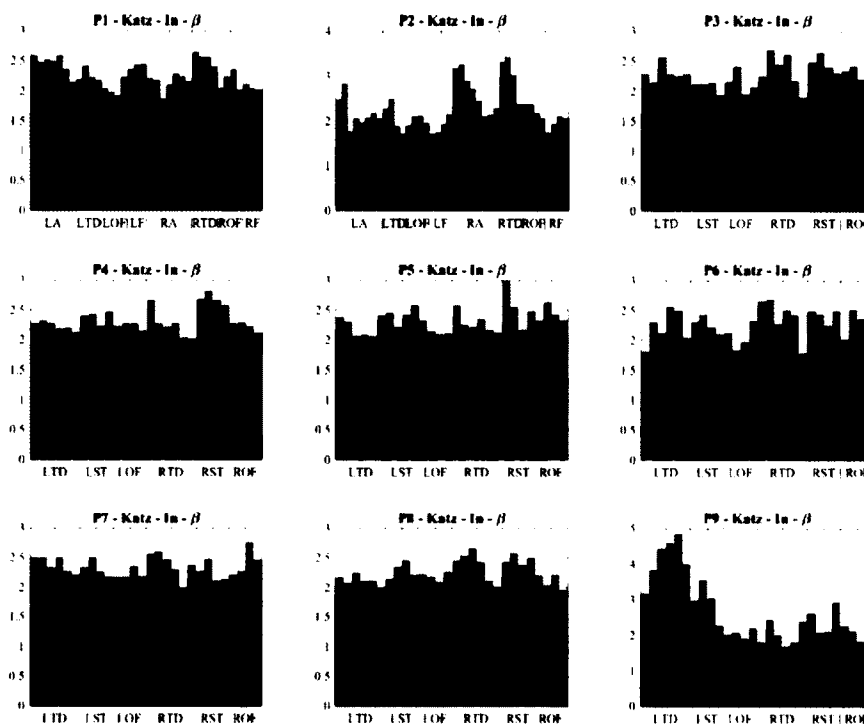
Figure B-19: Outward eigenvector centrality averaged for beta frequencies (13-30Hz) over early ictal epochs for each patient.
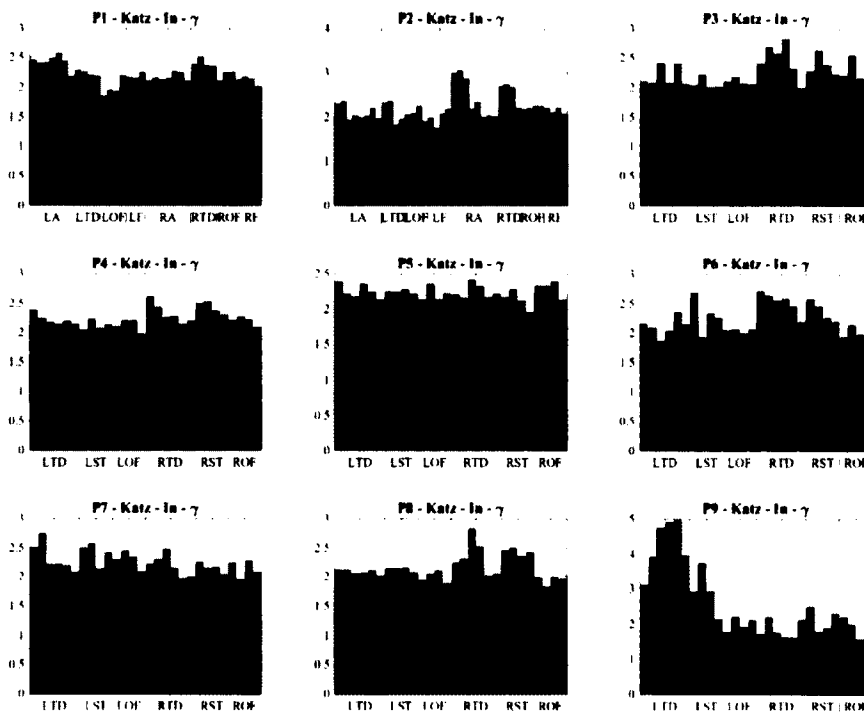

Figure B-20: Outward eigenvector centrality averaged for gamma frequencies (31-50Hz) over early ictal epochs for each patient.

Figures B-21 through B-25 show the show the grand average inward Katz

centrality per electrode for all patients P1-P9 where individual centralities were estimated

over the $\delta, \theta, \alpha, \beta$, and γ frequency bands, respectively. The first three epochs of each

clinical seizure were averaged per patient. Figures B-21 and B-22 show good examples of

issues that arise because of network connectivity as discussed in Subsection 5.4.1. Here,

relatively lower edge density leads to networks that may not be weakly connected, which

ultimately leads to issues with Katz centrality estimation. For networks derived from

higher frequency bands, edge density is relatively higher leading to more well connected

networks, which reduces the risk that networks estimation issue will occur that negatively

affect our focus localization methodology. For gamma frequencies (Figure B-25), these

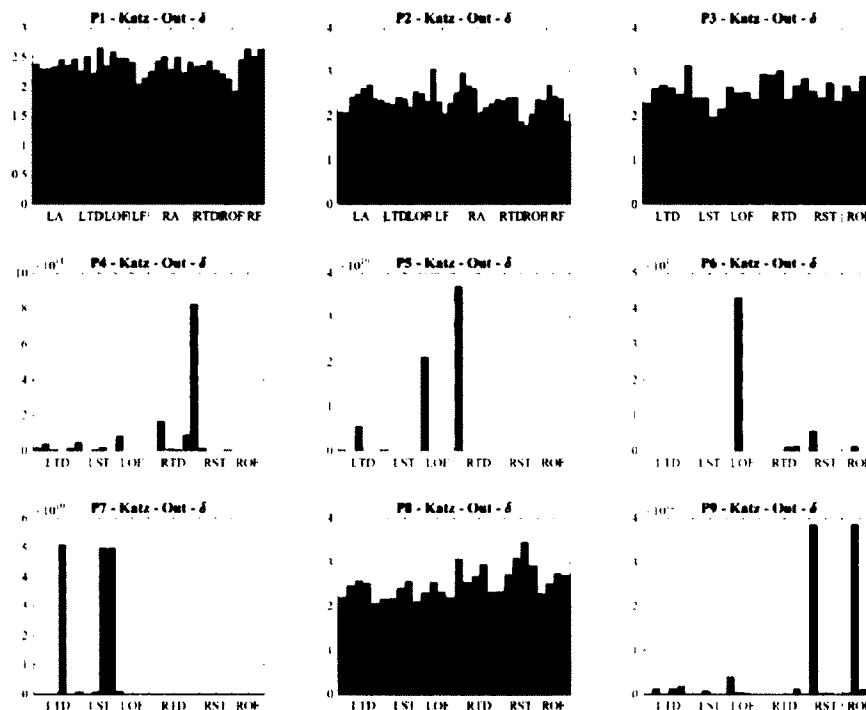issues have become minimal, leading to successful focus localization for each patient.

Figure B-21: Inward Katz centrality averaged for delta frequencies (1-4Hz) over early ictal epochs for each patient.
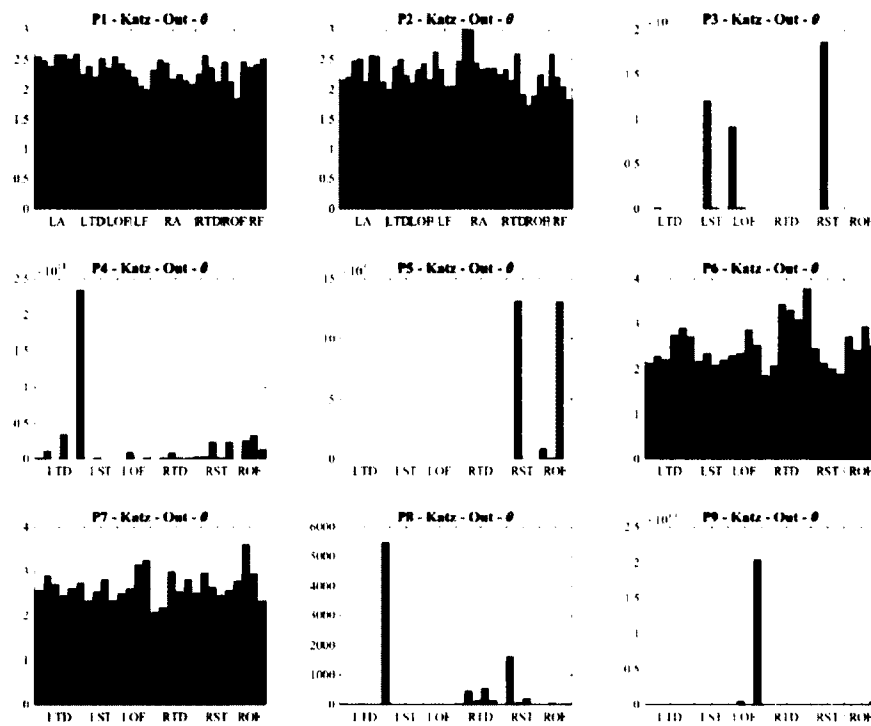
Figure B-22: Inward Katz centrality averaged for theta frequencies (5-8Hz) over early ictal epochs for each patient.

Figure B-23: Inward Katz centrality averaged for alpha frequencies (31-50Hz) over early ictal epochs for each patient.

Figure B-24: Inward Katz centrality averaged for beta frequencies (13-30Hz) over early ictal epochs for each patient.
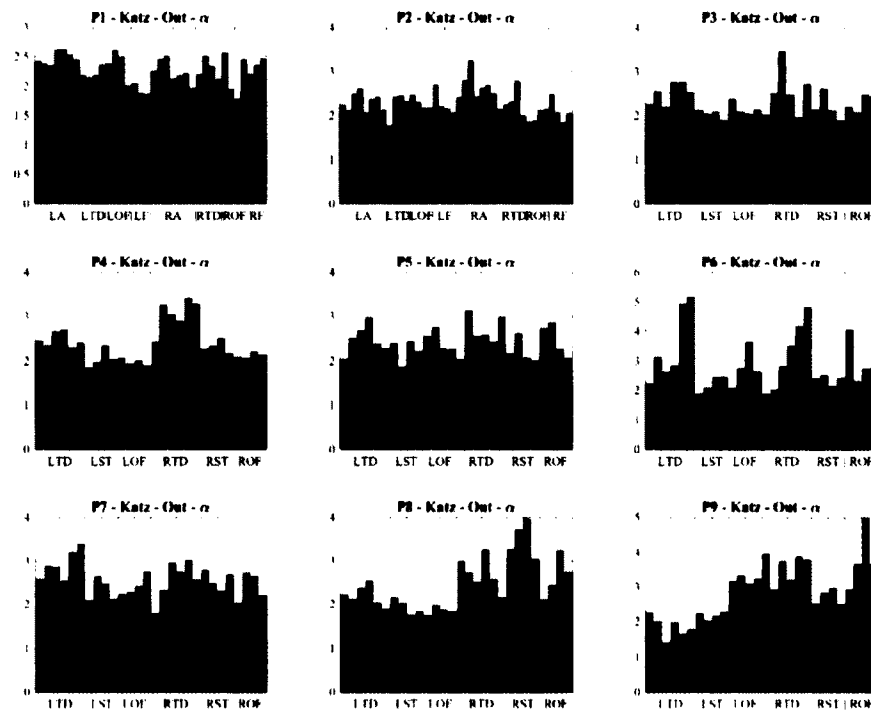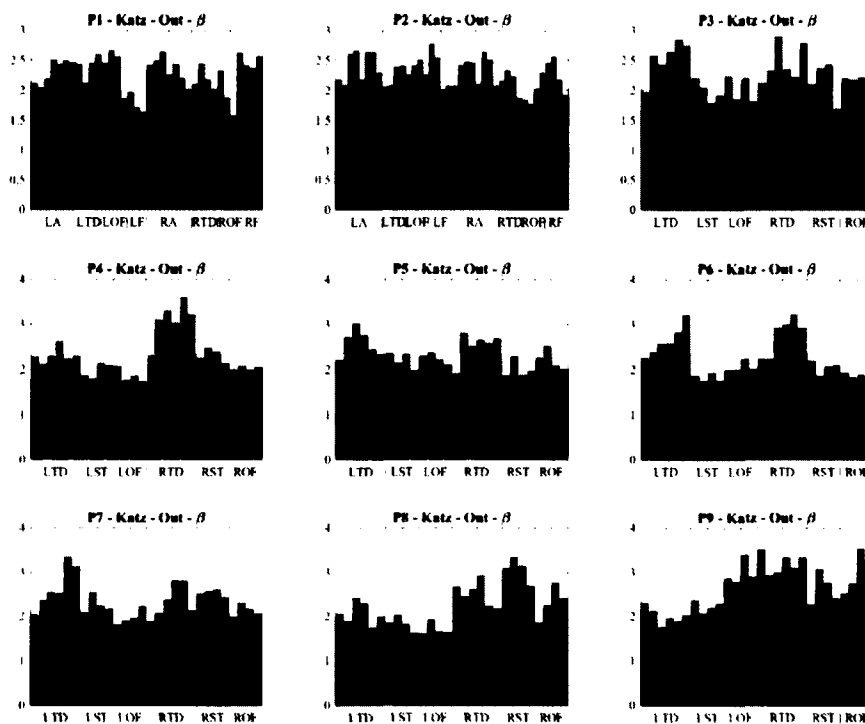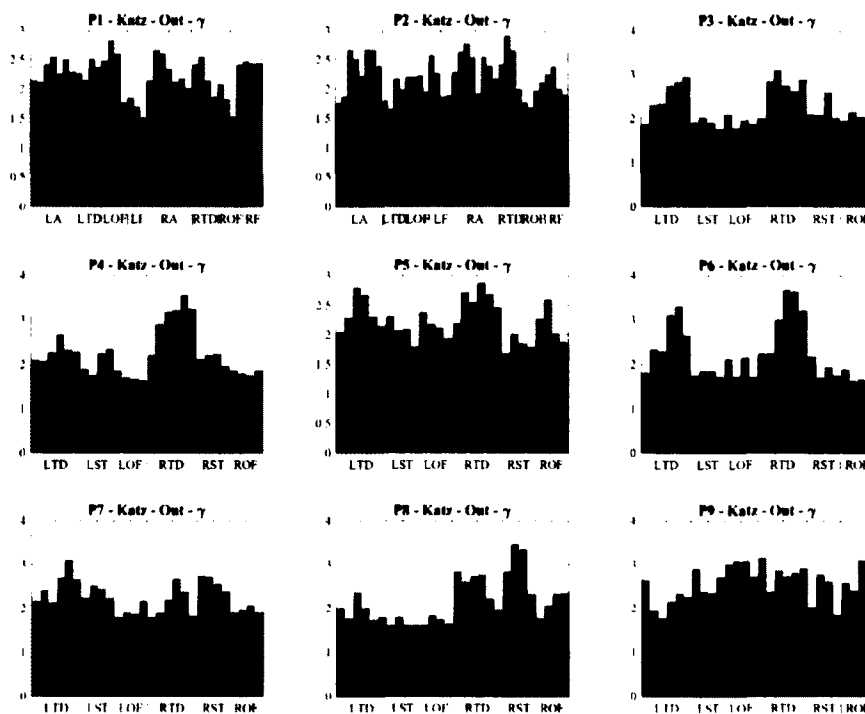

Figure B-25: Inward Katz centrality averaged for gamma frequencies (31-50Hz) over early ictal epochs for each patient.

Figures B-26 through B-30 show the show the grand average outward Katz

centrality per electrode for all patients P1-P9 where individual centralities were estimated

over the $\delta, \theta, \alpha, \beta$, and γ frequency bands, respectively. The first three epochs of each

clinical seizure were averaged per patient. Similar to the issues seen in inward Katz

centrality, lower frequency networks lead to estimation issues that negatively affect focus

localization in the delta and theta frequency bands, and again, these issues disappear in

higher frequency bands where higher edge density leads to more connected networks.

However, outward Katz centrality does not have the same success as inward Katz

centrality in the higher frequency bands. In the gamma frequency (Figure B-30) focus
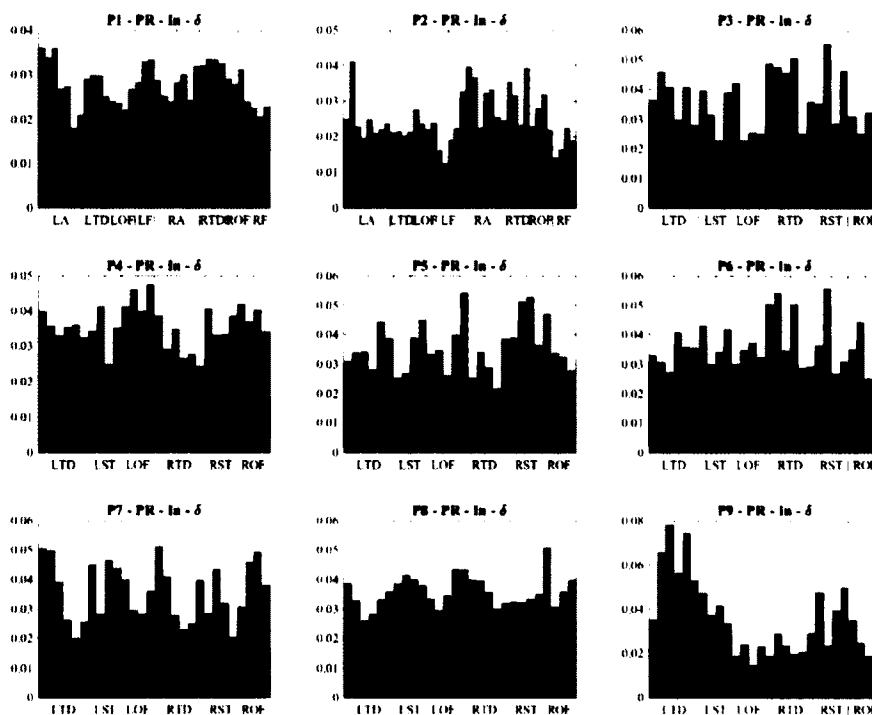
localization fails for patients P1, P8, and P9.

Figure B-26: Outward Katz centrality averaged for delta frequencies (1-4Hz) over early ictal epochs for each patient.

Figure B-27: Outward Katz centrality averaged for theta frequencies (5-8Hz) over early ictal epochs for each patient.

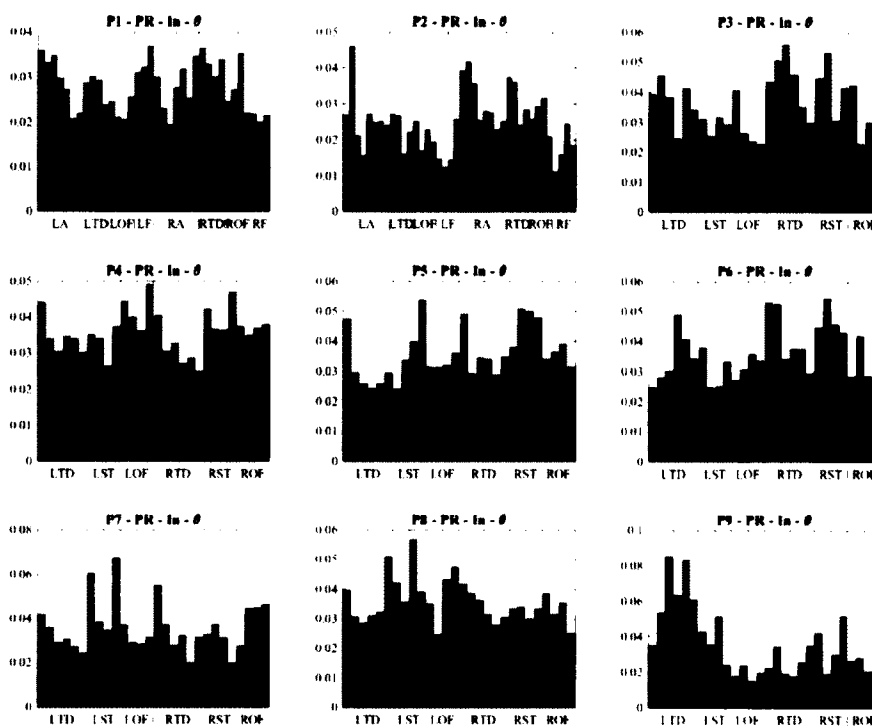Figure B-28: Outward Katz centrality averaged for alpha frequencies (9-12Hz) over early ictal epochs for each patient.

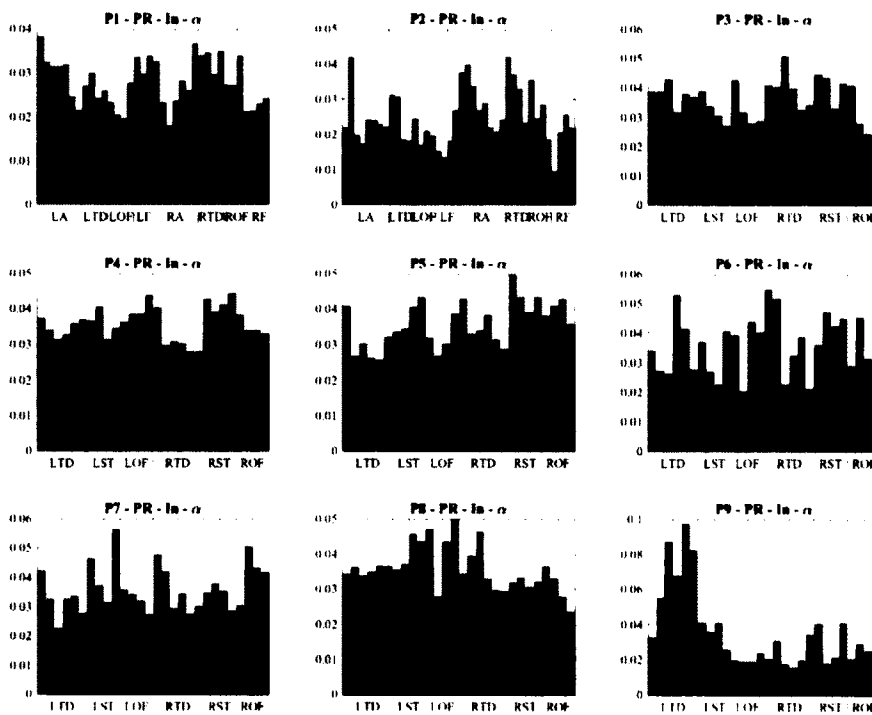Figure B-29: Outward Katz centrality averaged for beta frequencies (13-30Hz) over early ictal epochs for each patient.

Figure B-30: Outward Katz centrality averaged for gamma frequencies (31-50Hz) over early ictal epochs for each patient.

Figures B-31 through B-35 show the show the grand average inward PageRank centrality per electrode for all patients P1-P9 where individual centralities were estimated over the $\delta, \theta, \alpha, \beta$, and γ frequency bands, respectively. The first three epochs of each clinical seizure were averaged per patient. In higher frequencies, patients P2 and P9 shows markedly higher centrality values compared to non-focal electrodes, but in general, focus localization does not provide consistent localization results for other patients.

Figure B-31: Inward PageRank centrality averaged for delta frequencies (1-4Hz) over early ictal epochs for each patient.

Figure B-32: Inward PageRank centrality averaged for theta frequencies (5-8Hz) over early ictal epochs for each patient.

Figure B-33: Inward PageRank centrality averaged for alpha frequencies (9-12Hz) over early ictal epochs for each patient.
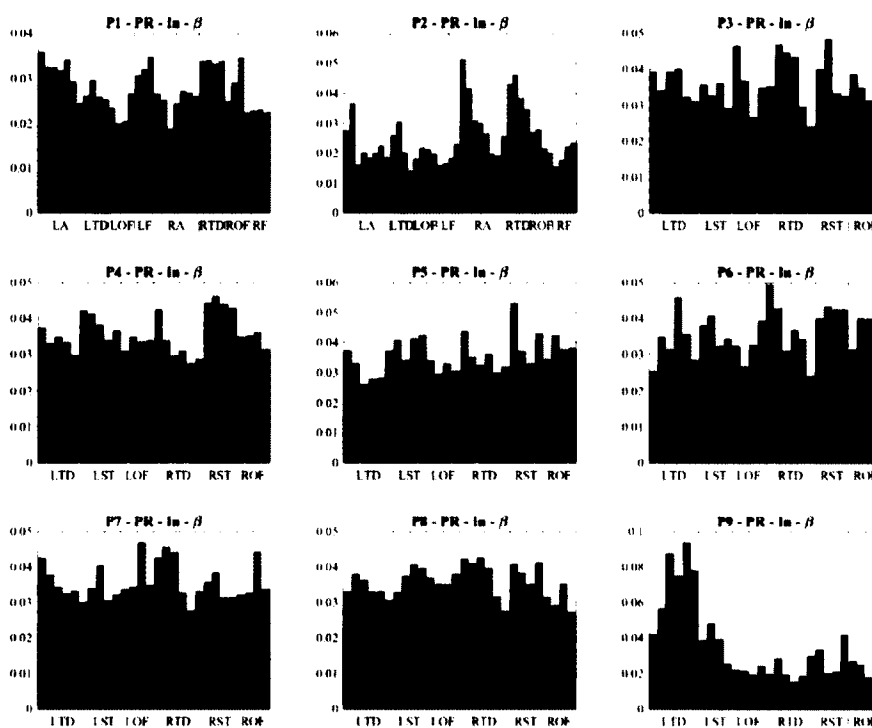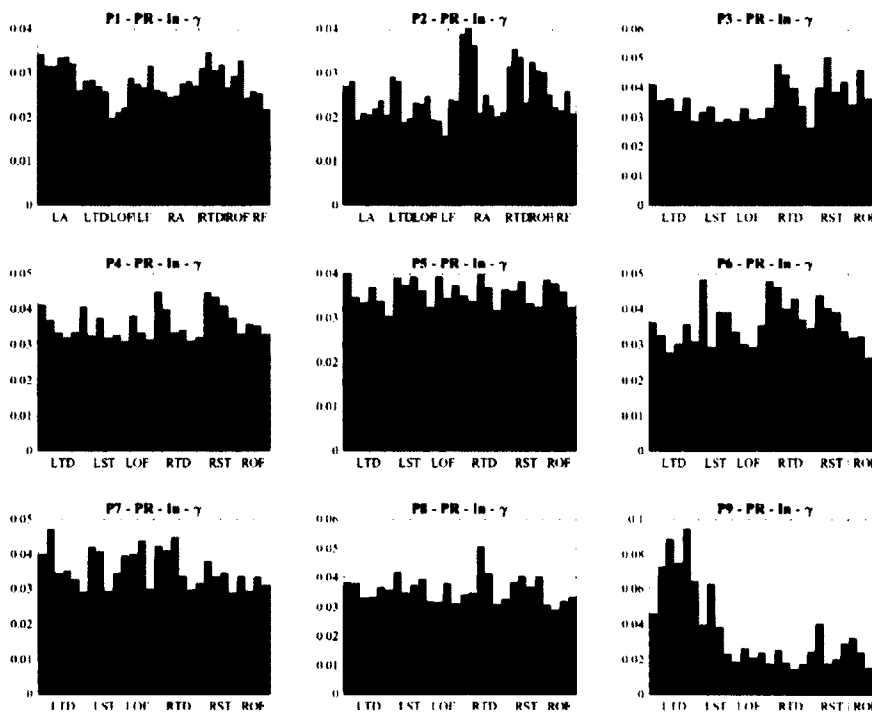
Figure B-34: Inward PageRank centrality averaged for beta frequencies (13-30Hz) over early ictal epochs for each patient.

Figure B-35: Inward PageRank centrality averaged for gamma frequencies (31-50Hz) over early ictal epochs for each patient.

Figures B-36 through B-40 show the show the grand average outward PageRank

centrality per electrode for all patients P1-P9 where individual centralities were estimated

over the $\delta, \theta, \alpha, \beta$, and γ frequency bands, respectively. The first three epochs of each

clinical seizure were averaged per patient. For higher frequencies, patients P3, P4, P6,

and P7 show comparatively higher centrality values compared to non-focal electrodes, all

of which have a maximum centrality in the focal electrodes, leading to successful focus

localization in these patients. Furthermore, these mentioned patients including patient P5

seem to have centrality results that are complementary to what is seen in inward
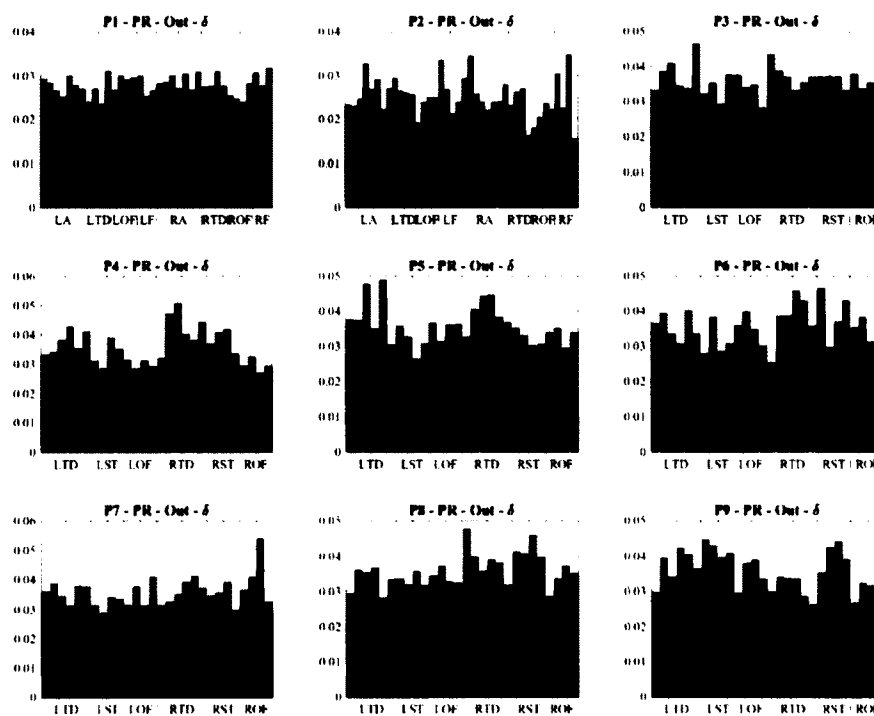
PageRank centrality.

Figure B-36: Outward PageRank centrality averaged for delta frequencies (1-4Hz) over early ictal epochs for each patient.
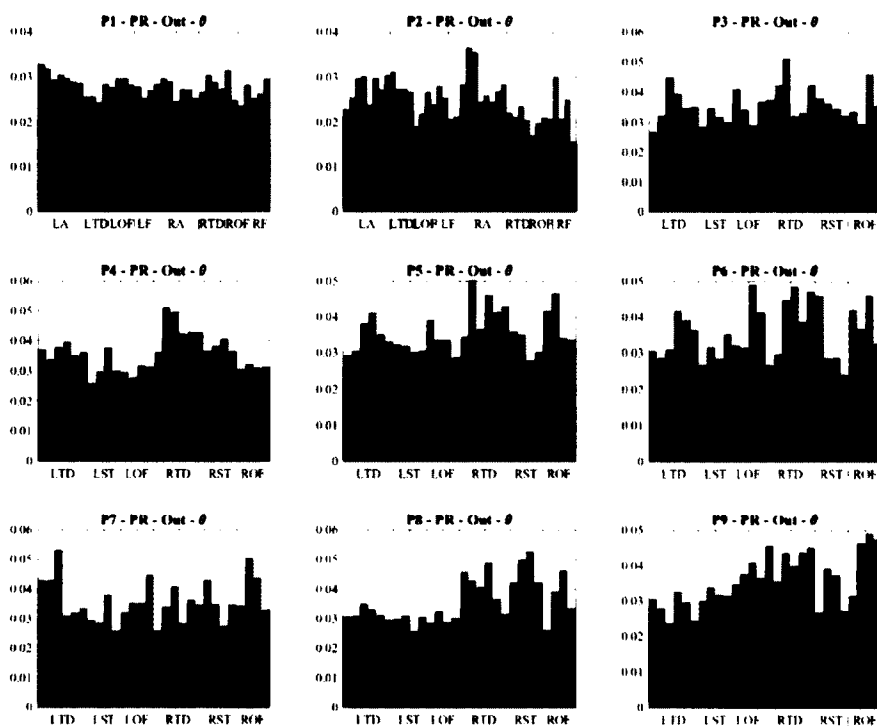
Figure B-37: Outward PageRank centrality averaged for theta frequencies (5-8Hz) over early ictal epochs for each patient.
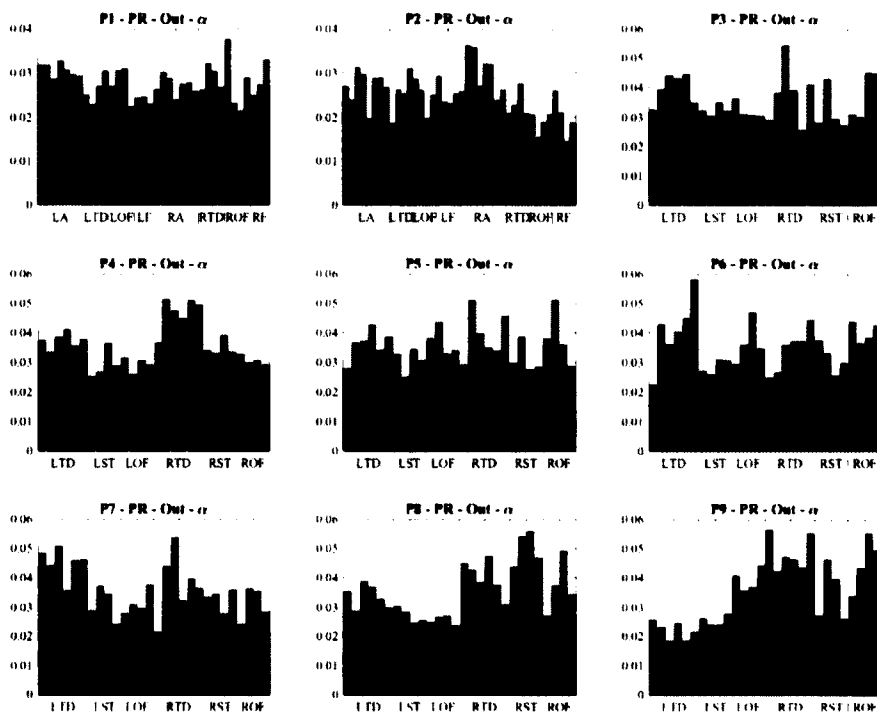

Figure B-38: Outward PageRank centrality averaged for alpha frequencies (9-12Hz) over early ictal epochs for each patient.
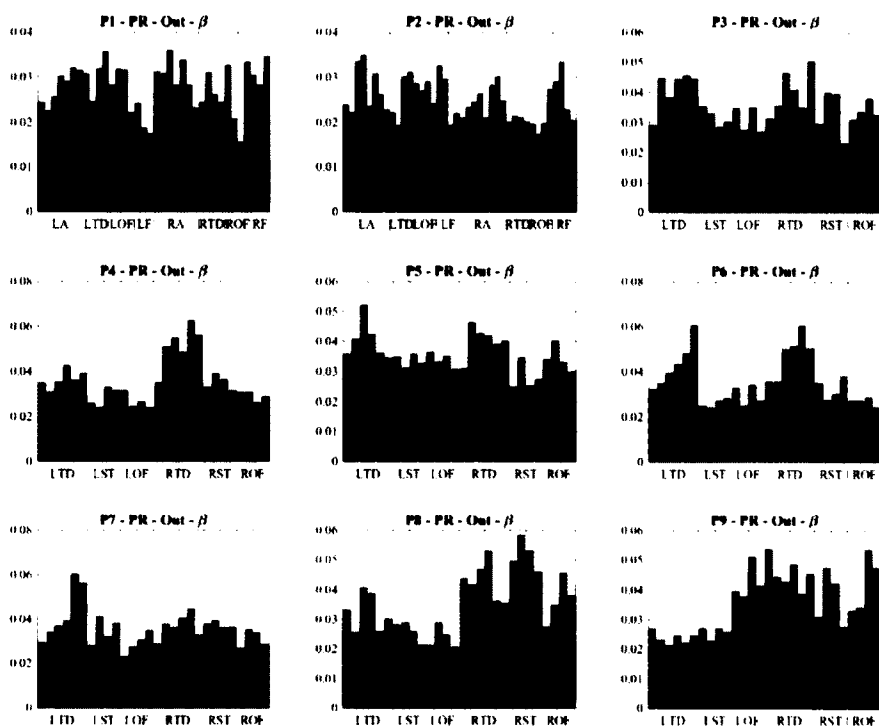
Figure B-39: Outward PageRank centrality averaged for beta frequencies (13-30Hz) over early ictal epochs for each patient.
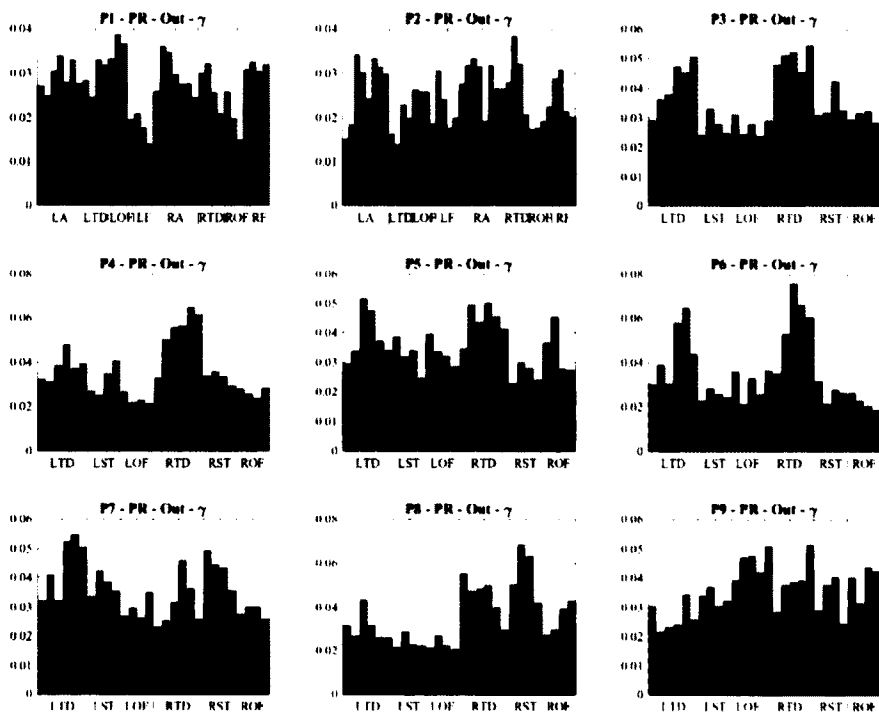

Figure B-40: Outward PageRank centrality averaged for gamma frequencies (31-50Hz) over early ictal epochs for each patient.

Figures B-41 through B-45 show the show the grand average authority scores

from the HITS algorithm per electrode for all patients P1-P9 where individual centralities

were estimated over the $\delta, \theta, \alpha, \beta$, and γ frequency bands, respectively. The first three

epochs of each clinical seizure were averaged per patient. Like many of the previously

shown centrality measures, certain patients show comparatively higher centrality values

in the focal electrode in the lower frequency bands, and these electrodes gain

comparatively higher centrality values than non-focal electrodes in higher frequency

networks. In this case, authority scores lead to successful focus localization in all
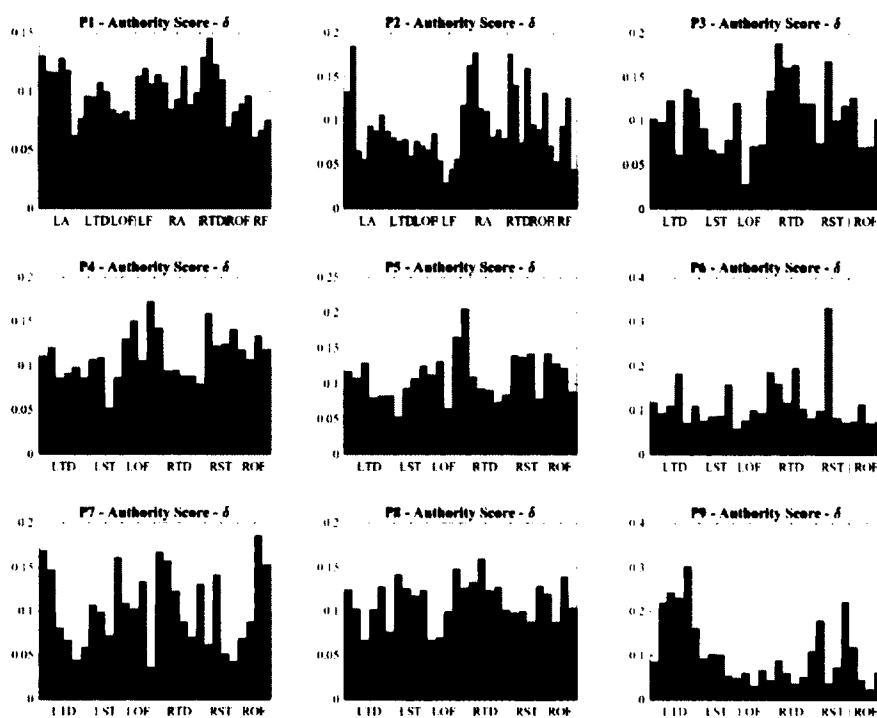
observed patients.

Figure B-41: Authority scores averaged for delta frequencies (1-4Hz) over early ictal epochs for each patient.
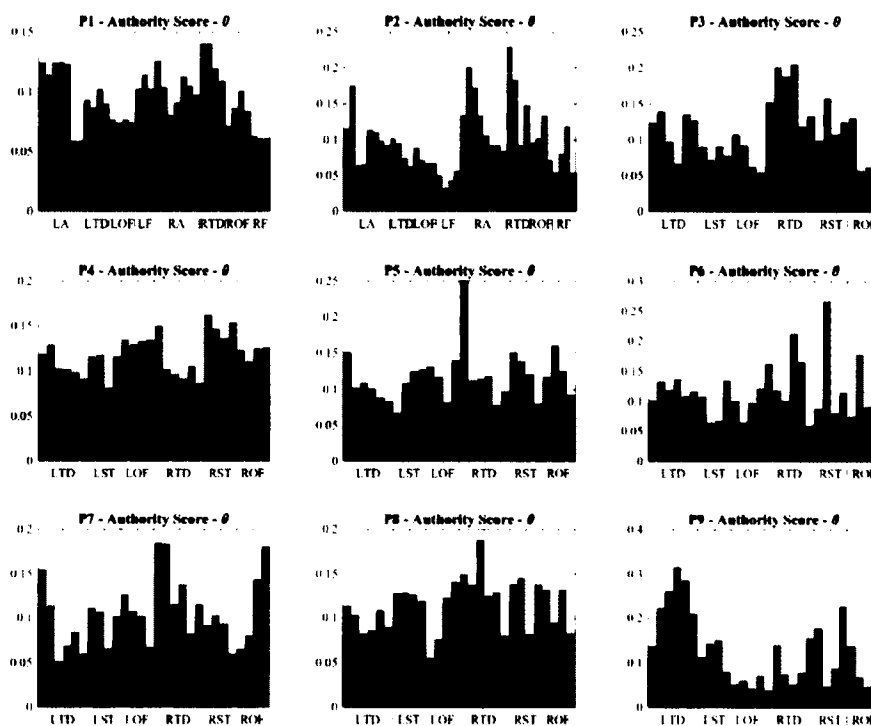
Figure B-42: Authority scores averaged for theta frequencies (5-8Hz) over early ictal epochs for each patient.
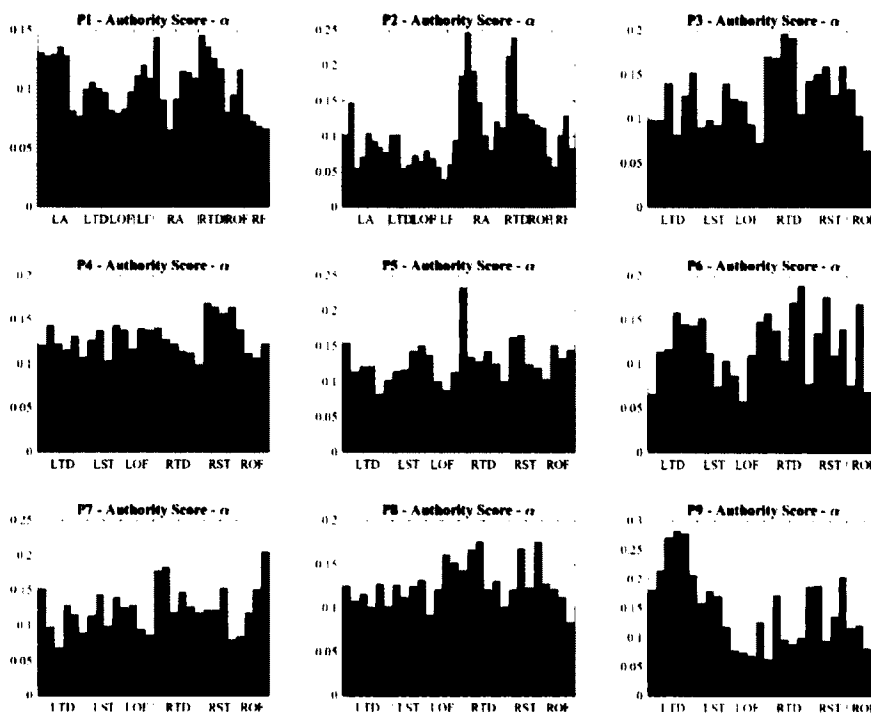

Figure B-43: Authority scores averaged for alpha frequencies (9-12Hz) over early ictal epochs for each patient.
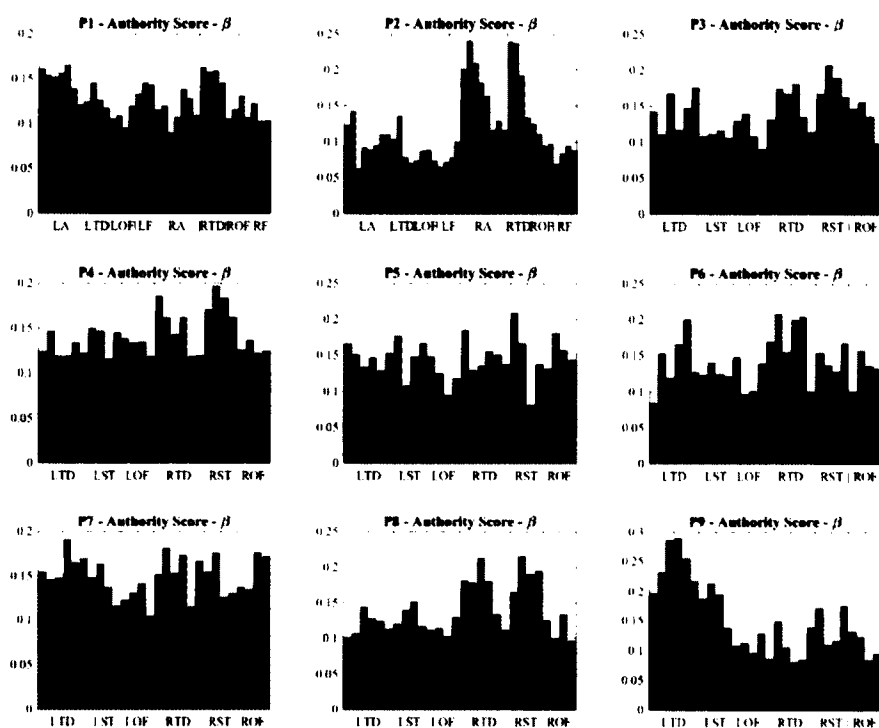
Figure B-44: Authority scores averaged for beta frequencies (13-30Hz) over early ictal epochs for each patient.
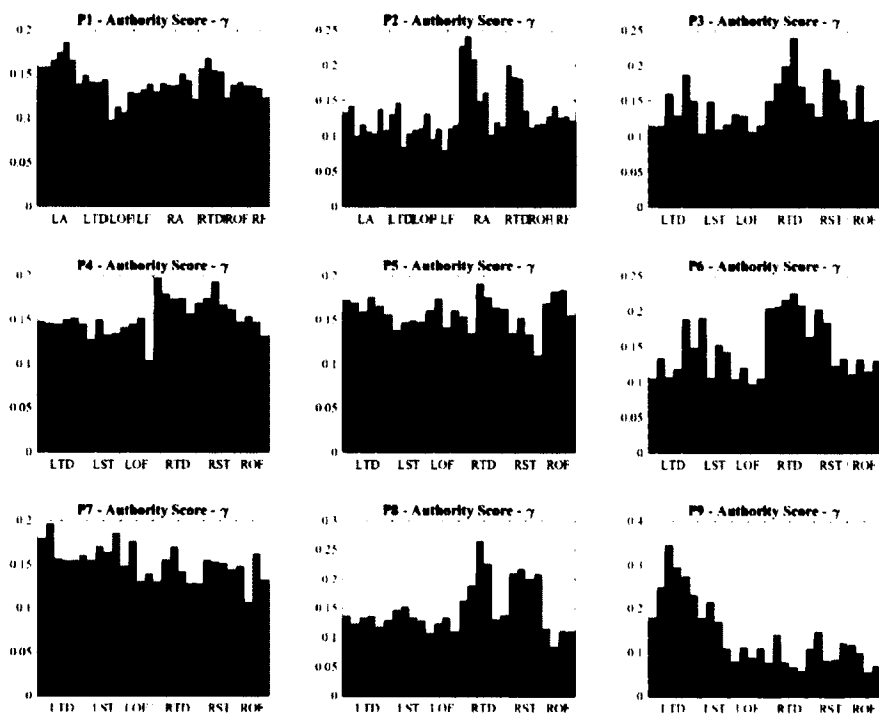

Figure B-45: Authority scores averaged for gamma frequencies (31-50Hz) over early ictal epochs for each patient.

Figures B-46 through B-50 show the show the grand average hub scores from the

HITS algorithm per electrode for all patients P1-P9 where individual centralities were

estimated over the $\delta, \theta, \alpha, \beta$, and γ frequency bands, respectively. The first three epochs

of each clinical seizure were averaged per patient. In patients P3, P6, and P7, focus

localization based on hub scores is successful in all frequency bands except for the delta

band, and for patient P5, focus localization is successful in all frequency bands except for

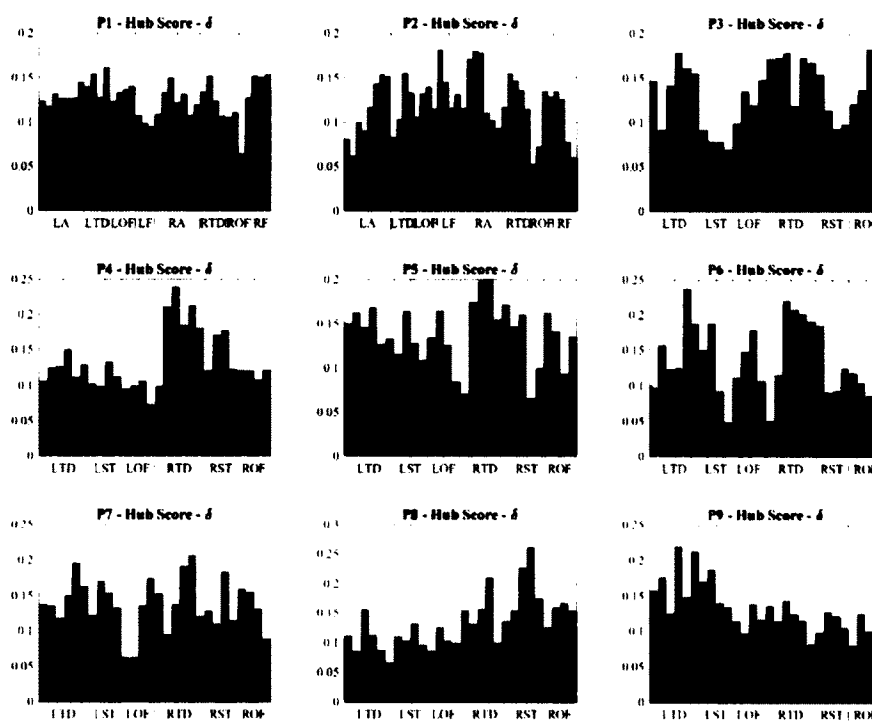the beta band. For patient P4, focus localization is successful at each frequency band.

Figure B-46: Hub scores averaged for delta frequencies (1-4Hz) over early ictal epochs for each patient.

Figure B-47: Hub scores averaged for theta frequencies (5-8Hz) over early ictal epochs for each patient.
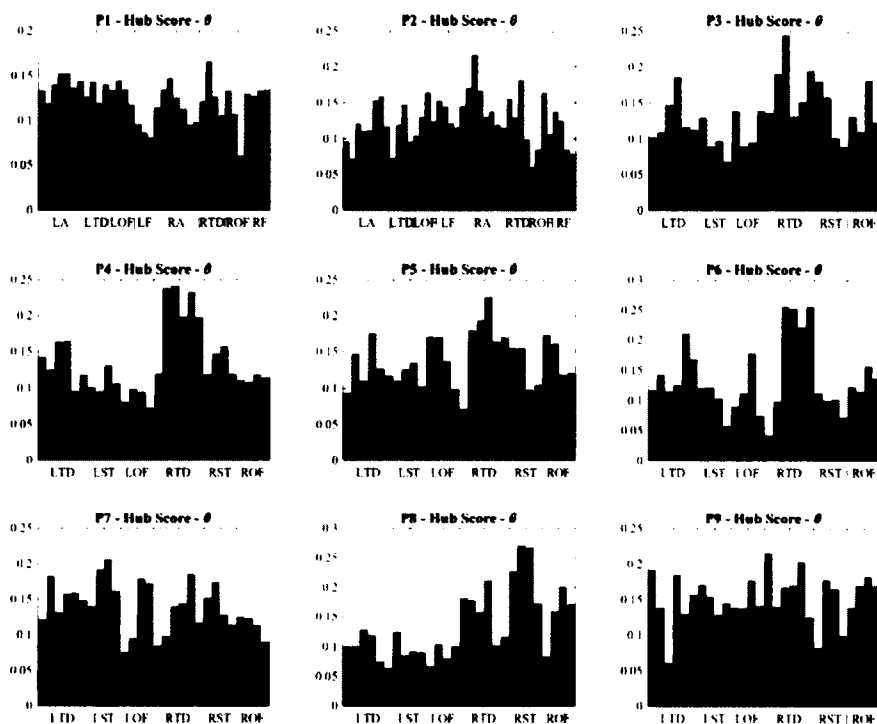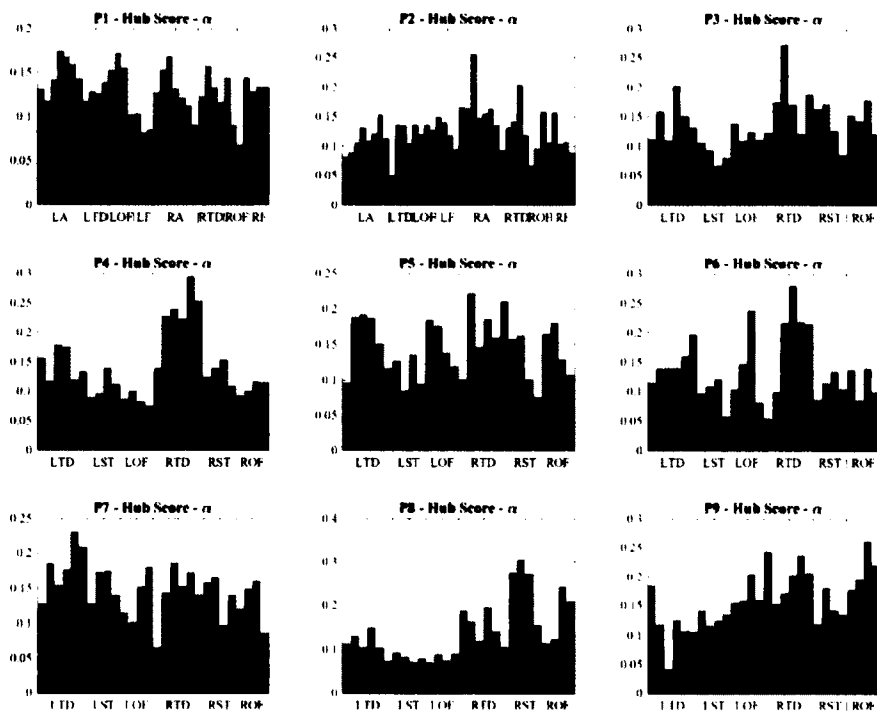

Figure B-48: Hub scores averaged for alpha frequencies (9-12Hz) over early ictal epochs for each patient.
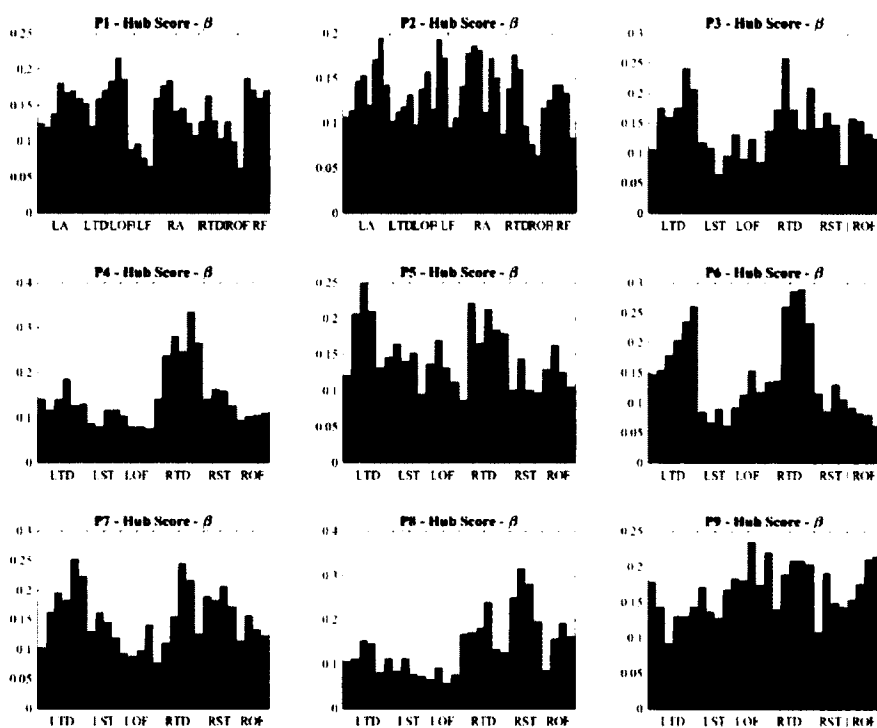
Figure B-49: Hub scores averaged for beta frequencies (13-30Hz) over early ictal epochs for each patient.

Figure B-50: Hub scores averaged for gamma frequencies (31-50Hz) over early ictal epochs for each patient.

Figures B-51 through B-55 show the show the grand average inward harmonic

centrality values per electrode for all patients P1-P9 where individual centralities were

estimated over the $\delta, \theta, \alpha, \beta,$ and γ frequency bands, respectively. The first three epochs

of each clinical seizure were averaged per patient. For all patients except patient P9, the

variation of inward harmonic centrality values decreases for higher frequency spectra,

with the maximum value moving into the epileptogenic focus. In the gamma band, the

focus is successfully localized in all patients based on our methodology.

Figure B-51: Inward harmonic centrality averaged for delta frequencies (1-4Hz) over early
ictal epochs for each patient.

Figure B-52: Inward harmonic centrality averaged for theta frequencies (5-8Hz) over early ictal epochs for each patient.

Figure B-53: Inward harmonic centrality averaged for alpha frequencies (9-12Hz) over early ictal epochs for each patient.

Figure B-54: Inward harmonic centrality averaged for beta frequencies (13-30Hz) over early ictal epochs for each patient.

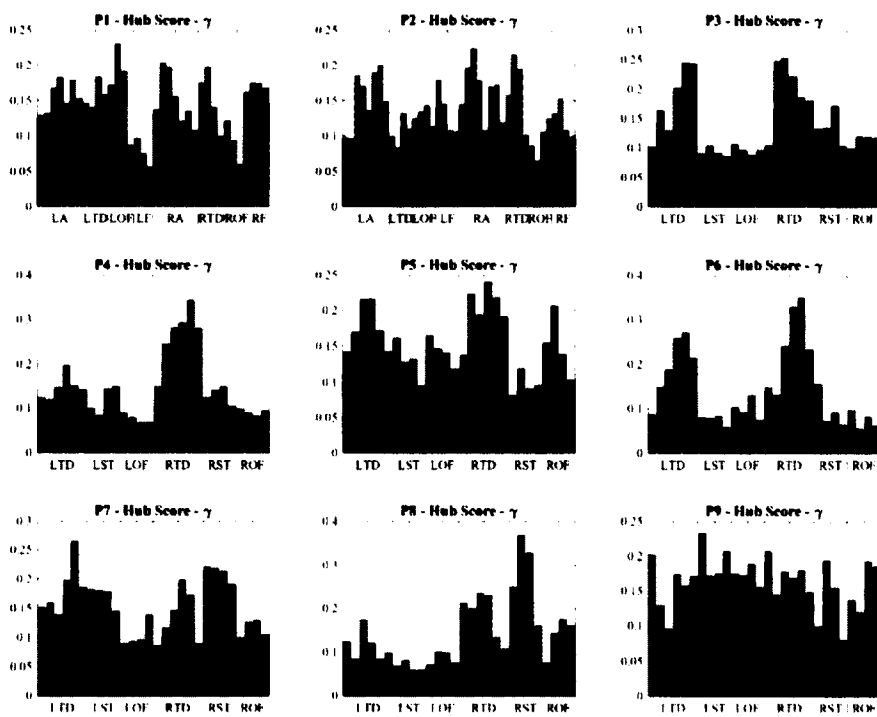Figure B-55: Inward harmonic centrality averaged for gamma frequencies (31-50Hz) over early ictal epochs for each patient.

Figures B-56 through B-60 show the show the grand average outward harmonic

centrality values per electrode for all patients P1-P9 where individual centralities were

estimated over the $\delta, \theta, \alpha, \beta$, and γ frequency bands, respectively. The first three epochs

of each clinical seizure were averaged per patient. For higher frequency bands, patients

P3 through P7 show relatively higher outward harmonic centrality values in the set of

focal electrodes compared to non-focal electrodes with the gamma band showing

successful focus localization based on our methodology for these patients. For patient P9,

the opposite behavior is seen in outward harmonic centrality values for increasing

frequency bands as compared to the behavior of inward harmonic centrality with the

focal electrodes having relatively smaller outward centrality values than the non-focal
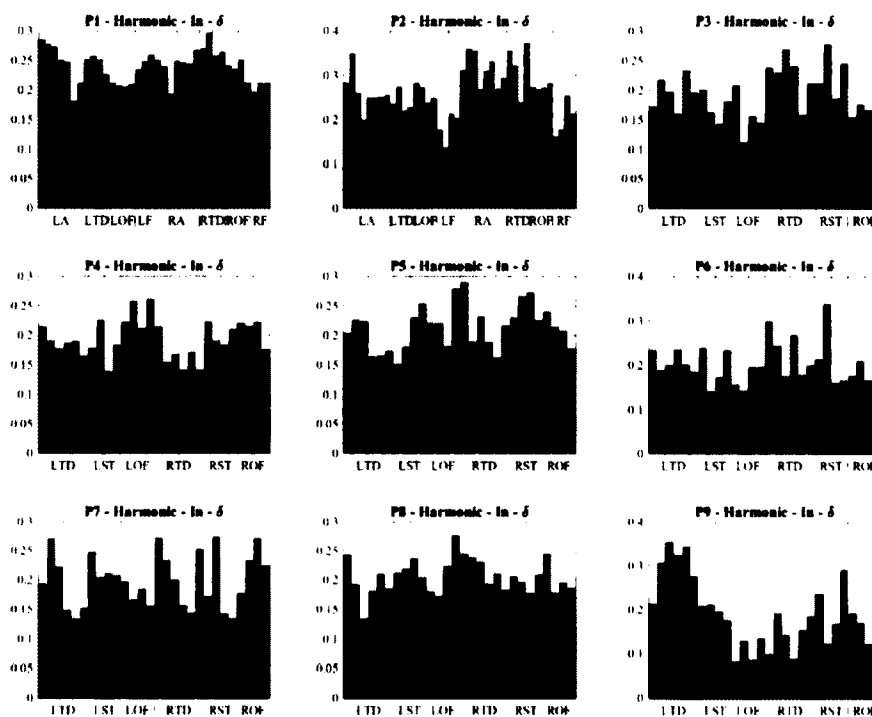
electrodes as frequency increases.

Figure B-56: Outward harmonic centrality averaged for delta frequencies (1-4Hz) over early ictal epochs for each patient.
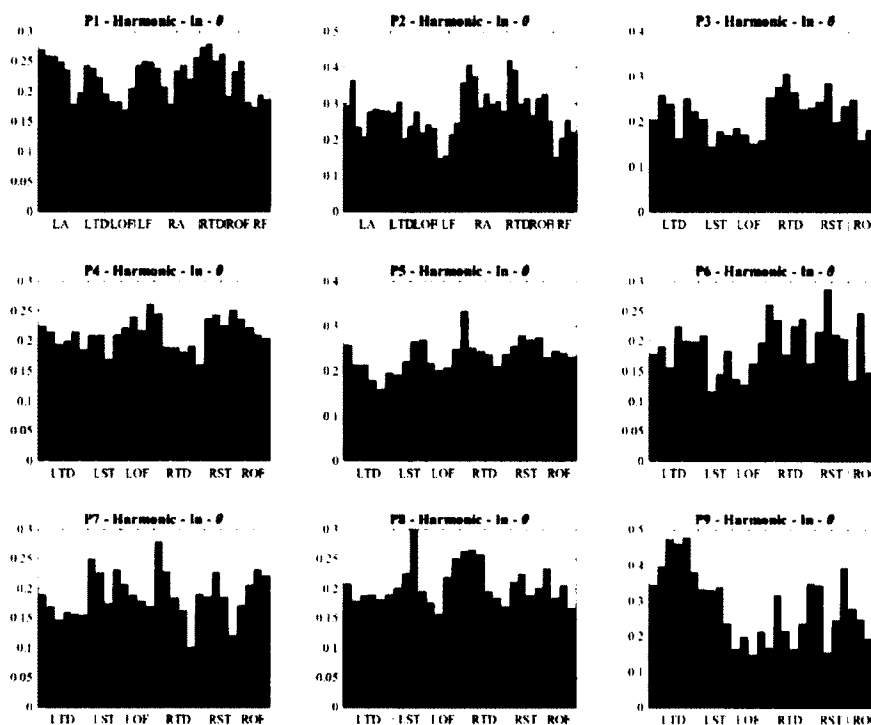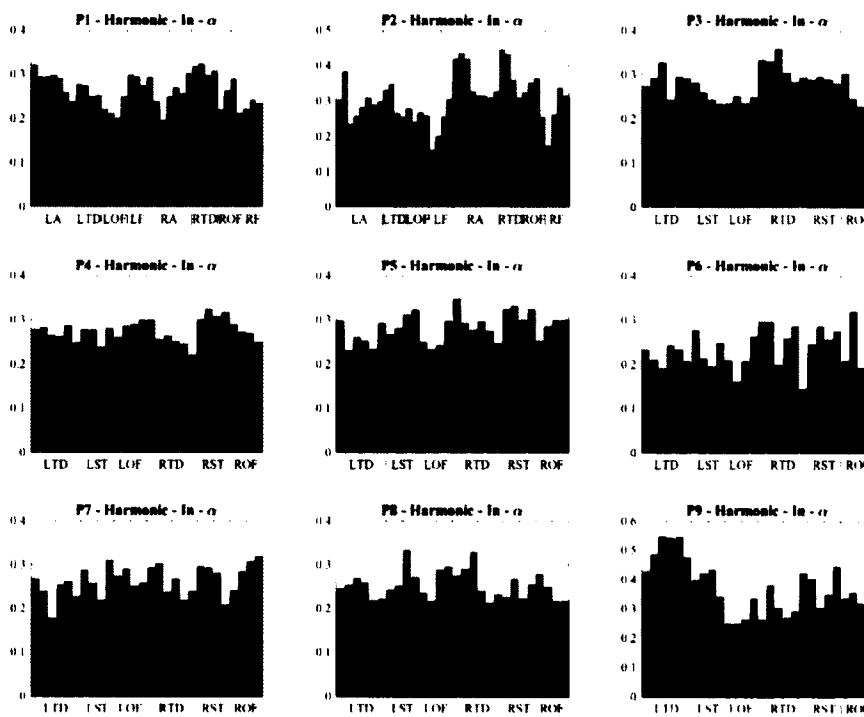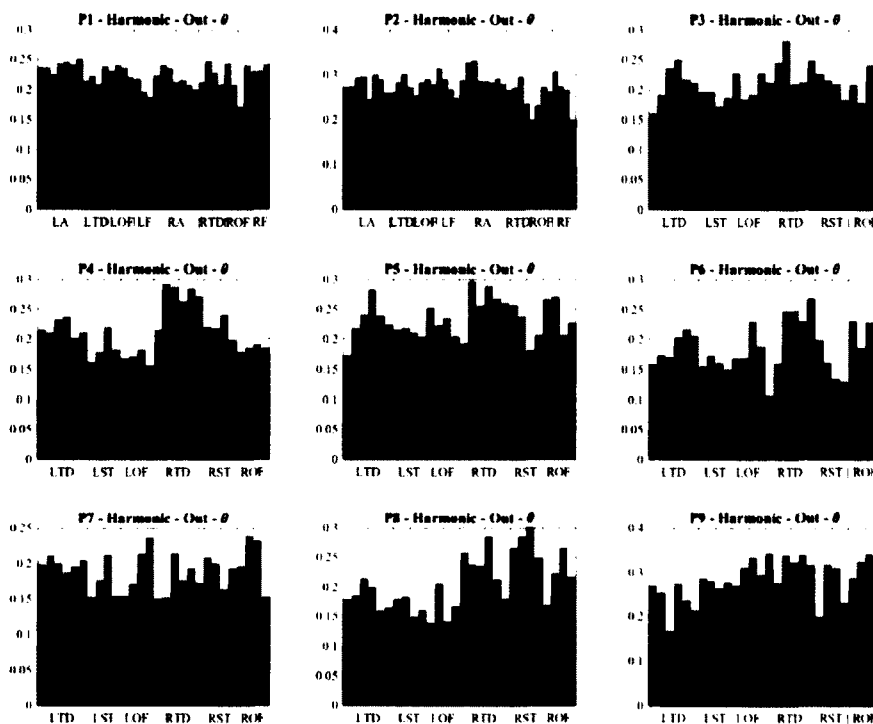
Figure B-57: Outward harmonic centrality averaged for theta frequencies (5-8Hz) over early ictal epochs for each patient.

Figure B-58: Outward harmonic centrality averaged for alpha frequencies (9-12Hz) over early ictal epochs for each patient.
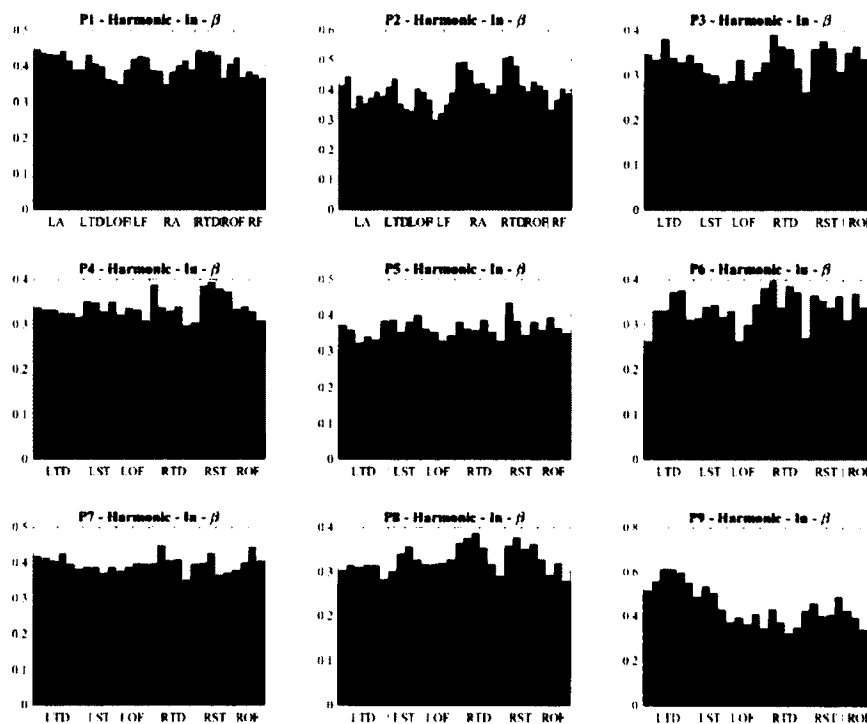
Figure B-59: Outward harmonic centrality averaged for beta frequencies (13-30Hz) over early ictal epochs for each patient.
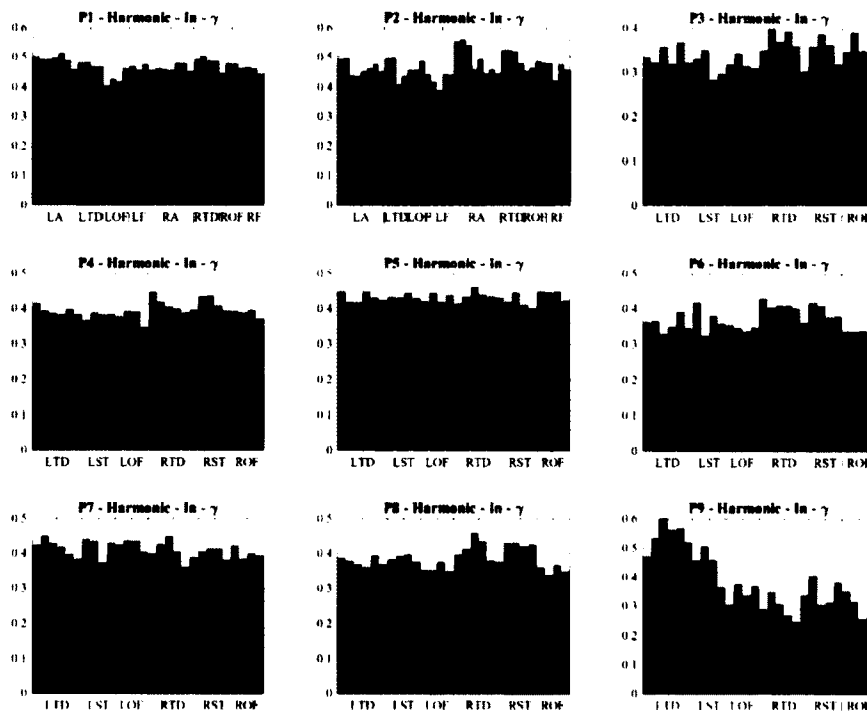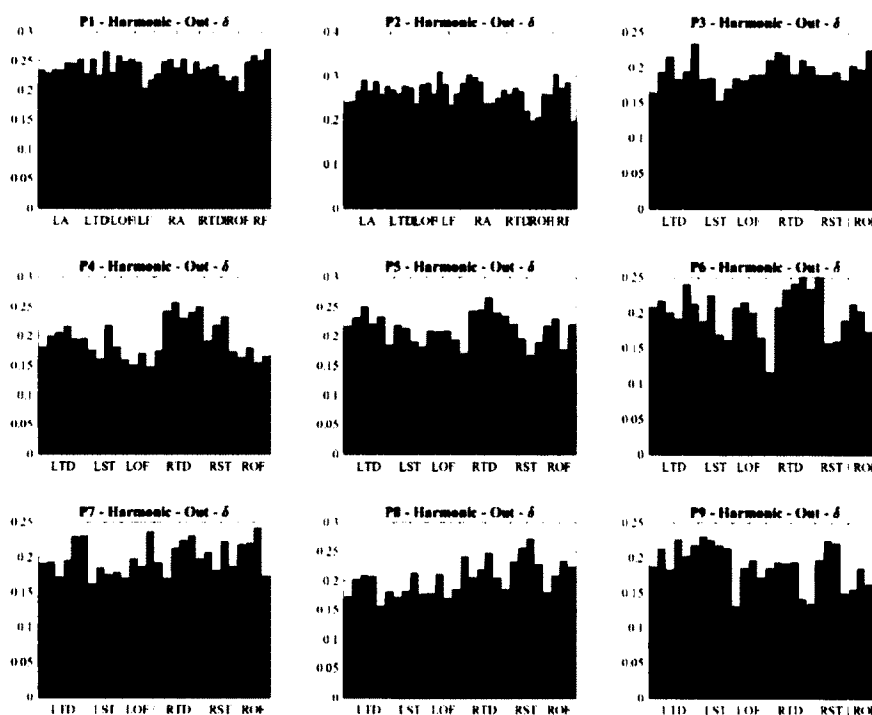

Figure B-60: Outward harmonic centrality averaged for gamma frequencies (31-50Hz) over early ictal epochs for each patient.

Figures B-61 through B-65 show the show the grand average betweenness

centrality values per electrode for all patients P1-P9 where individual centralities were

estimated over the $\delta, \theta, \alpha, \beta$, and γ frequency bands, respectively. The first three epochs

of each clinical seizure were averaged per patient. For patients P2 and P9, betweenness

centrality in the delta frequency band shows markedly higher values in the focal

electrodes compared to non-focal electrodes, but for higher frequency bands, this

prominent behavior seems to is lost for patient P9 and remains for patient P2. For patients

P3 through P7, betweenness centrality becomes relatively higher in focal electrodes

compared to non-focal electrodes as frequency increases. For patient P1, relative

betweenness values between electrodes does not seem to change dramatically for any

frequency band.

Figure B-61: Betweenness centrality averaged for delta frequencies (1-4Hz) over early ictal epochs for each patient.

Figure B-62: Betweenness centrality averaged for theta frequencies (5-8Hz) over early ictal epochs for each patient.

Figure B-63: Betweenness centrality averaged for alpha frequencies (9-12Hz) over early ictal epochs for each patient.
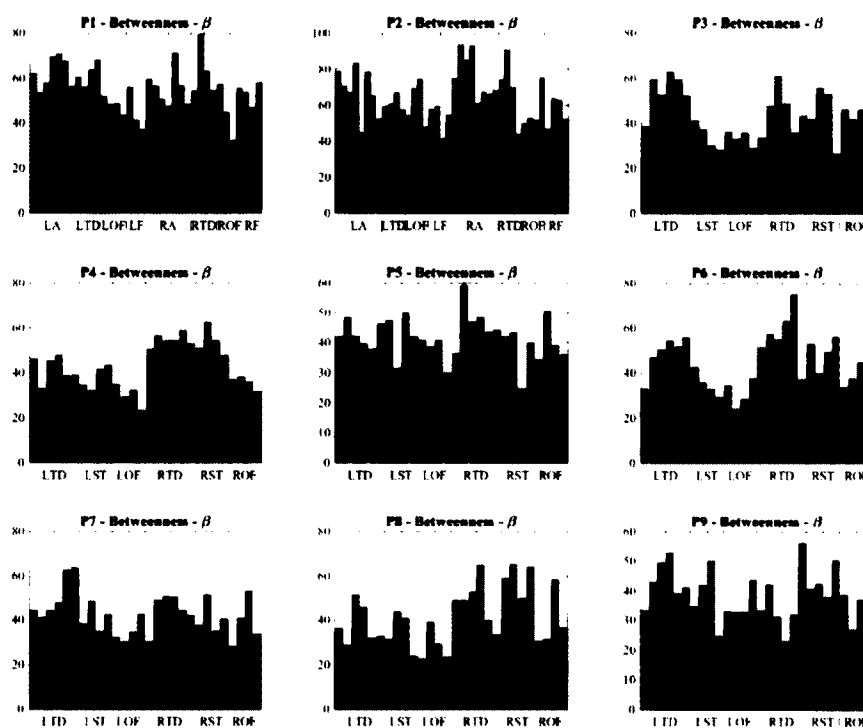
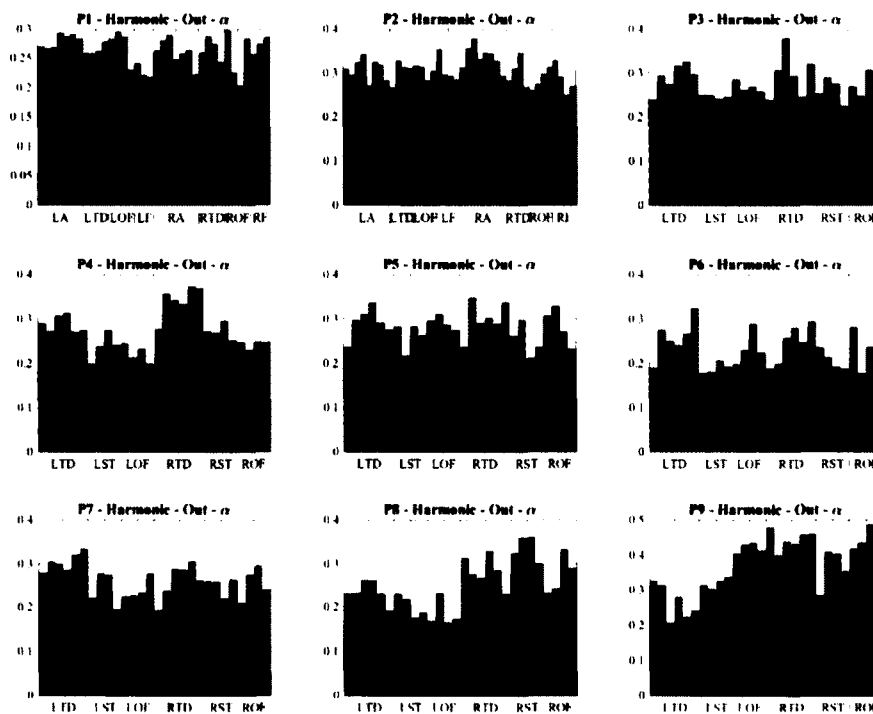Figure B-64: Betweenness centrality averaged for beta frequencies (13-30Hz) over early ictal epochs for each patient.

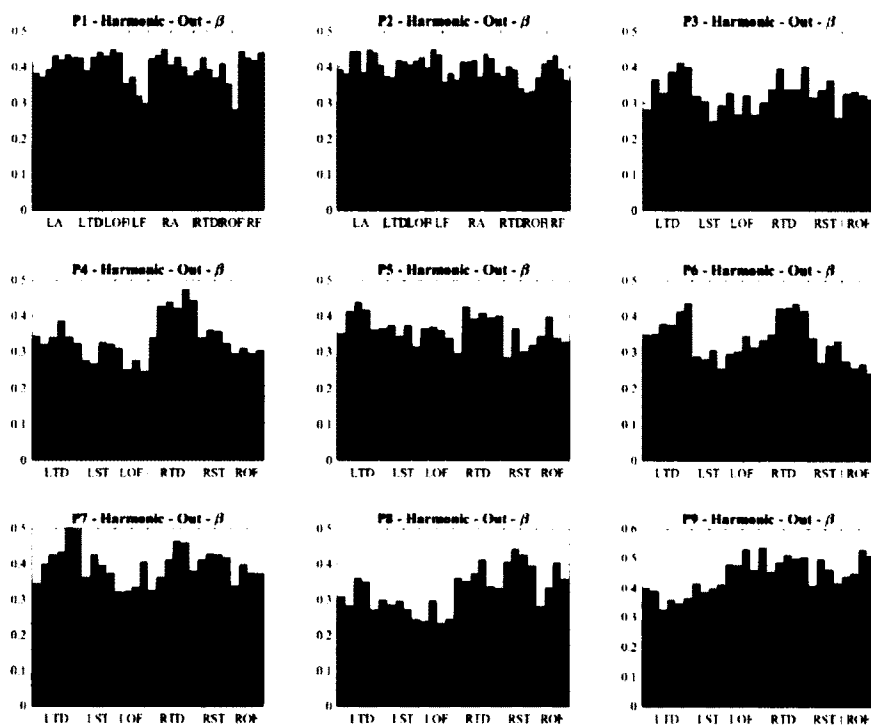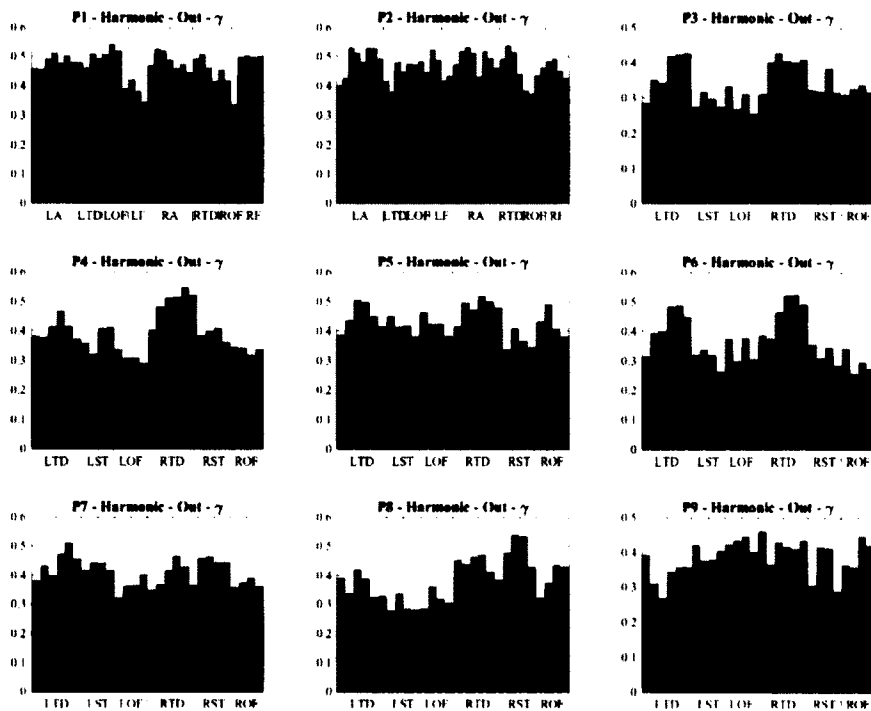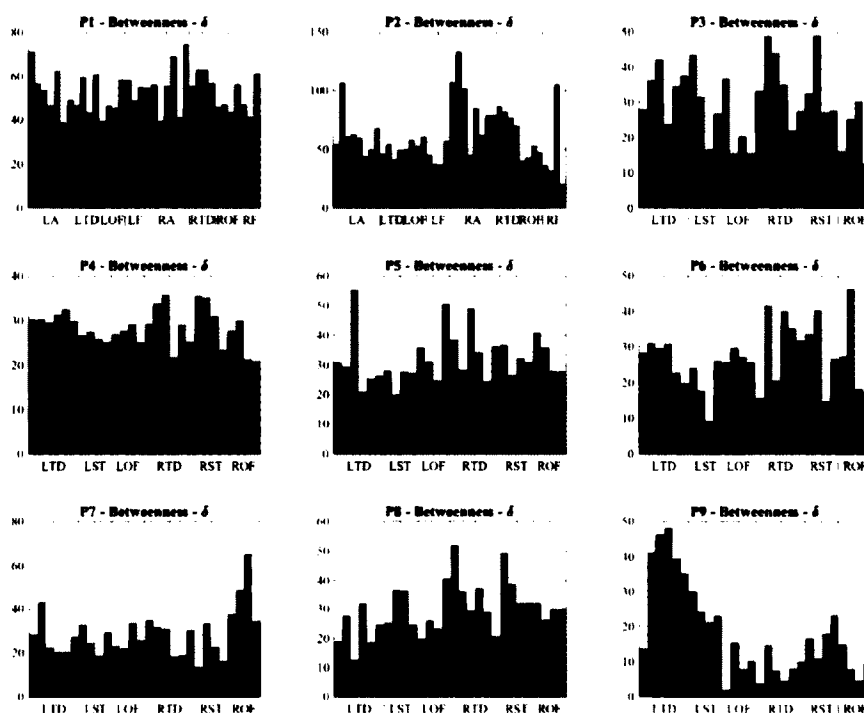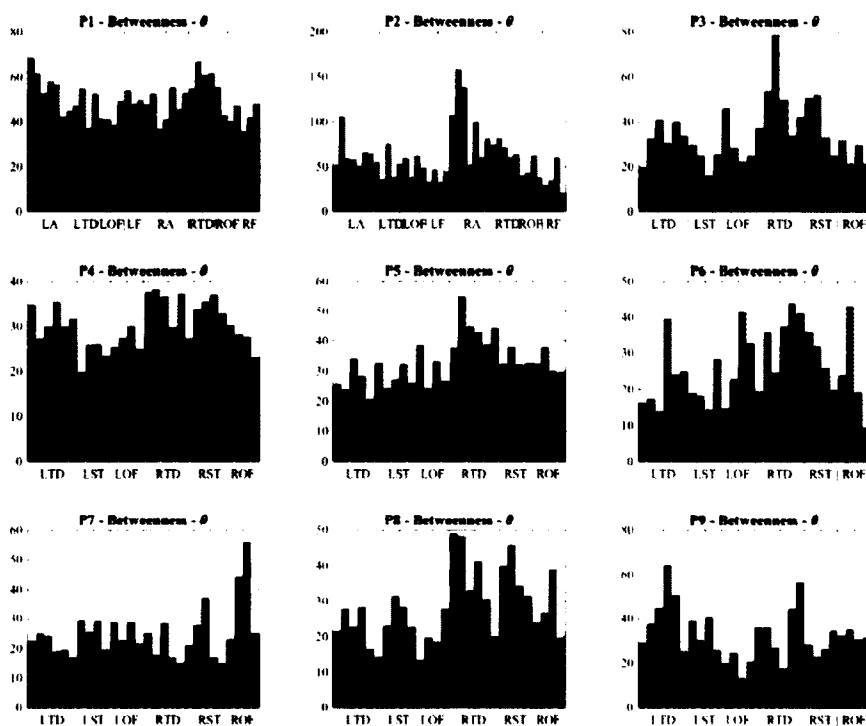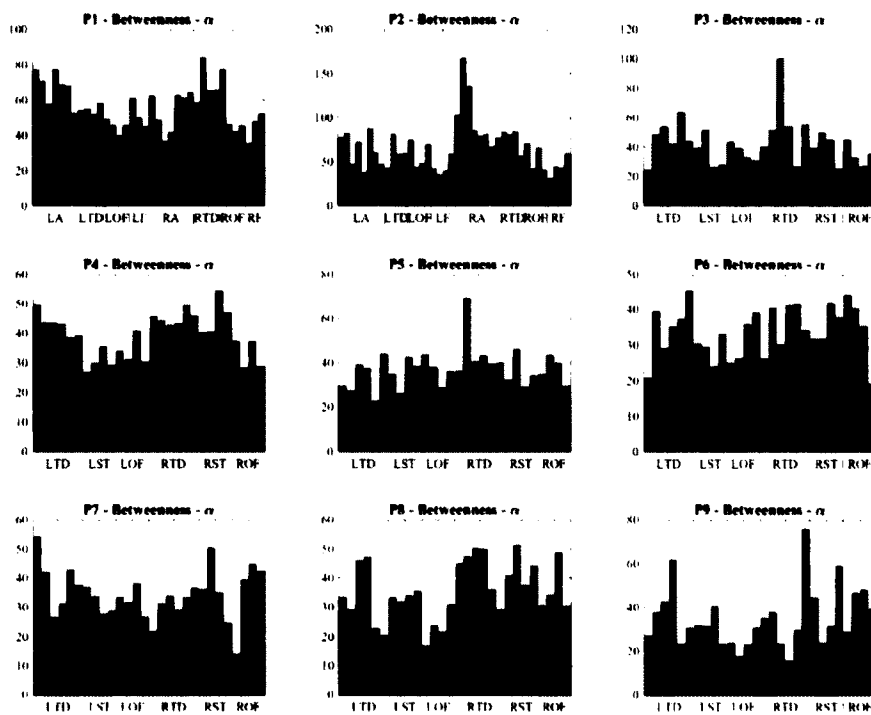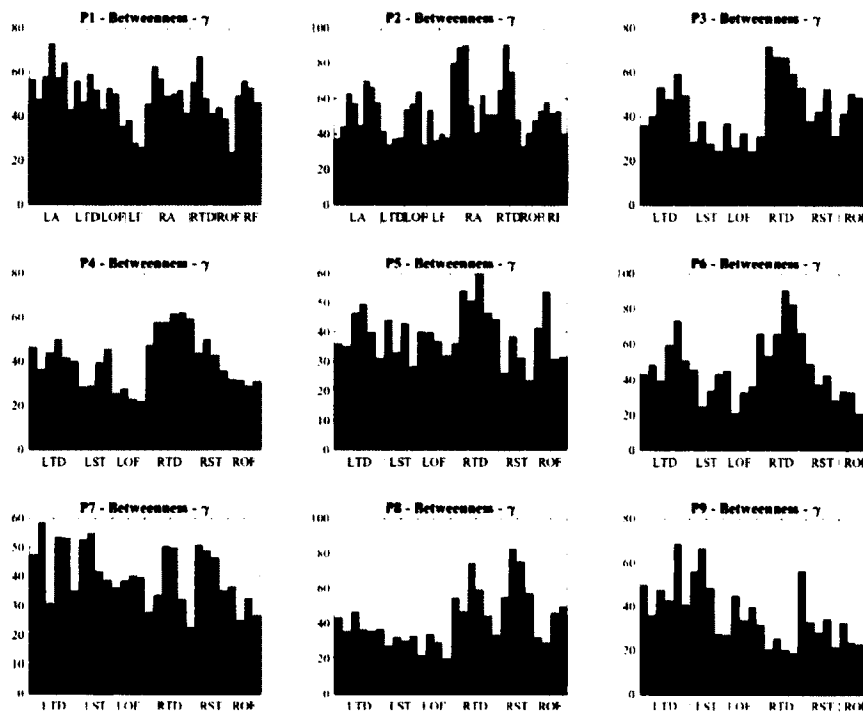Figure B-65: Betweenness centrality averaged for gamma frequencies (31-50Hz) over early ictal epochs for each patient.

BIBLIOGRAPHY

[1]   F. A. C. Azevedo, L. R. B. Carvalho, L. T. Grinberg, J. M. Farfel, R. E. L. Ferretti, R. E. P. Leite, W. J. Filho, R. Lent, and S. Herculano-Houzel, "Equal numbers of neuronal and nonneuronal cells make the human brain an isometrically scaled-up primate brain," *J. Comp. Neurol.*, vol. 513, no. 5, pp. 532–541, 2009.

[2]   R. W. Williams and K. Herrup, "The control of neuron number.," *Annu. Rev. Neurosci.*, vol. 11, pp. 423–53, 1988.

[3]   D. Purves, G. J. Augustine, D. Fitzpatrick, W. C. Hall, A.-S. Lamantia, J. O. Mcnamara, and S. M. Willians, *Neuroscience*, 4th ed. Sinauer Associates, Inc.

[4]   R. S. Fisher, C. Acevedo, A. Arzimanoglou, A. Bogacz, J. H. Cross, C. E. Elger, J. Engel, L. Forsgren, J. A. French, M. Glynn, D. C. Hesdorffer, B. I. Lee, G. W. Mathern, S. L. Moshé, E. Perucca, I. E. Scheffer, T. Tomson, M. Watanabe, and S. Wiebe, "ILAE Official Report: A practical clinical definition of epilepsy," *Epilepsia*, vol. 55, no. 4, pp. 475–482, 2014.

[5]   D. Hirtz, D. J. Thurman, K. Gwinn-Hardy, M. Mohamed, A. R. Chaudhuri, and R. Zalutsky, "How common are the 'common' neurologic disorders?," *Neurology*, vol. 68, no. 5, pp. 326–337, 2007.

[6]   D. Yoon, K. D. Frick, D. A. Carr, and J. K. Austin, "Economic impact of epilepsy in the United States," *Epilepsia*, vol. 50, no. 10, pp. 2186–2191, 2009.

[7]   C. E. Begley, M. Famulari, J. F. Annegers, D. R. Lairson, T. F. Reynolds, S. Coan, S. Dubinsky, M. E. Newmark, C. Leibson, E. L. So, and W. A. Rocca, "The cost of epilepsy in the United States: an estimate from population-based clinical and survey data.," *Epilepsia*, vol. 41, no. 3, pp. 342–51, 2000.

[8]   M. J. England, C. T. Liverman, A. M. Schultz, and L. M. Strawbridge, "Epilepsy across the spectrum: Promoting health and understanding. A summary of the Institute of Medicine report," *Epilepsy and Behavior*, vol. 25, no. 2. pp. 266–276, 2012.

[9]   Y. Schiller and Y. Najjar, "Quantifying the response to antiepileptic drugs: Effect of past treatment history," *Neurology*, vol. 70, no. 1, pp. 54–65, 2008.

161

[10] W. A. Hauser, J. F. Annegers, and W. A. Rocca, "Descriptive epidemiology of epilepsy: Contributions of population-based studies from Rochester, Minnesota.," *Mayo Clin. Proc.*, vol. 71, no. 6, pp. 576–586, 1996.

[11] B. C. Jobst and G. D. Cascino, "Resective Epilepsy Surgery for Drug-Resistant Focal Epilepsy: A Review.," *JAMA*, vol. 313, no. 3, pp. 285–293, 2015.

[12] M. Thom, G. W. Mathern, J. H. Cross, and E. H. Bertram, "Mesial temporal lobe epilepsy: How do we improve surgical outcome?," *Ann. Neurol.*, vol. 68, no. 4, pp. 424–434, 2010.

[13] J. Janszky, I. Janszky, R. Schulz, M. Hoppe, F. Behne, H. W. Pannek, and A. Ebner, "Temporal lobe epilepsy with hippocampal sclerosis: predictors for long-term surgical outcome.," *Brain*, vol. 128, no. 2, pp. 395–404, 2005.

[14] W. L. Ramey, N. L. Martirosyan, C. M. Lieu, H. A. Hasham, J. Lemole, and M. E. Weinand, "Current management and surgical outcomes of medically intractable epilepsy," *Clin. Neurol. Neurosurg.*, vol. 115, no. 12, pp. 2411–2418, 2013.

[15] C. H. Yun, S. K. Lee, S. Y. Lee, K. K. Kim, S. W. Jeong, and C. K. Chung, "Prognostic factors in neocortical epilepsy surgery: Multivariate analysis," *Epilepsia*, vol. 47, no. 3, pp. 574–579, 2006.

[16] S. K. Lee, S. Y. Lee, K. K. Kim, K. S. Hong, D. S. Lee, and C. K. Chung, "Surgical outcome and prognostic factors of cryptogenic neocortical epilepsy," *Ann. Neurol.*, vol. 58, no. 4, pp. 525–532, 2005.

[17] T. S. Walczak, R. a Radtke, and D. V Lewis, "Accuracy and interobserver reliability of scalp ictal EEG.," *Neurology*, vol. 42, no. 12, pp. 2279–2285, 1992.

[18] P. Widdess-Walsh, L. Jeha, D. Nair, P. Kotagal, W. Bingaman, and I. Najm, "Subdural electrode analysis in focal cortical dysplasia: Predictors of surgical outcome," *Neurology*, vol. 69, no. 7, pp. 660–667, 2007.

[19] J. C. Bulacio, L. Jehi, C. Wong, J. Gonzalez-Martinez, P. Kotagal, D. Nair, I. Najm, and W. Bingaman, "Long-term seizure outcome after resective surgery in patients evaluated with intracranial electrodes," *Epilepsia*, vol. 53, no. 10, pp. 1722–1730, 2012.

[20] M. Kamiński and K. Blinowska, "A new method of the description of the information flow in the brain structures," *Biol. Cybern.*, vol. 65, no. 3, pp. 203–210, 1991.

[21] L. A. Baccalá and K. Sameshima, "Partial directed coherence: a new concept in neural structure determination.," *Biol. Cybern.*, vol. 84, no. 6, pp. 463–74, Jun. 2001.

[22]   L. A. Baccalá, F. de Medicina, K. Sameshima, and D. Y. Takahashi, "Generalized partial directed coherence," in *Proc. of the 2007 15th Intl. Conf. on Digital Signal Processing*, 2007, no. 3, pp. 163–166.

[23]   W. Liao, Z. Zhang, Z. Pan, D. Mantini, J. Ding, X. Duan, C. Luo, G. Lu, and H. Chen, "Altered functional connectivity and small-world in mesial temporal lobe epilepsy.," *PLoS One*, vol. 5, no. 1, p. e8525, Jan. 2010.

[24]   S. Achard, R. Salvador, B. Whitcher, J. Suckling, and E. T. Bullmore, "A resilient, low-frequency, small-world human brain functional network with highly connected association cortical hubs.," *J. Neurosci.*, vol. 26, no. 1, pp. 63–72, Jan. 2006.

[25]   Y. Liu, M. Liang, Y. Zhou, Y. He, Y. Hao, M. Song, C. Yu, H. Liu, Z. Liu, and T. Jiang, "Disrupted small-world networks in schizophrenia.," *Brain*, vol. 131, no. 4, pp. 945–961, Apr. 2008.

[26]   M. P. van den Heuvel, C. J. Stam, M. Boersma, and H. E. Hulshoff Pol, "Small-world and scale-free organization of voxel-based resting-state functional connectivity in the human brain.," *Neuroimage*, vol. 43, no. 3, pp. 528–39, Nov. 2008.

[27]   E. van Diessen, W. M. Otte, K. P. J. Braun, C. J. Stam, and F. E. Jansen, "Improved Diagnosis in Children with Partial Epilepsy Using a Multivariable Prediction Model Based on EEG Network Characteristics," *PLoS One*, vol. 8, no. 4, 2013.

[28]   M. A. Quraan, C. McCormick, M. Cohn, T. A. Valiante, and M. P. McAndrews, "Altered Resting State Brain Dynamics in Temporal Lobe Epilepsy Can Be Observed in Spectral Power, Functional Connectivity and Graph Theory Metrics," *PLoS One*, vol. 8, no. 7, 2013.

[29]   C. Wilke, G. A. Worrell, and B. He, "Analysis of epileptogenic network properties during ictal activity," in *Proceedings of the 31st Annual International Conference of the IEEE Engineering in Medicine and Biology Society: Engineering the Future of Biomedicine, EMBC 2009*, 2009, pp. 2220–2223.

[30]   P. van Mierlo, E. Carrette, H. Hallez, K. Vonck, D. Van Roost, P. Boon, and S. Staelens, "Accurate epileptogenic focus localization through time-variant functional connectivity analysis of intracranial electroencephalographic signals.," *Neuroimage*, vol. 56, pp. 1122–1133, 2011.

[31]   P. Van Mierlo, E. Carrette, H. Hallez, R. Raedt, A. Meurs, S. Vandenberghe, D. Van Roost, P. Boon, S. Staelens, and K. Vonck, "Ictal-onset localization through connectivity analysis of intracranial EEG signals in patients with refractory epilepsy," *Epilepsia*, vol. 54, no. 8, pp. 1409–1418, 2013.

[32] S. P. Burns, S. Santaniello, R. B. Yaffe, C. C. Jouny, and N. E. Crone, "Network dynamics of the brain and influence of the epileptic seizure onset zone," in *Proceedings of the National Academy of Sciences of the United States of America*, 2014, vol. 111, no. 49, pp. E5321–5330.

[33] Z. Haneef and S. Chiang, "Clinical correlates of graph theory findings in temporal lobe epilepsy," *Seizure*, vol. 23, no. 10, pp. 809–818, 2014.

[34] P. van Mierlo, M. Papadopoulou, E. Carrette, P. Boon, S. Vandenberghe, K. Vonck, and D. Marinazzo, "Functional brain connectivity from EEG in epilepsy: Seizure prediction and epileptogenic focus localization," *Prog. Neurobiol.*, vol. 121, pp. 19–35, 2014.

[35] R. T. Constable, D. Scheinost, E. S. Finn, X. Shen, M. Hampson, F. S. Winstanley, D. D. Spencer, and X. Papademetris, "Potential use and challenges of functional connectivity mapping in intractable epilepsy," *Front. Neurol.*, vol. 4, 2013.

[36] H. Lütkepohl, "Comparison of Criteria for Estimating the Order of a Vector Autoregressive Process," *J. Time Ser. Anal.*, vol. 6, no. 1, pp. 35–52, 1985.

[37] M. Morf, a. Vieira, D. T. L. Lee, and T. Kailath, "Recursive Multichannel Maximum Entropy Spectral Estimation," *IEEE Trans. Geosci. Electron.*, vol. 16, no. 2, pp. 85–94, 1978.

[38] A. Schlögl, "A comparison of multivariate autoregressive estimators," *Signal Processing*, vol. 86, no. 9, pp. 2426–2429, 2006.

[39] M. R. Gevers and B. D. O. Anderson, "Representations of jointly stationary stochastic feedback processes†," *Int. J. Control*, vol. 33, no. 5, pp. 777–809, 1981.

[40] L. Faes, S. Erla, and G. Nollo, "Measuring connectivity in linear multivariate processes: definitions, interpretation, and practical analysis.," *Comput. Math. Methods Med.*, vol. 2012, p. 140513, Jan. 2012.

[41] D. Kugiumtzis, "Surrogate Data Test on Time Series," in *Modelling and Forecasting Financial Data: Techniques of Nonlinear Dynamics*, 2002, pp. 267–282..

[42] T. Schreiber and A. Schmitz, "Improved surrogate data for nonlinearity tests," *Phys. Rev. Lett.*, vol. 77, pp. 635–638, Sep. 1999.

[43] J. L. Gross and J. Yellen, *Graph Theory and Its Applications*, 2nd ed. Boca Raton, FL: Chapman & Hall/CRC, 2006.

[44] D. Poole, *Linear Algebra: A Modern Introduction*, Third. Brooks/Cole, Cengage Learning, 2011.

[45]   M. E. J. Newman, *Networks: An Introduction*. Oxford: Oxford University Press, 2010.

[46]   P. R. Gould, "On the Geographical Interpretation of Eigenvalues," *Trans. Inst. Br. Geogr.*, no. 42, pp. 53–86, 1967.

[47]   L. Page, S. Brin, R. Motwani, and T. Winograd, "The PageRank Citation Ranking: Bringing Order to the Web," *World Wide Web Internet Web Inf. Syst.*, vol. 54, no. 1999–66, pp. 1–17, 1998.

[48]   J. M. Kleinberg, "Authoritative Sources in a Hyperlinked Environment," *J. ACM*, vol. 46, no. May 1997, pp. 668–677, 1999.

[49]   L. Katz, "A new status index derived from sociometric analysis," *Psychometrika*, vol. 18, no. 1, pp. 39–43, 1953.

[50]   Y. Rochat, "Closeness centrality extended to unconnected graphs: The harmonic centrality index," in *Applications of Social Network Analysis*, 2009.

[51]   L. C. Freeman, "A Set of Measures of Centrality Based on Betweenness," *Sociometry*, vol. 40, no. 1, pp. 35–41, 1977.

[52]   I. Vlachos, B. Krishnan, J. Sirven, K. Noe, J. Drazkowski, and L. D. Iasemidis, "Frequency-based Connectivity Analysis of Interictal iEEG to Localize the Epileptogenic Focus," in *Proceedings of the 29th Southern Biomedical Engineering Conference*, 2013.

[53]   L. D. Iasemidis, J. C. Sackellares, H. P. Zaveri, and W. J. Williams, "Phase space topography and the Lyapunov exponent of electrocorticograms in partial seizures," *Brain Topogr.*, vol. 2, no. 3, pp. 187–201, 1990.

[54]   K. J. Blinowska, "Review of the methods of determination of directed connectivity from multichannel data," *Med. Biol. Eng. Comput.*, vol. 49, no. 5, pp. 521–529, May 2011.

[55]   L. D. Brown, T. T. Cai, and A. DasGupta, "Interval Estimation for a Binomial Proportion," *Stat. Sci.*, vol. 16, no. 2, pp. 101–117, 2001.

[56]   R. J. Morgan and I. Soltesz, "Nonrandom connectivity of the epileptic dentate gyrus predicts a major role for neuronal hubs in seizures," in *Proceedings of the National Academy of Sciences of the United States of America*, 2008.

[57]   R. S. Sloviter, "Permanently altered hippocampal structure, excitability, and inhibition after experimental status epilepticus in the rat: the 'dormant basket cell' hypothesis and its possible relevance to temporal lobe epilepsy," *Hippocampus*, vol. 1, pp. 41–66, 1991.

[58] M. de Curtis and V. Gnatkovsky, "Reevaluating the mechanisms of focal ictogenesis: The role of low-voltage fast activity.," *Epilepsia*, vol. 50, no. 12, pp. 2514–2525, 2009.

[59] L. D. Iasemidis, "Epileptic seizure prediction and control.," *IEEE Trans. Biomed. Eng.*, vol. 50, no. 5, pp. 549–558, 2003.

[60] L. D. Iasemidis, "Seizure Prediction and its Applications.," *Neurosurg. Clin. N. Am.*, vol. 22, no. 4, pp. 489–506, vi, Oct. 2011.

[61] K. S. Tsakalis, N. Chakravarthy, Sabesan, L. D. Iasemidis, and Pardalos, "A feedback control systems view of epileptic seizures," *Cybern. Syst. Anal.*, vol. 42, no. 4, pp. 483–495, 2006.

[62] K. S. Tsakalis and L. D. Iasemidis, "Control aspects of a theoretical model for epileptic seizures," *Int. J. Bifurc. Chaos*, vol. 16, no. 07, pp. 2013–2027, 2006.

[63] N. Chakravarthy, S. Sabesan, K. S. Tsakalis, and L. Iasemidis, "Controlling epileptic seizures in a neural mass model," *J. Comb. Optim.*, vol. 17, no. 1, pp. 98–116, 2009.

[64] N. Chakravarthy, K. S. Tsakalis, S. Sabesan, and L. D. Iasemidis, "Homeostasis of brain dynamics in epilepsy: a feedback control systems perspective of seizures.," *Ann. Biomed. Eng.*, vol. 37, no. 3, pp. 565–85, Mar. 2009.

[65] R. S. Fisher, W. R. Webber, R. P. Lesser, S. Arroyo, and S. Uematsu, "High-frequency EEG activity at the start of seizures.," *J. Clin. Neurophysiol.*, vol. 9, pp. 441–448, 1992.

[66] G. Alarcon, C. D. Binnie, R. D. Elwes, and C. E. Polkey, "Power spectrum and intracranial EEG patterns at seizure onset in partial epilepsy.," *Electroencephalogr. Clin. Neurophysiol.*, vol. 94, pp. 326–337, 1995.

[67] G. A. James, S. P. Tripathi, J. G. Ojemann, R. E. Gross, and D. L. Drane. "Diminished default mode network recruitment of the hippocampus and parahippocampus in temporal lobe epilepsy.," *J. Neurosurg.*, vol. 119, no. 2, pp. 288–300, 2013.

[68] L. Lacasa, B. Luque, F. Ballesteros, J. Luque, and J. C. Nuño, "From time series to complex networks: the visibility graph.," *Proc. Natl. Acad. Sci. U. S. A.*, vol. 105, no. 13, pp. 4972–4975, 2008.

[69] J. Kim and T. Wilhelm, "What is a complex graph?," *Phys. A Stat. Mech. its Appl.*, vol. 387, no. 11, pp. 2637–2652, 2008.

[70] X. Tang, L. Xia, Y. Liao, W. Liu, Y. Peng, T. Gao, and Y. Zeng, "New approach to epileptic diagnosis using visibility graph of high-frequency signal.," *Clin. EEG Neurosci.*, vol. 44, no. 2, pp. 150–6, 2013.

[71] C. Wilke, G. Worrell, and B. He, "Graph analysis of epileptogenic networks in human partial epilepsy," *Epilepsia*, vol. 52, no. 1, pp. 84–93, 2011.

[72] E. Gombay, "Change detection in autoregressive time series," *J. Multivar. Anal.*, vol. 99, no. 3, pp. 451–464, 2008.

[73] S. Chen and P. Gopalakrishnan, "Speaker, environment and channel change detection and clustering via the Bayesian Information Criterion," *Proc. DARPA Broadcast News Transcr. Underst. Work.*, vol. 6, pp. 127–132, 1998.

[74] X. Shao and X. Zhang, "Testing for Change Points in Time Series," *J. Am. Stat. Assoc.*, vol. 105, no. 491, pp. 1228–1240, 2010.

[75] V. Lawhern, W. D. Hairston, and K. Robbins, "DETECT: A MATLAB Toolbox for Event Detection and Identification in Time Series, with Applications to Artifact Detection in EEG Signals," *PLoS One*, vol. 8, no. 4, p. e62944, 2013.

[76] E. S. Page, "Continuous Inspection Schemes," *Biometrika*, vol. 41, no. 12, pp. 100–115, 1954.

[77] C. Bilgin and B. Yener, "Dynamic network evolution: Models, clustering. anomaly detection," *IEEE Networks*, no. 1, 2006.

[78] P. Holme and J. Saramäki, "Temporal networks," *Phys. Rep.*, vol. 519, no. 3, pp. 97–125, 2012.

[79] P. Grindrod and D. J. Higham, "A Matrix Iteration for Dynamic Network Summaries," *SIAM Rev.*, vol. 55, no. 1, pp. 118–128, 2013.

[80] J. Tang, M. Musolesi, C. Mascolo, V. Latora, and V. Nicosia, "Analysing Information Flows and Key Mediators through Temporal Centrality Metrics Categories and Subject Descriptors," in *Proceedings of the 3rd Workshop on Social Network Systems*, p.3, 2010.

[81] P. Grindrod, M. C. Parsons, D. J. Higham, and E. Estrada, "Communicability across evolving networks," *Phys. Rev. E - Stat. Nonlinear, Soft Matter Phys.*, vol. 83, no. 4, p. 046120, 2011.

[82] P. Grindrod and D. J. Higham, "A dynamical systems view of network centrality," *Proc. Math. Phys. Eng. Sci.*, vol. 470, no. 2165, p. 20130835, 2014.

[83] S. Praprotnik and V. Batagelj, "Spectral centrality measures in temporal networks," *Ars Math. Contemp.*, vol. 11, no. 1, pp. 11–33, 2016.

[84] F. E. Grubbs, "Sample criteria for testing outlying observations," *Ann. Math. Stat.*, vol. 21, no. 1, pp. 27–58, 1950.